九州大学学術情報リポジトリ
Kyushu University Institutional Repository

Negative Catalysis-Driven Asymmetric Azlactone Ring-Opening with Hydrazines Using Quinine-Thiourea Catalysts: Access to Optically Active α-Amino Acid Hydrazides and Their Preferential Enrichment Phenomenon

ウォン, ソンヨン

https://hdl.handle.net/2324/7396162

出版情報：Kyushu University, 2025, 博士（理学）, 課程博士
バージョン：
権利関係：

KYUSHU UNIVERSITY

Negative Catalysis-Driven Asymmetric Azlactones Ring-Opening with Hydrazines Using Quinine-Thiourea Catalysts: Access to Optically Active *α*-Amino Acid Hydrazides and Their Preferential Enrichment Phenomenon

Sungyong WON

Catalysis Organic Chemistry Laboratory

Department of Chemistry
Graduate School of Science
Kyushu University

August 2025

Abbreviation

Boc	*tert*-butyloxycarbonyl
BTM	benzotetramisole
CPA	chiral phosphoric acid
CSA	camphorsulfonic aicd
CSP	crystal structure prediction
DABCO	1,4-diazabicyclo[2.2.2]octane
DCM	dichloromethane
DFT	density functional theory
DKR	dynamic kinetic resolution
DMAP	4-dimethylaminopyridine
ee	enantiomeric excess
er	enantiomeric ratio
IGM	independent gradient model
Int	intermediate
NAC	near attack conformation
NBSA	*o*-nitrobenzene sulfonic acid
PMP	*para*-methoxyphenyl
PTC	phase-transfer catalyst
rt	room temperature
THF	tetrahydrofuran
TMS	tetramethylsilane
Troc	2,2,2-trichloroethoxycarbonyl
TS	transition state

Table of Contents

1. Introduction

1-1. General Introduction of Azlactone

α-Amino acids and their derivatives are fundamental building blocks in the fields of medicinal chemistry and biochemistry.[1] Among them, non-proteinogenic α-substituted amino acids have received increasing attention, in part due to their potential for improved metabolic stability and target selectivity.[2] However, the stereoselective synthesis of such *α*-chiral amino acid derivatives remains a synthetic challenge.

Among the various strategies developed to address this challenge, the use of azlactones (also known as oxazolones or oxazol-5(4*H*)-ones) as electrophilic intermediates has proven especially powerful.[3] Easily accessible from *α*-amino acids via simple dehydration, azlactones offer both synthetic flexibility and high reactivity, making them highly suitable for catalytic enantioselective ring-opening to generate optically active *α*-amino acid derivatives.

Historically, azlactones have held significant importance in classical organic chemistry. Their earliest documented use dates back to the 19th century, notably in the Erlenmeyer–Plöchl reaction, in which azlactones were synthesized from *N*-acylated amino acids and condensed with aromatic aldehydes to yield *α*-arylidenamino acids.[4] This reaction demonstrated azlactones' synthetic potential as masked amino acid equivalents and established their fundamental role in nitrogen-containing heterocycle chemistry.

Despite this early discovery, broader attention toward azlactones resurfaced in the mid-20th century. A pivotal moment occurred during the total synthesis of penicillin V by Sheehan and Henery-Logan in 1959, wherein azlactones were unexpectedly detected not only as synthetic intermediates but also as side products.[5] This observation prompted renewed interest in azlactones, leading to deeper mechanistic investigations and the development of azlactone-based synthetic methodologies. In 1964, Goodman and Levine conducted kinetic studies on racemization of azlactone derivatives, showing that racemization proceeds to varying extents under mildly basic conditions.[6] Notably, pyridine induced only slow racemization, while more strongly basic conditions accelerated the process. Subsequent studies by de Jersey and Zerner in 1969 determined the pK_a of the *α*-proton of several azlactones to be approximately 9, highlighting the importance of this acidity in facilitating base-promoted racemization through enolization.[7]

Subsequently, in 1988, Benoiton and co-workers conducted a detailed kinetic investigation of the base-catalyzed racemization of 2,4-disubstituted oxazolones, systematically evaluating the influence of C(2) electronic and C(4) steric effects (Figure 1).[8] By determining activation parameters ($\Delta H^{\ddagger}$, $\Delta S^{\ddagger}$), they demonstrated that C(2) substituents accelerate racemization through resonance or inductive effects, while bulky C(4) substituents markedly suppress the rate by increasing steric hindrance. Importantly, they clarified that the racemization tendency of azlactones does not directly reflect the intrinsic configurational stability of the corresponding amino acid residues. In addition, more recent computational and experimental studies, including those of Tokunaga and co-workers, have pointed to the involvement of a carbanion-like transition state in racemization, complementing the traditional enolate pathway.[3e,9]

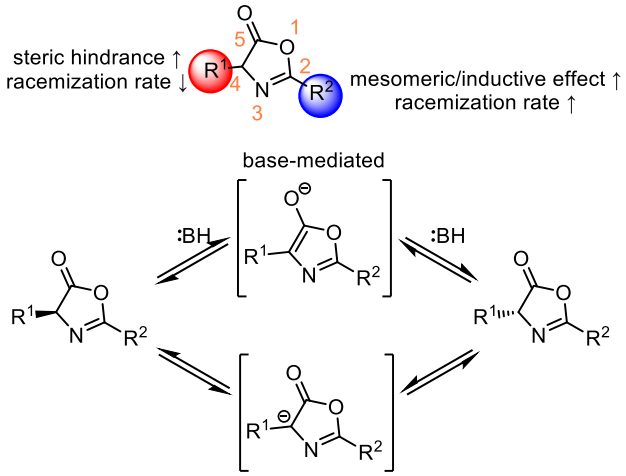

Figure 1. Substituent effects on racemization of azlactones: C(2) electron-donating groups accelerate the rate, while bulky C(4) groups suppress it via steric hindrance.

Given their high electrophilicity and structural versatility, azlactones are particularly well-suited for nucleophilic ring-opening reactions, which allow direct functionalization and access to diverse α-amino acid derivatives under mild conditions. In this research, catalytic asymmetric ring-opening reactions have been developed based on dynamic kinetic resolution (DKR) strategies, with particular emphasis on their mechanistic underpinnings. The following sections will thus explore the behavior of azlactones in such transformations, with an emphasis on catalyst-controlled selectivity, nucleophile tuning, and associated kinetic phenomena.

1-2. Development of Azlactone DKR for Enantioselective Ring-Opening

1-2-1. Alcoholysis-Based DKR of Azlactones

The first demonstration of catalyst-mediated DKR of azlactones was reported by Fu and co-workers in 1998, where a planar chiral DMAP derivative was used as the catalyst (Scheme 1).[10] In this system, the alcoholysis of azlactones was promoted using 5 mol% of the catalyst and 10 mol% benzoic acid as additive, under mild conditions (toluene, rt, 7 d), affording ring-opened amino acid derivatives in high yields. A total of 7 azlactone substrates were examined, affording the corresponding amino acid esters in consistently high yields (93–98%) with low to modeate enantioselectivity (44–78 %ee). Despite the limited enantiocontrol, this work established a key precedent in the development of catalytic dynamic kinetic resolution of azlactones using alcohol nucleophiles under nonenzymatic conditions.

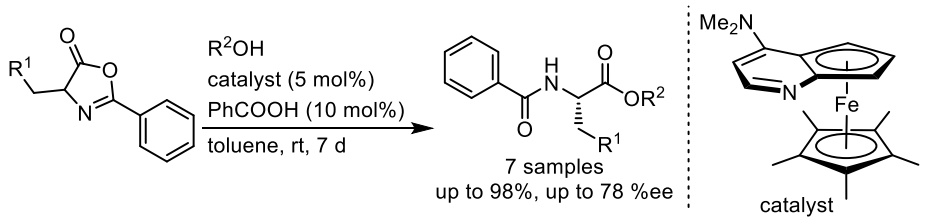

Scheme 1. The DKR of azlactones with alcohols, first demonstrated by Fu *et al.* using a planar chiral DMAP catalyst.

The Berkessel and Lex group reported a DKR of azlactones via alcoholysis using a series of bifunctional (thio)urea-*tert*-amine-based organocatalysts in 2005 (Scheme 2).[11] In their system, the framework of the catalyst was designed to promote both racemization of the azlactone and activation of the alcohol through hydrogen bonding. Various azlactone substrates were subjected to nucleophilic ring opening with allyl alcohol in the presence of 5 mol% of catalyst, and the transformation proceeded under mild conditions (toluene, rt, 48 h) without the need for metal additives. At room temperature, the reaction proceeded to high conversion (up to 96%) but gave moderate enantioselectivity (72–87 %ee, enantiomeric excess). To improve the ee, the temperature was lowered to –20 °C, leading to enhanced enantioselectivity of up to 91%; however, the conversion dropped significantly to 16% under these conditions. This study demonstrated that efficient DKR of azlactones can be achieved under metal-free conditions using a structurally tunable class of organocatalysts, although the trade-off between conversion and enantioselectivity remained a notable limitation.

Further mechanistic insight was provided through NMR analysis, which indicated that the catalyst operates via hydrogen bonding between the urea moiety and the carbonyl group of the azlactone (Scheme 2). In addition to this primary interaction, the amino group of the catalyst was found to engage in hydrogen bonding with the hydroxyl proton of the alcohol nucleophile. This dual hydrogen-bonding framework was proposed to play a critical role in both substrate activation and stereocontrol.

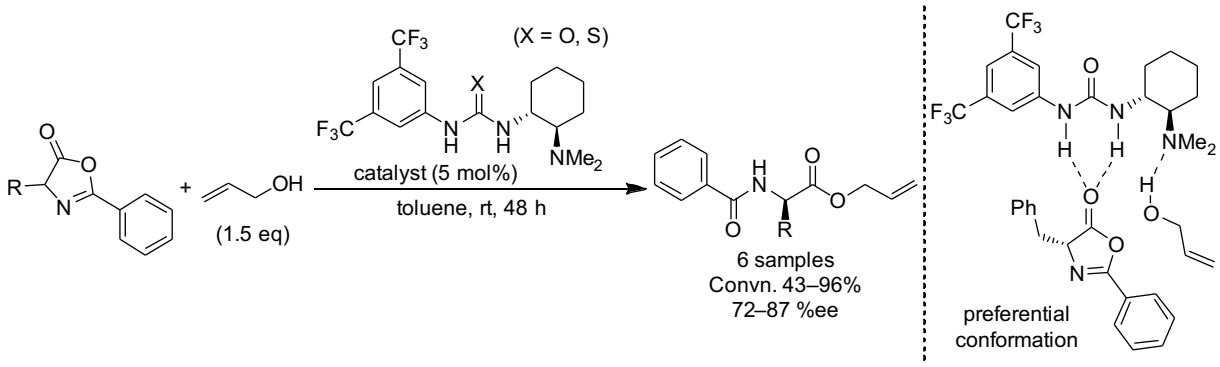

Scheme 2. Organocatalytic DKR of azlactones via alcoholysis and proposed hydrogen-bonding transition state.

In a subsequent study, the same group addressed the limitations observed in their earlier work (Scheme 3).[12] To overcome, they introduced a second-generation thiourea-*tert*-amine catalyst. This modified one significantly enhanced the stereodifferentiation, enabling the DKR of various azlactone substrates to proceed efficiently at room temperature. For instance, the reaction between the azlactone and allyl alcohol afforded the corresponding amino acid derivative in 95 %ee with over 90% conversion after 96 reaction hours.

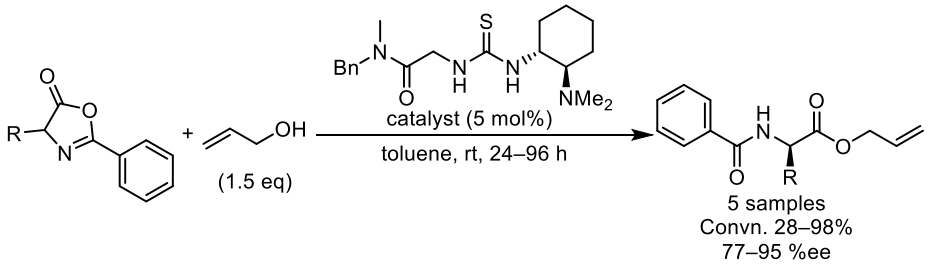

Scheme 3. Enhanced enantioselectivity in DKR of azlactones using second-generation thiourea-*tert*-amine catalyst.

In 2008, Connon and co-workers demonstrated a DKR of azlactones using another bifunctional (thio)urea organocatalysts that based on cinchona alkaloid structures (Scheme 4).[13] The catalysts, designed to activate both the azlactone and the alcohol nucleophile via hydrogen bonding, promoted the enantioselective alcoholysis of various azlactones bearing *α*-amino acid-derived side chains such as valine, methionine, and phenylalanine. Among the tested catalysts, the dihydroquinine-derived urea catalyst exhibited the best performance, delivering the desired amino acid derivatives with up to 85 %ee and nearly quantitative conversion at room temperature. Notably, the catalytic system showed good tolerance to steric bulk at the azlactone's *α*-position, enabling efficient DKR of both hindered and unhindered substrates. A control experiment clearly demonstrated that no reaction occurred in the absence of catalyst, confirming the essential role of the bifunctional catalyst in promoting both racemization and nucleophilic activation. While an improvement in enantioselectivity was observed upon lowering the reaction temperature to –20 °C, this came at the cost of longer reaction time.

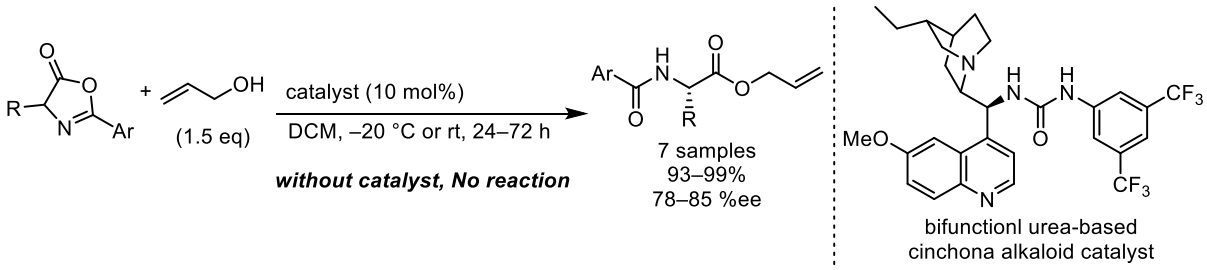

Scheme 4. Enantioselective alcoholysis of azlactones using bifunctional urea-based cinchona alkaloid catalysts (Connon, 2008).

In 2009, Song and co-workers reported a DKR of azlactones employing a series of squaramide-based dimeric cinchona alkaloid organocatalysts designed to suppress self-aggregation of the catalyst in solution (Scheme 5).[14] These catalysts, featuring a bifunctional architecture with hydrogen-bonding squaramide units and sterically constrained quinuclidine cores, enabled the enantioselective ring-opening of racemic azlactones with allyl alcohol. The reaction proceeded delivering the desired amino acid derivatives in excellent yields (up to 99%) and enantioselectivities (up to 94 %ee) within 3–8 h. Even at reduced catalyst loading (2 mol%), high selectivity (94 %ee) was retained, and further improvement to 97 %ee was achieved by lowering the reaction temperature to –20 °C. While this study provided important mechanistic insight into catalyst aggregation and stereocontrol, the substrate scope was limited to a single azlactone derivative, leaving the generality of the system yet to be demonstrated.

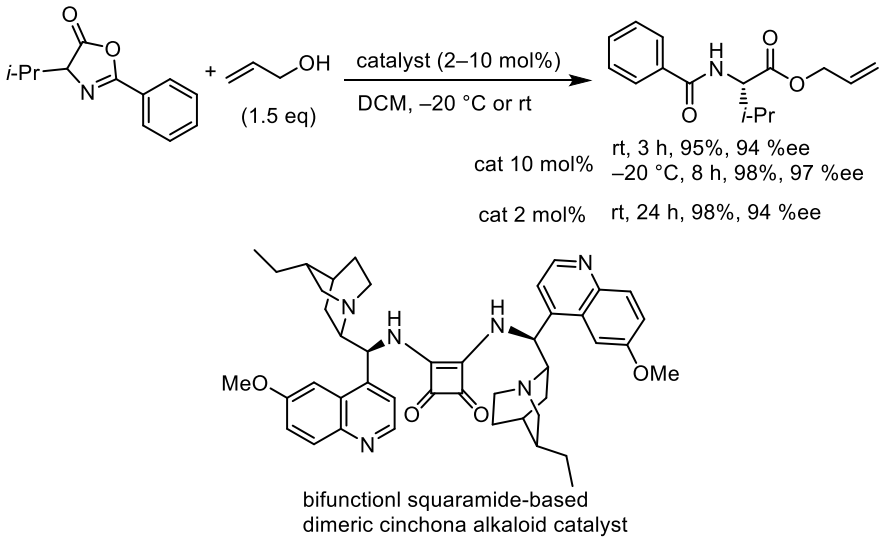

Scheme 5. Enantioselective DKR of azlactones using bifunctional squaramide-based dimeric cinchona alkaloid catalysts (Song, 2009).

In 2010, Birman and co-workers reported a DKR of azlactones employing the enantioselective acyl transfer catalyst benzotetramisole (BTM), marking the first successful example of this transformation via an acylation mechanism (Scheme 6).[15] The catalytic system utilized benzoic acid as a co-promoter and di(1-naphthyl)methanol as the alcohol nucleophile, enabling highly enantioselective ring-opening of various azlactone substrates under mild conditions. Among the catalysts tested, BTM proved most effective,

delivering the desired ester products in up to 97% and 96 %ee. A broad substrate scope was demonstrated, with both alkyl- and aryl-substituted azlactones undergoing efficient transformation, while the reaction of sterically hindered substrates such as isopropyl analogues remained challenging. The overall process was limited by its reliance on acid additives and relatively long reaction times, which often extended to several days.

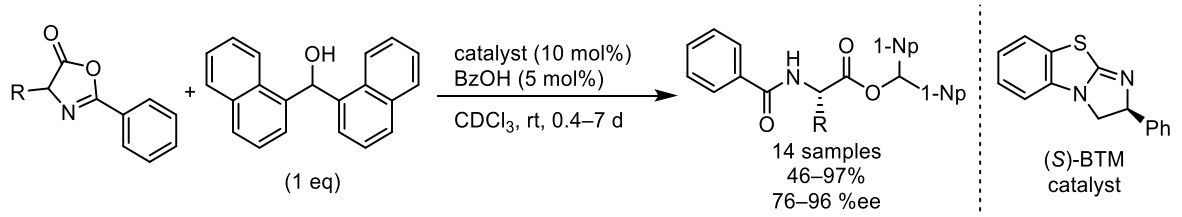

Scheme 6. Enantioselective ring-opening of azlactones via BTM-catalyzed acyl transfer.

Following their successful report on the DKR of azlactones via BTM-catalyzed enantioselective acyl transfer, Birman and co-workers developed a conceptually distinct strategy using chiral Brønsted acids as the sole catalyst (Scheme 7).[16] This new approach eliminated the need for benzoic acid co-promoters and enabled direct asymmetric alcoholysis of azlactones. Among the catalysts screened, 3,3′-bis(9-anthryl)-BINOL phosphoric acid demonstrated superior efficiency, particularly with 4-aryl-substituted azlactones, achieving up to 92 %ee.

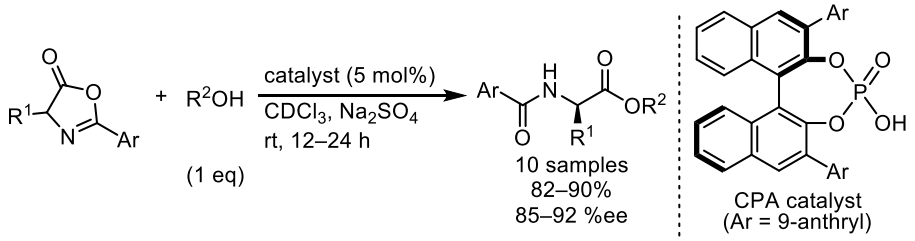

Scheme 7. Chiral phosphoric acid-catalyzed dynamic kinetic resolution of azlactones via enantioselective alcoholysis.

Connon and co-workers again developed a structurally tunable library of bifunctional cinchona alkaloid catalysts, building on their earlier work (Scheme 8).[17] By introducing various aryl substituents—including naphthol groups—at the C9 position of the quinidine core, they modulated the spatial proximity between the Brønsted base and hydrogen-bond donor functionalities. This design enabled the room-temperature DKR of representative substrates, achieving up to 99% yield and 99 %ee. The modular approach demonstrated comparable or superior enantioselectivity for selected substrates under milder conditions.

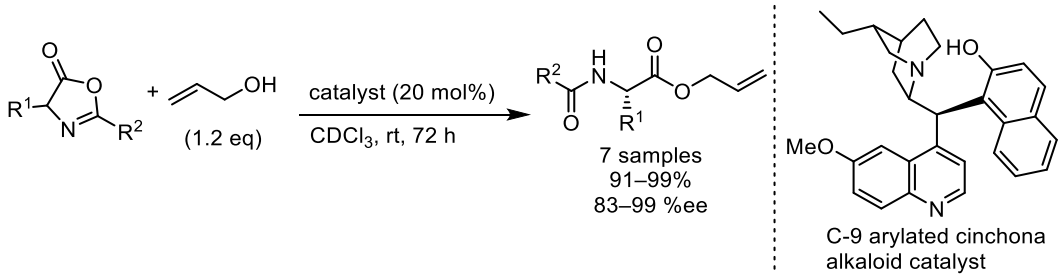

Scheme 8. DKR of azlactones via alcoholysis catalyzed by C9-arylated cinchona alkaloid derivatives (Connon, 2012).

Tetrapeptide-based catalysts have been demonstrated to promote the enantioselective DKR of azlactones through multifunctional activation reminiscent of enzymatic catalysis (Scheme 9).[18] Unlike conventional small-molecule organocatalysts, these low-molecular-weight peptides can adopt defined secondary structures, such as β-hairpin motifs, enabling multiple, spatially organized noncovalent interactions to stabilize developing charges in the transition state. Under optimized conditions, this approach achieved up to 99% yield and 94% ee across a diverse substrate set, highlighting the effectiveness of peptide scaffolds.

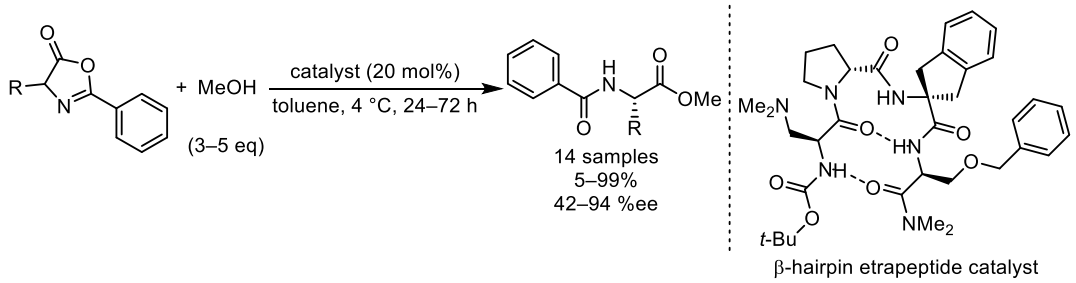

Scheme 9. *β*-Hairpin tetrapeptide-catalyzed DKR of azlactones, giving up to 99% yield and 94 %ee.

In a subsequent study, Connon and co-workers addressed a key limitation of earlier alcoholysis-based azlactone DKR protocols—namely, the lack of orthogonally removable protecting groups in the products (Scheme 10).[19] They designed a novel class of aryl azlactones bearing a tetrachlorophthalimide moiety and an isopropyl ester at the *α*-position to enable selective ring-opening with amino alcohol nucleophiles. This strategy provided access to diastereomerically pure intermediates (up to 99:1 d.r.), which could undergo efficient post-DKR ring-closure to generate phthalimide-protected amino acid derivatives.

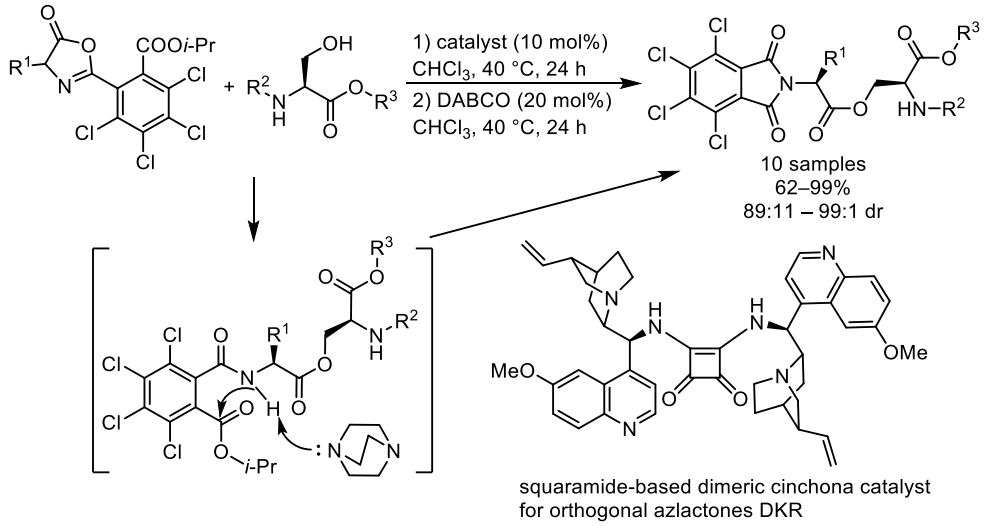

Scheme 10. Orthogonally protected amino acid derivatives obtained via diastereoselective DKR of aryl azlactones using a dimeric cinchona-squaramide catalyst.

In 2018, Suga and co-workers applied a binaphthyl-based chiral *N*,*N*-dimethylaminopyridine (DMAP) derivative to the DKR of azlactones (Scheme 11).[20] Originally developed as a powerful nucleophilic catalyst for Steglich-type rearrangements and acylation of alcohols, the catalyst features two amide groups at the 3,3′-positions of the binaphthyl scaffold. Although the study was not focused on overcoming specific structural challenges of azlactones, its purpose was to evaluate the performance of the catalyst in a benchmark transformation. Under cooperative Brønsted acid catalysis, the reaction proceeded at room temperature with as little as 3 mol% of the catalyst, delivering enantioenriched α-amino acid derivatives in up to 91% yield and 96:4 er.

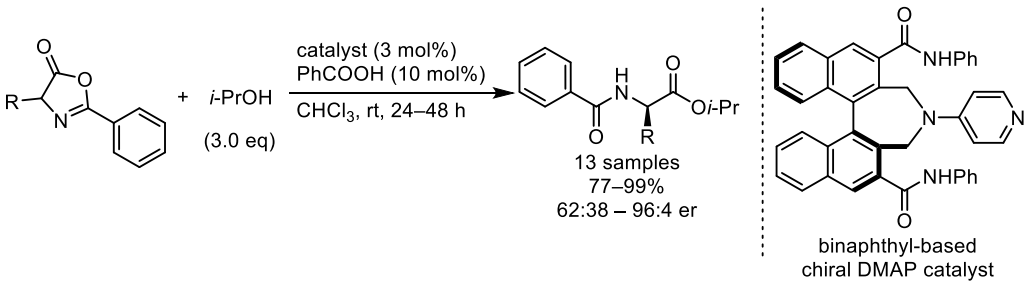

Scheme 11. Suga's chiral DMAP catalyst enables DKR of azlactones at room temperature with high enantioselectivity.

Among the catalytic strategies for the DKR of azlactones, most existing systems have relied on Brønsted acids or nucleophilic organocatalysts, which are often limited in their substrate scope or require relatively harsh conditions. In particular, the efficient stereocontrol of sterically hindered azlactone substrates bearing tertiary α-substituents has remained a persistent challenge. In this context, Tokunaga and co-workers reported a phase-transfer catalytic (PTC) asymmetric alcoholysis of azlactones, which enabled the synthesis of α-chiral amino acid esters in up to 98% yield and 99:1 er under biphasic basic conditions, using as little as 0.1 mol% catalyst loading (Scheme 12).[9b] Notably, this method proved applicable even to HFIP esters and

structurally hindered substrates, overcoming a critical limitation in prior alcoholysis-based approaches.

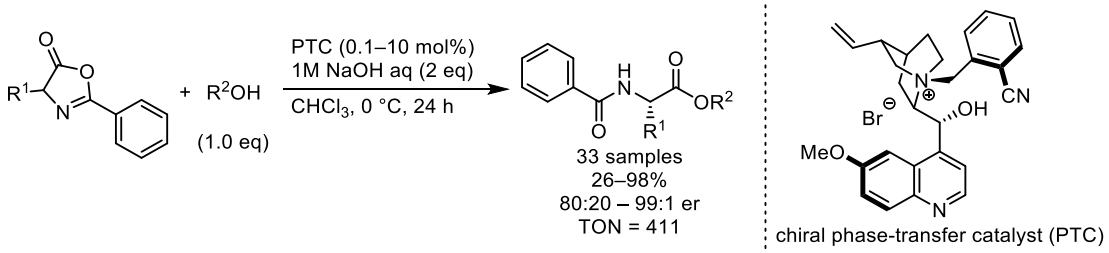

Scheme 12. Tokunaga's chiral phase-transfer catalyst enabled highly enantioselective alcoholysis of azlactones, affording α-amino acid esters with up to 99:1 er at catalyst loadings as low as 0.1 mol%.

To elucidate the origin of stereoselectivity in this transformation, the authors employed a computational strategy involving a pseudo-transition state (pseudo-TS) conformational search using the ConFinder program,[9a,21] coupled with density functional theory (DFT) calculations (Figure 2). This approach allowed identification of the key noncovalent interactions between the azlactone substrate and the chiral PTC in the stereodetermining transition state conformation. Through this analysis, the authors demonstrated how subtle electronic and steric modifications at the azlactone C(2)-position significantly affect reactivity and enantioselectivity by perturbing the accessible transition-state geometry.

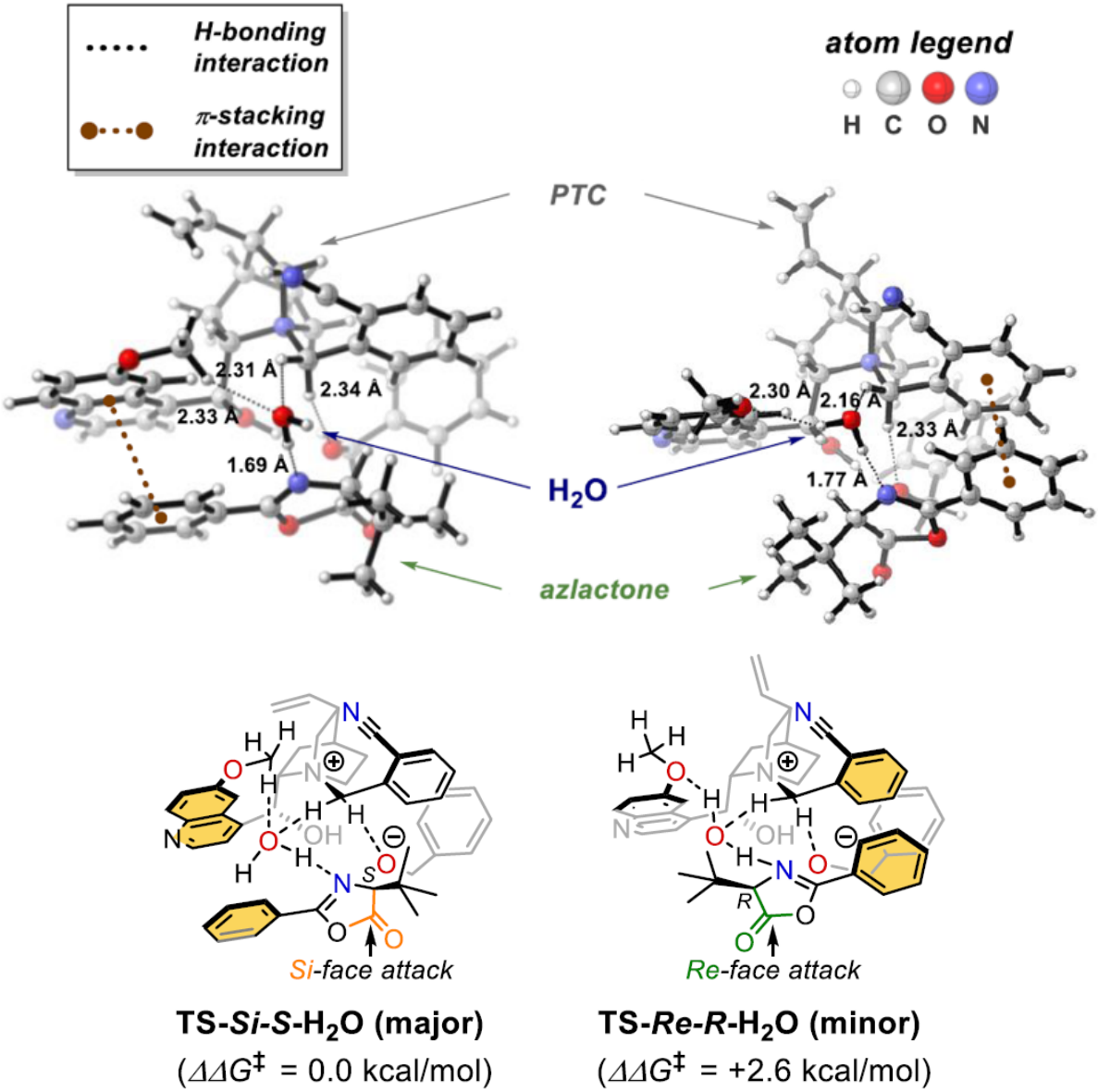

Figure 2. Calculated transition-state (TS) structures for the formation of each enantiomer at the B97D/TZVP level, highlighting key noncovalent interactions between the azlactone, chiral phase-transfer catalyst, and water. The major TS (left) is stabilized by multiple hydrogen bonds and a π-stacking interaction, while the minor TS (right) exhibits a distorted geometry with weakened interactions (Reproduced figures from ref 9a).

1-2-2. Thiolysis-Based DKR of Azlactones

In the course of developing their alcoholysis-based DKR of azlactones, Connon and co-workers also reported the first example of a thiolysis-based DKR using a synthetic organocatalyst in 2008 (Scheme 13).[12] Under similar conditions to those employed for alcoholysis, the bifunctional urea-type catalyst effectively promoted the ring-opening of azlactones with thiol nucleophiles. Within 2 subjects, the corresponding thioester products yielded in up to 98%, but showed low 64 %ee as the highest result.

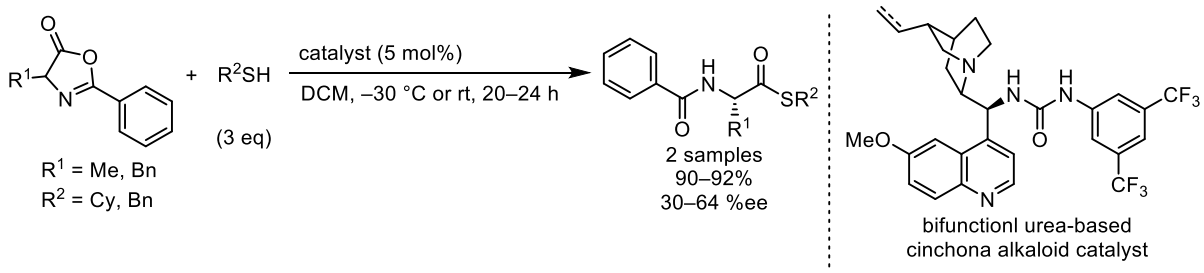

Scheme 13. Thiolysis-based DKR of azlactones using a bifunctional urea organocatalyst.

Following their success in alcoholytic DKR, Connon and co-workers extended their earlier study on the DKR of azlactones via thiolysis in 2012 (Scheme 14).[22] They developed new C9-naphthol-substituted cinchona alkaloid catalysts for this purpose. However, the enhancement in both reactivity and enantioselectivity was limited, requiring prolonged reaction times (3–28 days), with the best results reaching only up to 73% ee—a slight improvement over their 2008 study.

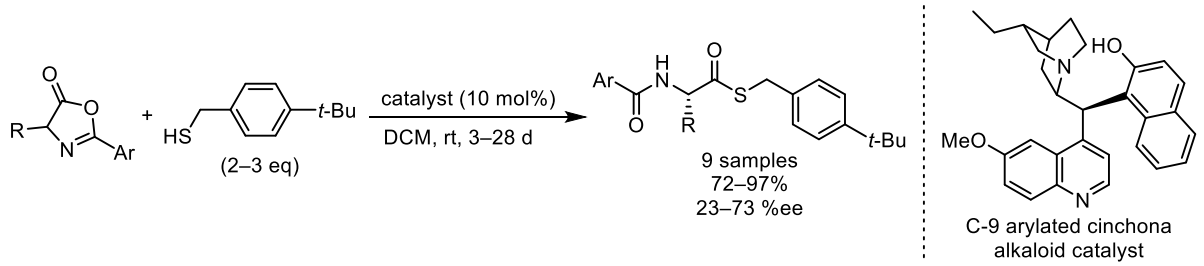

Scheme 14. C9-arylated cinchona-catalyzed DKR of azlactones via thiolysis.

In a subsequent study, they evaluated cupreine-derived catalysts to improve the thiolytic DKR (Scheme 15).[23] The best-performing hydroxylated catalyst promoted the reaction with up to 92 %ee. However, the transformation remained limited by moderate yields, which range from 24 to 60% due to catalyst-promoted hydrolysis of the azlactone. Moreover, achieving high enantioselectivity required extremely low temperatures (–70 °C) and extended reaction times (up to 92 h). Control experiments confirmed that the reaction does not proceed without a catalyst.

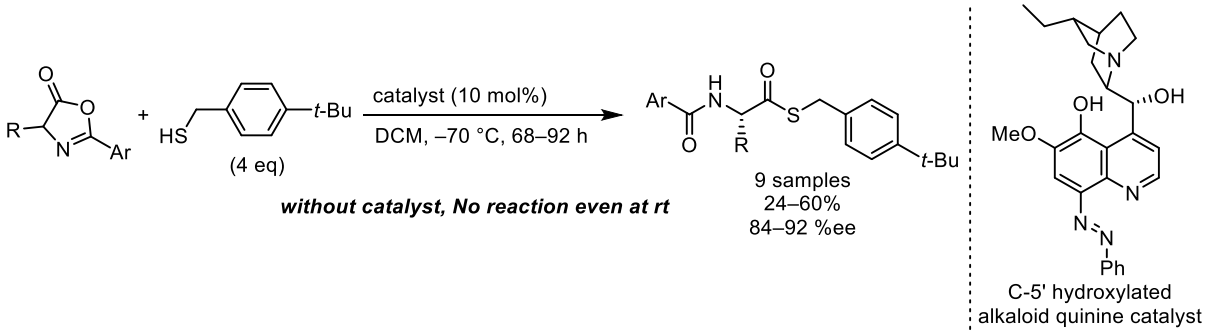

Scheme 15. Thiolytic DKR of azlactones using hydroxylated cupreine catalyst: high enantioselectivity under cryogenic and prolonged conditions.

1-2-3. Oxime-Based DKR of Azlactones

A representative example of azlactone transformation employing oximes as nucleophiles was reported by Feng and co-workers in 2015 (Scheme 16).[24] In this study, a series of chiral *N*-acyl amino acid oxime esters were synthesized through the DKR of azlactones with oximes, catalyzed by a chiral bisguanidinium hemi-salt. The reaction proceeded with high efficiency, affording the desired products in up to 99% yield and 97 %ee across a broad substrate scope. Oximes were highlighted as valuable oxygen nucleophiles, offering enhanced acidity and nucleophilicity relative to typical alcohols. However, the reaction was strictly conducted under cryogenic conditions (typically –40 to –50 °C), and no results were reported at ambient temperature, which may limit the practicality of this method.

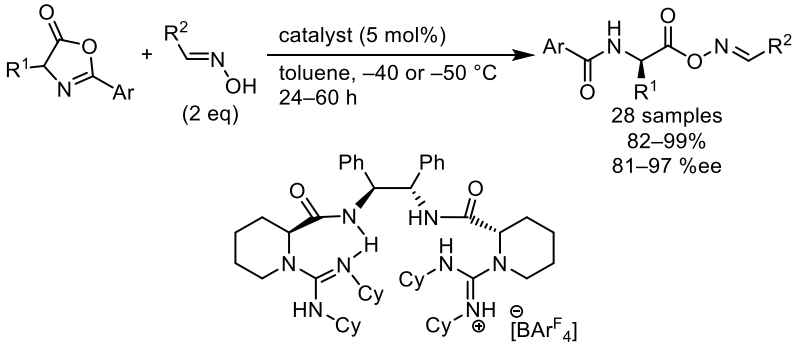

Scheme 16. Bisguanidinium salt-catalyzed asymmetric oxime addition to azlactones.

1-2-4. Aminolysis-Based DKR of Azlactones

Shi and co-workers reported the first catalytic asymmetric aminolysis of azlactones using aniline derivatives as nucleophiles under chiral phosphoric acid (CPA) catalysis, (*R*)-**TRIP** (Scheme 17).[25] This strategy enabled highly enantioselective formation of bisamide products (up to 99% yield, 96 %ee), and demonstrated the feasibility of using nitrogen nucleophiles in DKR of azlactones. However, their system required a specific structural motif on the aniline, featuring both a bulky substituent and a hydroxy group, to achieve high stereocontrol. This strict structural requirement significantly limited substrate generality, confining the method to a narrow set of nucleophiles and products. Although further developments allowed extension to related KR systems, the original approach underscores the need for more flexible strategies to harness the potential of nitrogen nucleophiles in asymmetric catalysis. The development of such methods remains a key challenge in the field.

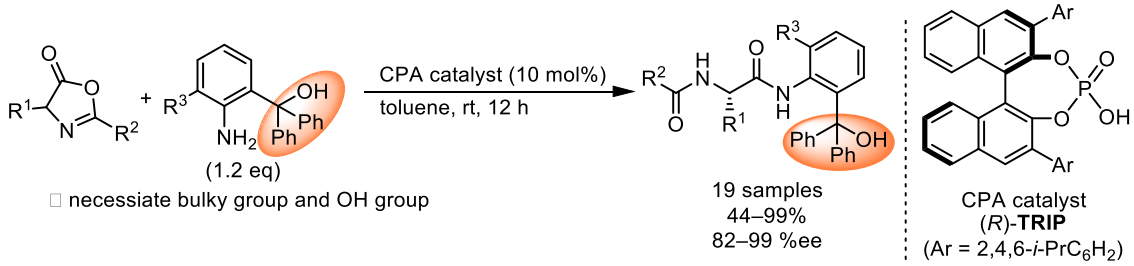

Scheme 17. Enantioselective DKR of azlactones with aniline derivatives under CPA catalysis.

1-2-5. Summary and Outlook

As discussed above, the DKR of azlactones has been explored with various nucleophiles for enantioselective ring-opening. Alcohols have served as the most representative nucleophiles, and notable advances have also been made using thiols, oximes, and anilines. However, it is evident that as the nucleophile class deviates from alcohols, the extent of development becomes increasingly limited. In particular, nitrogen-based nucleophiles have seen only a single successful example, in which a bulky moiety substituted aniline was employed by the Shi group (Figure 3).

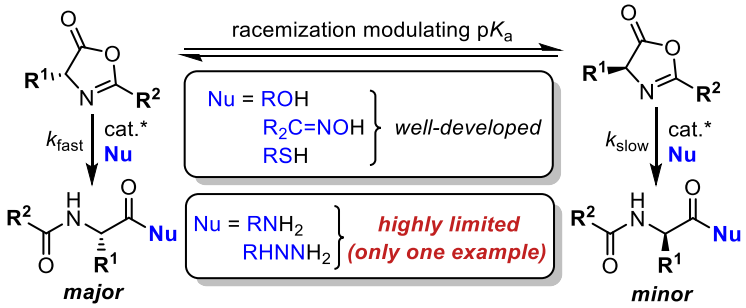

Figure 3. Development status of nucleophiles in azlactone DKR: well-established for *O*-, *S*-nucleophiles, highly limited for *N*-nucleophiles.

Considering the intrinsic reactivity of azlactones toward nucleophilic attack, this lack of diversity in the nucleophiles applicable to DKR is counterintuitive. Before exploring the catalytic conditions necessary for asymmetric induction, it is essential to first understand how various nitrogen-based nucleophiles behave under non-catalytic and Brønsted acid-promoted conditions. In the following sections, comparative studies are presented to assess the fundamental ring-opening reactivity of azlactones with representative nucleophiles.

1-3. Effect of Nucleophiles on Azlactones

Despite the electrophilicity of azlactones, nitrogen-based nucleophiles remain underexplored in DKR strategies. This section aims to clarify this comparatively little attention by examining their innate reactivity under non-catalytic conditions. Given azlactone's inherent susceptibility toward nucleophilic attack, it is worth examining why examples with nitrogen nucleophiles are scarce. To address this knowledge gap, it is crucial to first examine how these nucleophiles behave under catalyst-free conditions. In the following sections, comparative studies of catalyst-free ring-opening reactions of azlactones with various nitrogen nucleophiles are presented to elucidate their intrinsic reactivities.

1-3-1. Ring-Opening Reactivity of Azlactones with Nitrogen-Based Nucleophiles

During their kinetic studies on azlactone racemization between 1979 and 1988, Benoiton and co-workers optimized the non-catalyzed nucleophilic ring-opening with hydrazine monohydrate in methanol, shortening reaction times from cryogenic conditions (0–5 °C, 6 h) to just 10 minutes at 35 °C, affording chiral α-amino

acid hydrazides in 75–80% yield (Scheme 18).[8,26] These findings revealed that under such conditions, the rate of hydrazinolysis outpaces racemization, highlighting the effectiveness of hydrazine as a selective nucleophile. Moreover, they provide clear evidence that extremely rapid, non-catalyzed ring-opening reactions can proceed under mild conditions.

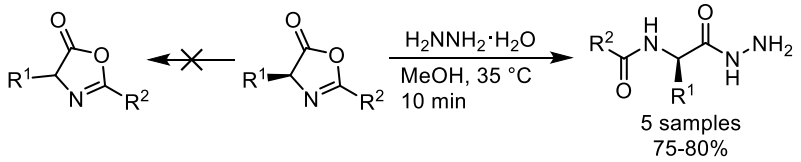

Scheme 18. Catalyst-free hydrazinolysis of azlactones under mild conditions, enabling rapid formation of *α*-amino acid hydrazides with high yield.

Despite this early and striking demonstration, hydrazine remained largely overlooked in subsequent developments, particularly in the context of asymmetric synthesis such as DKR. In contrast, the period between 2004 and 2020 saw a resurgence of interest in non-catalyzed azlactone transformations, particularly with amines.[27] A series of practical reports, including gram-scale examples, demonstrated that both primary and secondary amines can effectively promote ring-opening under mild, catalyst-free conditions, even at room temperature and with near-stoichiometric quantities of reagents (Scheme 19). Notably, several patents from 3M® and SYRICI® disclosed efficient large-scale protocols involving aliphatic primary and secondary amines, achieving high yields under ambient conditions.

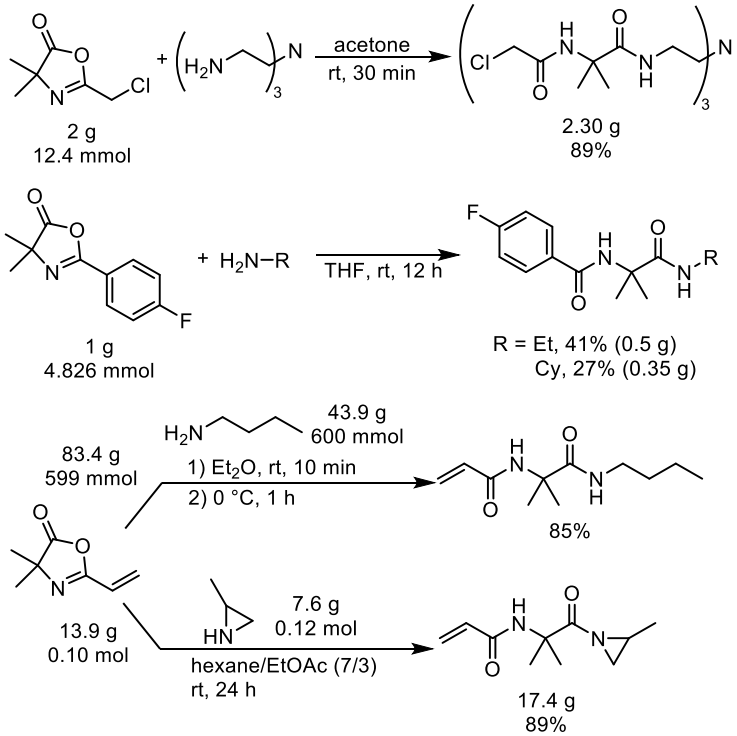

Scheme 19. Gram-scale, catalyst-free azlactone ring-opening with primary and secondary amines under ambient conditions, reported in industrial patents by 3M® and SYRICI®.

Non-catalyzed azlactone ring-opening with amines has also been widely explored in academic settings.

Early work by Shriner (1948) showed that secondary amines like piperidine could promote the reaction in excellent yield, albeit under harsh conditions.[28] Later, Gibson (2013)[29] and Fontaine (2018)[30] demonstrated that primary amines such as allylamine and benzylamine efficiently react with azlactones at room temperature without catalysts, highlighting the broad applicability of this transformation in both polymer and small-molecule contexts.

Collectively, these examples underscore the pronounced intrinsic reactivity of azlactones toward nitrogen-based nucleophiles under catalyst-free conditions. This observation not only challenges the prevailing notion that catalysts are necessary to drive such nucleophilic ring-opening transformations but also provides a foundation for systematically investigating the fundamental reactivity trends of azlactones across a wider range of nucleophilic species. The following section, therefore, explores the contrasting behavior exhibited by weaker nucleophiles, aiming to delineate clearer mechanistic insights and expand the synthetic applicability of azlactone chemistry.

1-3-2. Ring-Opening Reactivity of Azlactones with Weak Nucleophiles

In sharp contrast, when oxygen- or sulfur-based nucleophiles such as alcohols or thiols are employed, azlactone ring-opening proceeds far less readily under non-catalyzed conditions. Unlike nitrogen nucleophiles, these species lack the α-effect and typically display insufficient reactivity to promote efficient ring-opening without activation.

Efficient azlactone ring-opening has also been demonstrated using oxime, as reported by Mukerjee and co-workers in 1979 (Scheme 20).[31] In their study, oxime nucleophiles reacted with azlactones without any catalysts or bases under refluxing benzene (about 80 °C), providing the corresponding *O*-acyl oximes in high yields (73–83%) within 30 minutes. Notably, this reaction required elevated temperatures to proceed efficiently, in contrast to the room-temperature or cryogenic conditions sufficient for nitrogen-based nucleophiles such as amines and hydrazines.

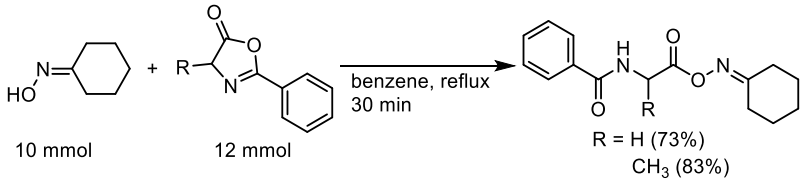

Scheme 20. Oxime-induced ring-opening of azlactones requires high temperature (80 °C) to give *O*-acyl oximes in 73–83% yield.

To date, no successful reports exist of catalyst-free, base-free, or acid-free ring-opening of azlactones using alcohol or thiol nucleophiles (Figure 4). Notably, in the DKR studies introduced earlier sections, Connon and co-workers explicitly demonstrated that under their developed catalytic conditions, azlactone alcoholysis[12] or thiolysis[22] does not proceed in the absence of the catalyst. Similarly, Amarante and co-workers reported that in the presence of a camphorsulfonic aicd (CSA) Brønsted acid catalyst, ring-opening with alcohols occurs efficiently, whereas under catalyst-free conditions no conversion was observed.[32] These findings collectively underscore the inherently low nucleophilicity of alcohols and thiols toward azlactone

ring-opening, in stark contrast to the high reactivity of nitrogen nucleophiles under non-catalyzed conditions.

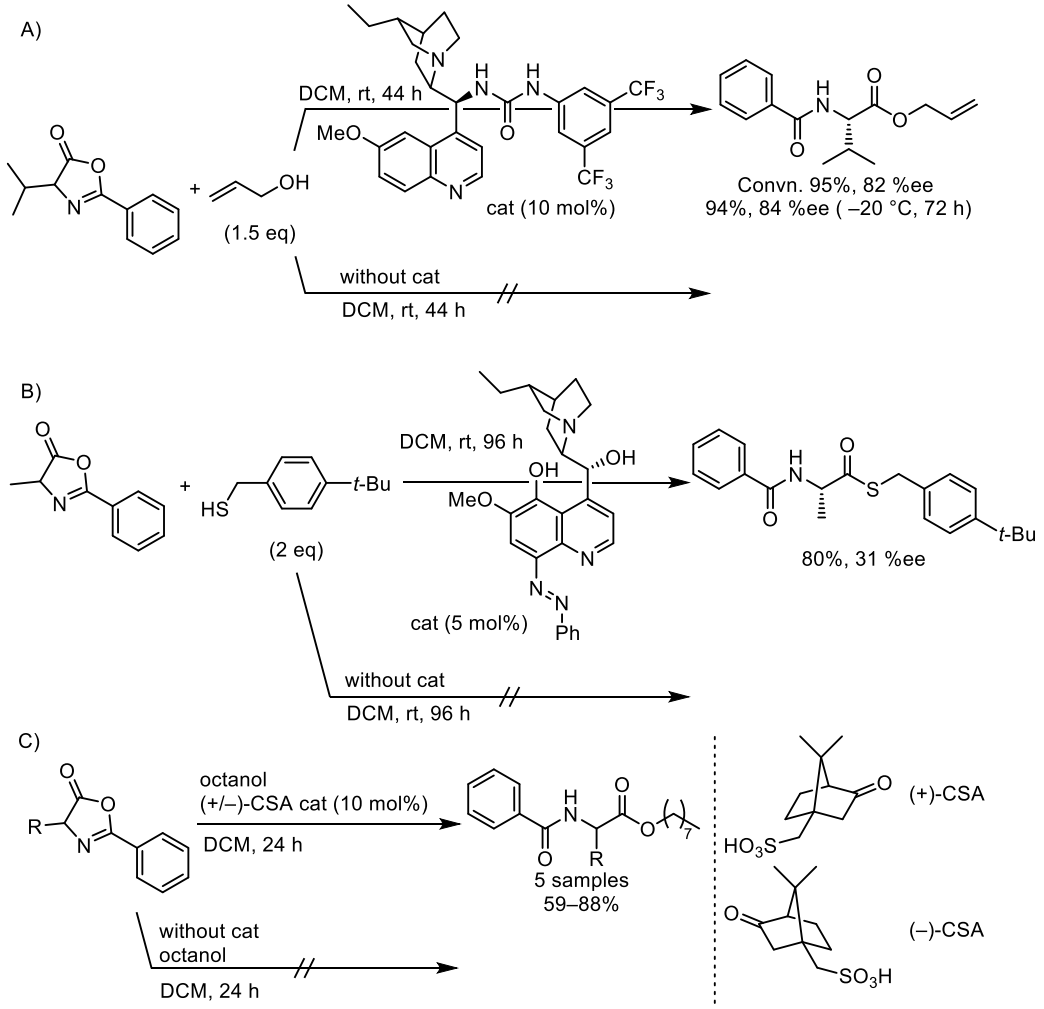

Figure 4. Catalyst-dependence in the ring-opening of azlactones with alcohols and thiols. (A) Alcoholysis with a chiral bifunctional thiourea catalyst proceeds with high yield and enantioselectivity, while no conversion occurs without the catalyst. (B) Thiolysis proceeds only in the presence of an organocatalyst; no product forms without catalyst. (C) Alcoholysis with CSA (camphorsulfonic acid) gives moderate-to-high yields; no reaction occurs under catalyst-free conditions.

Taken together, these observations highlight the stark contrast in nucleophilic performance between oxygen/sulfur-based and nitrogen-based species under non-catalyzed conditions. To further quantify and contextualize these differences, systematic comparisons based on nucleophilicity parameters (*N*) are warranted, providing a unified framework to rationalize the distinct reactivity trends observed across nucleophile classes.

1-3-3. Nucleophilicity Parameters (*N*)

The Mayr nucleophilicity parameter (*N*) is a quantitative scale developed to evaluate and compare the nucleophilic reactivity of diverse compounds under standardized conditions. Introduced in the 1990s by Herbert Mayr and co-workers,[33] the system was established through extensive kinetic studies measuring reaction rates between a reference series of electrophiles (such as benzhydrylium ions) and a wide range of nucleophiles, including amines, hydrazines, alcohols, thiols, phosphines, and others. The resulting parameters are expressed through the linear free-energy relationship: $\log k = s(N + E)$, where k is the second-order rate constant, s is a nucleophile-specific sensitivity factor, N is the nucleophilicity parameter, and E is the electrophilicity parameter of the reaction partner.

Introducing the *N*-parameter framework allows the subsequent discussion to quantitatively rationalize the observed differences in azlactone ring-opening reactivity. This empirical approach enables direct comparison of nucleophilic reactivities across diverse chemical classes, offering a mechanistic rationale for why only specific nucleophiles, such as amines and hydrazines, effectively promote non-catalyzed ring-opening, whereas others, like alcohols and thiols, require additional activation. The following table summarizes representative *N* values for various nucleophiles (Table 1).

Table 1. Representative Mayr nucleophilicity parameters (*N*) for various nucleophiles in MeCN and other solvents (reported only).

molecule	name	solvent	*N*	s_N	ref
	methanol	MeCN	6.86	0.73	34
	methanol	MeOH	7.54	0.92	35
	methanolate	MeOH	15.78	0.56	36
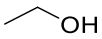	ethanol	MeCN	7.13	0.71	34
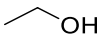	ethanol	EtOH	7.44	0.90	35
	ethanolate	EtOH	15.78	0.65	36
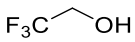	trifluoroethanol	TFE	1.11	0.96	37
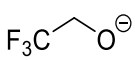	trifluoroethanolate	H_2O	12.66	0.59	38
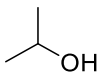	*i*-propanol	MeCN	6.82	0.70	34
	*iso*propanolate	*i*PrOH	17.03	0.63	36
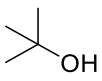	*t*-butanol	MeCN	5.35	0.72	34
 (O attack)	dimethylsulfoxide	DMSO	11.30	0.74	39

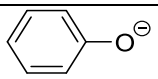	phenolate	MeCN	18.53	0.85	40
	water	MeCN	5.79	0.72	34
	hydroxide	H_2O	10.47	0.61	38
	dimethylsulfide	MeCN	12.70	0.72	41
	tetrahydrothiophene	MeCN	13.30	0.72	41
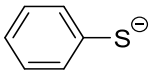	thiophenolate	DMSO	23.36	0.74	42
NH_3	ammonia	MeCN	11.39	0.69	43
$MeNH_2$	methylamine	MeCN	15.19	0.68	43
Me_2NH	dimethylamine	MeCN	17.96	0.63	43
Me_3N	trimethylamine	MeCN	23.05	0.45	43
$EtNH_2$	ethylamine	H_2O	12.87	0.58	44
Et_2NH	diethylamine	MeCN	15.10	0.73	45
Et_3NH	triethylamine	MeCN	17.10	0.52	46
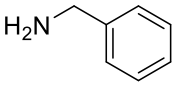	benzylamine	MeCN	14.29	0.67	45
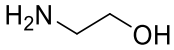	ethanolamine	MeCN	14.11	0.71	45
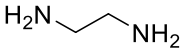	ethylenediamine	H_2O	13.28	0.58	44
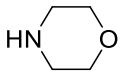	morpholine	MeCN	15.65	0.74	45
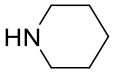	piperidine	MeCN	17.35	0.68	45
	pyrrolidine	MeCN	18.58	0.61	47
	quinuclidine	MeCN	20.54	0.60	48
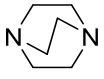	DABCO	MeCN	18.80	0.70	48
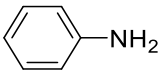	aniline	MeCN	12.64	0.68	44
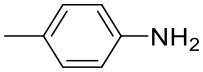	*p*-toluidine	MeCN	13.19	0.69	44
	pyridine	MeCN	13.60	0.60	49

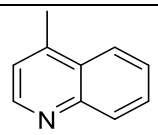	lepidine	MeCN	11.60	0.62	50
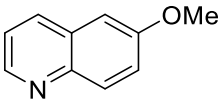	6-methoxy-quinoline	MeCN	10.86	0.66	50
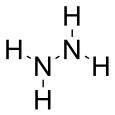	hydrazine	MeCN	16.45	0.56	51
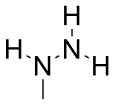	methylhydrazine	MeCN	17.73	0.58	52
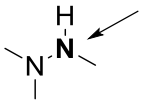	trimethylhydrazine	MeCN	12.43	0.75	51
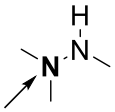	trimethylhydrazine	MeCN	17.75	0.53	51
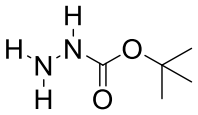	Boc-hydrazine	MeCN	11.40	0.70	43
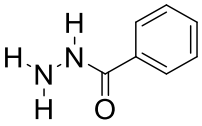	benzoylhydrazine	MeCN	12.49	0.66	43

The *N* parameter values, while dependent to some extent on the solvent used during their determination, generally display consistent trends across nucleophile classes. Simple aliphatic alcohols, for example, exhibit *N*-values in the range of approximately 5–7, reflecting their inherently weak nucleophilic character. Upon deprotonation to the corresponding alkoxides, however, the nucleophilicity increases markedly, often nearly doubling the *N*-value of 15–18, which rationalizes the well-established requirement for basic conditions to promote efficient azlactone alcoholysis. In contrast, thiols remain challenging to position within this framework, as no direct *N* parameter measurements for simple thiols have been reported to date. However, a few isolated studies have investigated the reactivity of thiolethers or thiophenolates in related nucleophilic processes. Among amines, a notable increase in *N*-values is observed when moving from primary to secondary and tertiary amines, reaching values between ~13–20. However, it is important to note that tertiary amines, while possessing high *N*-values, lack an available free N–H site for nucleophilic addition, effectively limiting their role to that of bases rather than nucleophiles. Hydrazines display also notably high *N*-values, typically in the range of 11–18, with hydrazine itself reported at 16.45. This strong nucleophilic character provides a clear mechanistic rationale for earlier observations by Goodman and Benoiton, where hydrazinolysis efficiently outcompeted racemization during azlactone reactions under non-catalyzed

conditions. Altogether, the high nucleophilicity observed across nitrogen-based nucleophiles in subsequent studies, explains why efficient, catalyst-free ring-opening of azlactones has been consistently reported in reactions.

1-3-4. Summary and Outlook

Taken together, these insights emphasize that while the use of highly nucleophilic species, such as hydrazines and amines, enables efficient, catalyst-free ring-opening of azlactones, this very reactivity imposes intrinsic limitations when DKR is pursued. In contrast to alcohols, thiols, or oximes, which display inherently low nucleophilicity and thus require catalytic or basic activation to engage in azlactone ring-opening, nitrogen-based nucleophiles often react too rapidly under mild conditions, bypassing the stereocontrolled pathways mediated by chiral catalysts. This duality has shaped the historical focus of DKR studies toward weaker nucleophiles, where the catalyst can exert meaningful control over the stereochemical outcome (Figure 5).

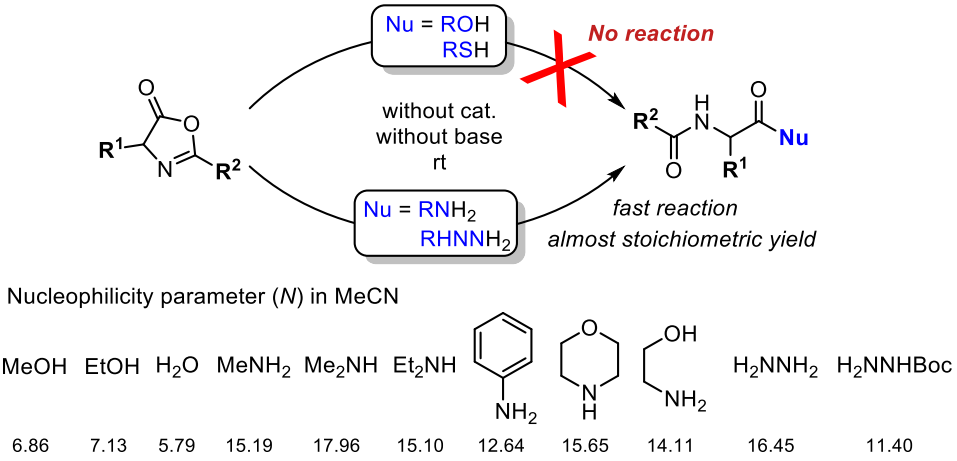

Figure 5. Comparison of nucleophilic reactivities in azlactone ring-opening. Strong nitrogen nucleophiles enable rapid, uncatalyzed azlactone ring-opening, unlike weaker nucleophiles requiring activation.

Notably, the only reported example of DKR with nitrogen nucleophiles—Feng Shi group's pioneering work employing aniline derivatives—achieved successful stereocontrol by deliberately attenuating the nucleophilicity of the amine through the introduction of bulky substituents and hydroxyl groups (see the section 1-2-4).[24] This strategic design allowed the CPA catalyst, (*R*)-TRIP, to govern the reaction pathway without interference from background, catalyst-free processes.

Therefore, to enable DKR of azlactones with nitrogen nucleophiles, it becomes essential not merely to lower the activation barrier through catalysis but to simultaneously suppress the innate reactivity of the nucleophile itself. In effect, this calls for the introduction of negative catalysis concepts—approaches that intentionally retard background reactivity—to achieve stereocontrol in systems where the nucleophile is otherwise too reactive for conventional catalytic modulation.

1-4. Negative Catalysis: Historical and Modern Perspectives

While catalysis is commonly defined as the acceleration of a chemical reaction through stabilization of the transition state or reduction of the activation energy, the concept of negative catalysis offers a counterpoint to this traditional understanding. In the context of this study, negative catalysis refers to the suppression of a reaction pathway through preferential stabilization of the ground state or selective destabilization of a competing transition state, thereby increasing the overall activation energy and diverting the reaction through a slower route (Figure 5).[52] Such an approach to negative catalysis has also been conceptualized in enzyme catalysis, where selective destabilization of competing transition states controls enzymatic selectivity and specificity.

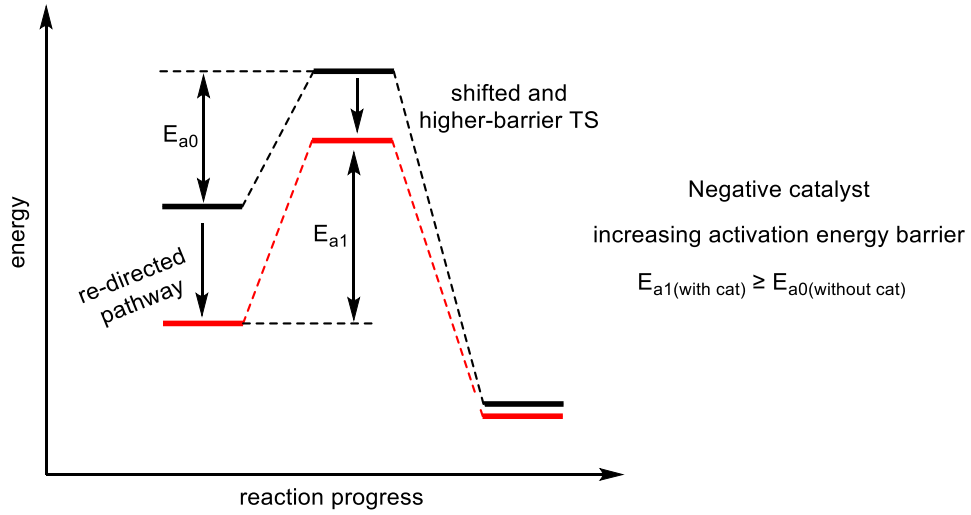

Figure 5. Conceptual illustration of negative catalysis as a strategy to suppress an undesired reaction pathway.

The uncatalyzed reaction (black) proceeds along a lower-energy pathway with activation energy E_{a0}. In contrast, the introduction of a negative catalyst redirects the system to an alternative route (red) characterized by a higher energy barrier ($E_{a1} \geq E_{a0}$), resulting in delayed transition state formation and overall rate suppression. Such a phenomenon is not merely inhibitory but represents a strategy for kinetic pathway control through selective remodeling of the reaction coordinate.

1-4-1. Early Controversies and Theoretical Instability (1920s–1970s)

The concept of negative catalysis — wherein the presence of an additive leads to suppression, rather than acceleration, of a chemical reaction — has long intrigued chemists. As early as 1923, Taylor systematically reviewed a diverse array of inhibitory phenomena, ranging from the hydrolysis of halogenated acids to the autoxidation of organic compounds, and emphasized the mechanistic ambiguity underlying these effects.[53] While some cases could be rationalized by competition for catalytic species or formation of inhibitory complexes, a unified theoretical framework was lacking. Shortly thereafter, Christiansen critically engaged with the Taylor's interpretations, highlighting the inadequacy of simple molecular complexation models and drawing attention to the then-nascent notion of chain reactions as a potential explanation for inhibitory

effects.[54] In 1927, this perspective gained experimental traction through Bäckström's pioneering studies, which demonstrated that both thermal and photochemical systems, such as the autooxidation of benzaldehyde, exhibit negative catalysis by virtue of chain-breaking mechanisms, wherein inhibitors disrupt the propagation of highly energetic intermediates.[55] Despite these early insights, the concept of negative catalysis continued to resist consensus. In 1950, Tamura offered a new mechanistic angle, showing that catalyst deactivation via polymeric byproducts and selective poisoning of surface-active sites could also manifest as reaction suppression, particularly in heterogeneous hydrogenation.[56]

However, the definitional ambiguity persisted well into the latter half of the 20th century. In 1968, Young group posed the question in *Journal of Chemical Education* of whether a negative catalyst is meaningfully distinct from an inhibitor, sparking renewed attention to the issue.[57] In 1969, the Singh group addressed this question by emphasizing the need to distinguish between thermodynamic and kinetic perspectives.[58] They questioned whether an increase in activation energy could still be considered catalysis. This debate revealed a clear division of opinions. Some researchers adopted a formalist view, defining catalysis simply as the provision of an alternative reaction pathway, regardless of whether it speeds up or slows down the reaction. Others preferred a phenomenological view, where only a measurable decrease in reaction rate would qualify as negative catalysis. This difference in definitions highlights the lack of agreement on the concept of negative catalysis and shows that its interpretation depends heavily on how catalysis itself is defined.

1-4-2. From Enzyme Selectivity to Reaction Channel Control (1990s)

In 1990, Rétey suggested that enzymes can achieve selectivity not only by accelerating desired reactions, but also by actively suppressing undesired ones through structural control and selective substrate binding.[59] This notion of "negative catalysis" emphasized how binding energy and conformational restriction could prevent side reactions, particularly in radical-mediated processes. While developed in the context of enzymatic systems, this concept hinted at broader strategies later explored in synthetic catalysis — where reaction selectivity can arise not solely from promoting a target pathway, but from *constraining* competing ones.

A notable demonstration of negative catalysis in small-molecule systems was provided by Breslow in his mechanistic investigation of RNA cleavage using imidazole buffers.[60] He showed that imidazole redirected a common intermediate away from an undesired rearrangement pathway and toward RNA cleavage. This redirection suppressed the side reaction without slowing the overall substrate consumption, illustrating how a catalyst can selectively inhibit one pathway while promoting another—a defining feature of negative catalysis.

1-4-3. Applications in Modern Asymmetric Catalysis

A notable milestone in the development of negative catalysis in non-enzymatic systems was reported by Jacobsen and co-workers in 2008, who demonstrated that selective suppression of undesired pathways could serve as a viable strategy for inducing enantioselectivity in strongly Brønsted acid–promoted reactions (Scheme 21).[61a] In their study on the Povarov reaction, a chiral urea catalyst was shown to form hydrogen

bonds with the iminium ion intermediate, attenuating its inherent reactivity and thereby suppressing non-selective background reactions. Importantly, this attenuation did not simply inhibit the overall process but instead channeled the reactivity through a more controlled and selective catalytic cycle, enabling high enantioselectivity. Although the term "negative catalysis" was consciously avoided throughout the paper, the core principle—selective deactivation rather than acceleration—clearly aligns with the modern interpretation of the concept.

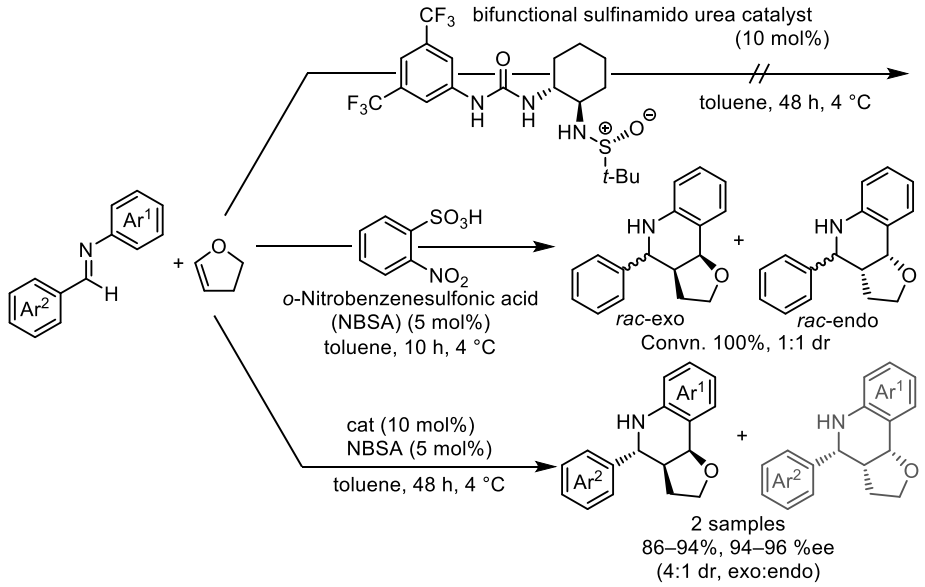

Scheme 21. Enantioselective Povarov reaction via chiral urea catalyst. A bifunctional urea catalyst enables exo-selective cycloaddition with high enantioselectivity by attenuating iminium ion reactivity.

This mechanistic strategy was further substantiated by computational studies, which revealed that the catalyst–substrate complex exhibited decreased electrophilicity due to stabilization of the intermediate through hydrogen bonding (Figure 6 & 7).[61] Rather than acting as a classical inhibitor that halts the reaction, the catalyst functioned to reshape the energetic landscape, disfavoring unproductive or racemic pathways while preserving access to the desired enantioselective outcome. As such, this work represents one of the earliest and clearest demonstrations of negative catalysis within a realistic organic synthesis context—extending the conceptual framework beyond enzymatic systems and into the domain of rational catalyst design.

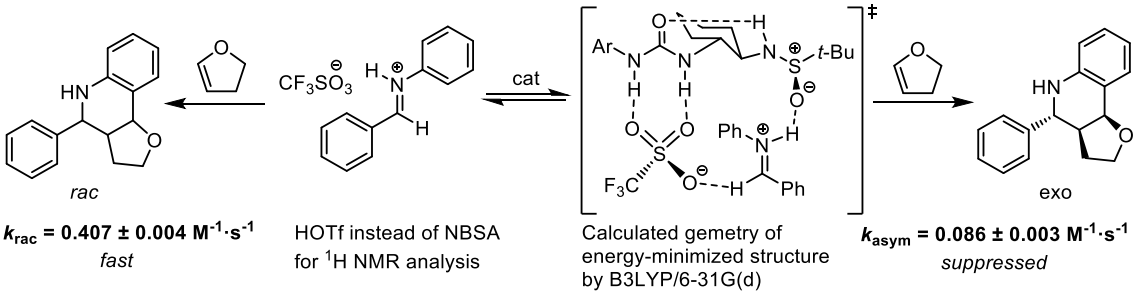

Figure 6. Suppression of racemic background pathway. The catalyst slows the background reaction and stabilizes a selective pathway, as supported by rate data and computed structure.

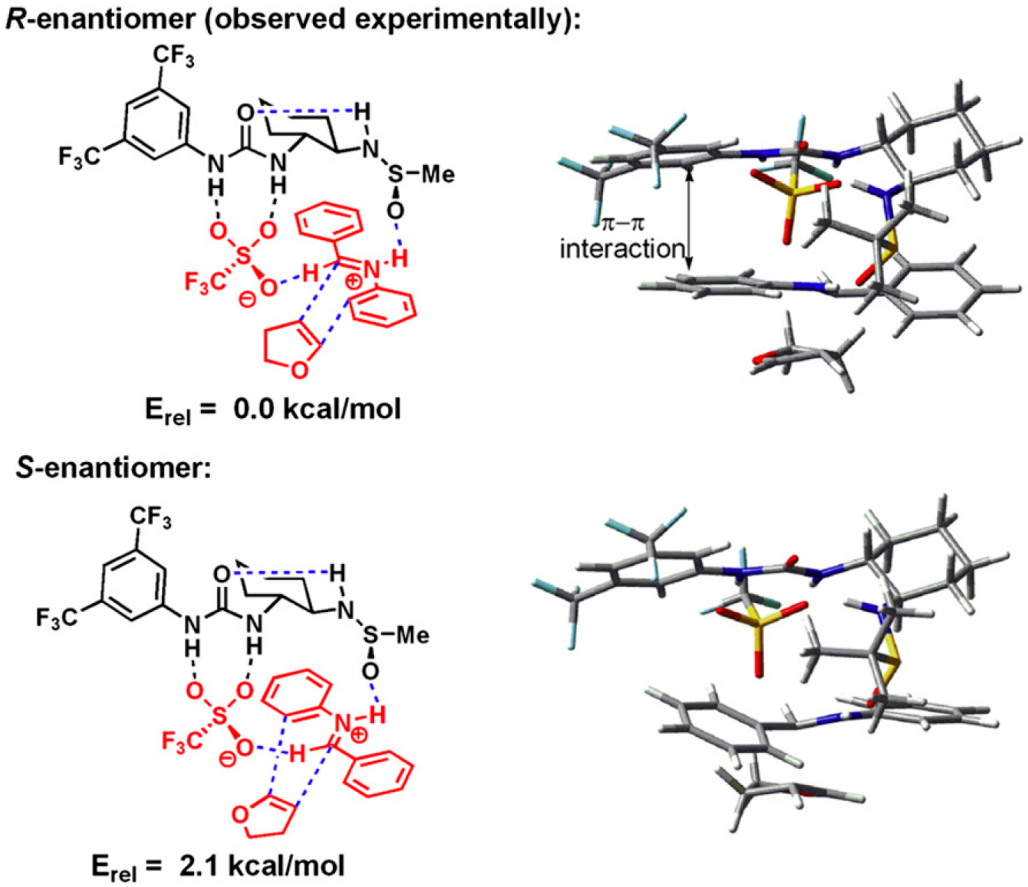

Figure 7. Computed transition states explaining enantioselectivity. The favored *R*-TS is stabilized by π–π and H-bonding, showing a 2.1 kcal/mol energy gap over the *S*-TS (Reproduced figures from ref 61b).

The other notable example of a negative catalysis-inspired strategy was reported by Denmark and co-workers in their investigation of the enantioselective sulfenocyclization of alkenes in 2014 (Scheme 22).[62] In this system, a Brønsted acid such as methanesulfonic acid was required for activation of the catalyst and generation of the sulfenylating agent. However, in the absence of the chiral catalyst, the reaction proceeded readily to give racemic product—a classic background reaction scenario. Interestingly, the researchers observed that the inclusion of components inherently present under catalytic conditions, such as the conjugate base of the acid (methanesulfonate) and phthalimide, led to a substantial suppression of this racemic background reaction. This suggested that these components act not as inert byproducts but as inhibitors under catalytic conditions.

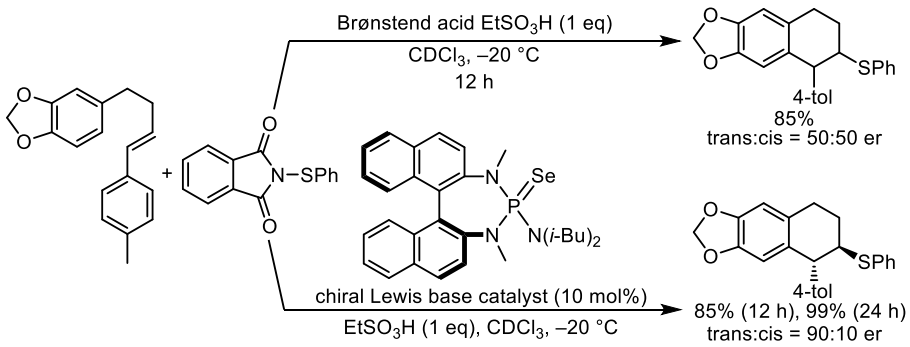

Scheme 22. Chiral Lewis base diverts racemic background in sulfenocyclization toward enantioselective pathway.

Mechanistically, the inhibition was attributed to a buffering effect arising from *homoconjugation* between the Brønsted acid and its conjugate base (Figure 8 & Scheme 23). In particular, the sulfonic acid and sulfonate ion formed *triple ion complexes*, effectively sequestering free acid molecules and thereby lowering the acidity of the medium. This reduction in proton activity suppressed the background protonation of the sulfenylating agent, thus minimizing uncatalyzed reactivity. Importantly, this suppressive effect was not observed when the reaction was simply conducted without the chiral catalyst, indicating that the true background reaction under catalytic conditions is far more attenuated than previously assumed. The result is a system where the catalytic pathway is selectively enhanced while the racemic background is actively inhibited—a defining feature of negative catalysis.

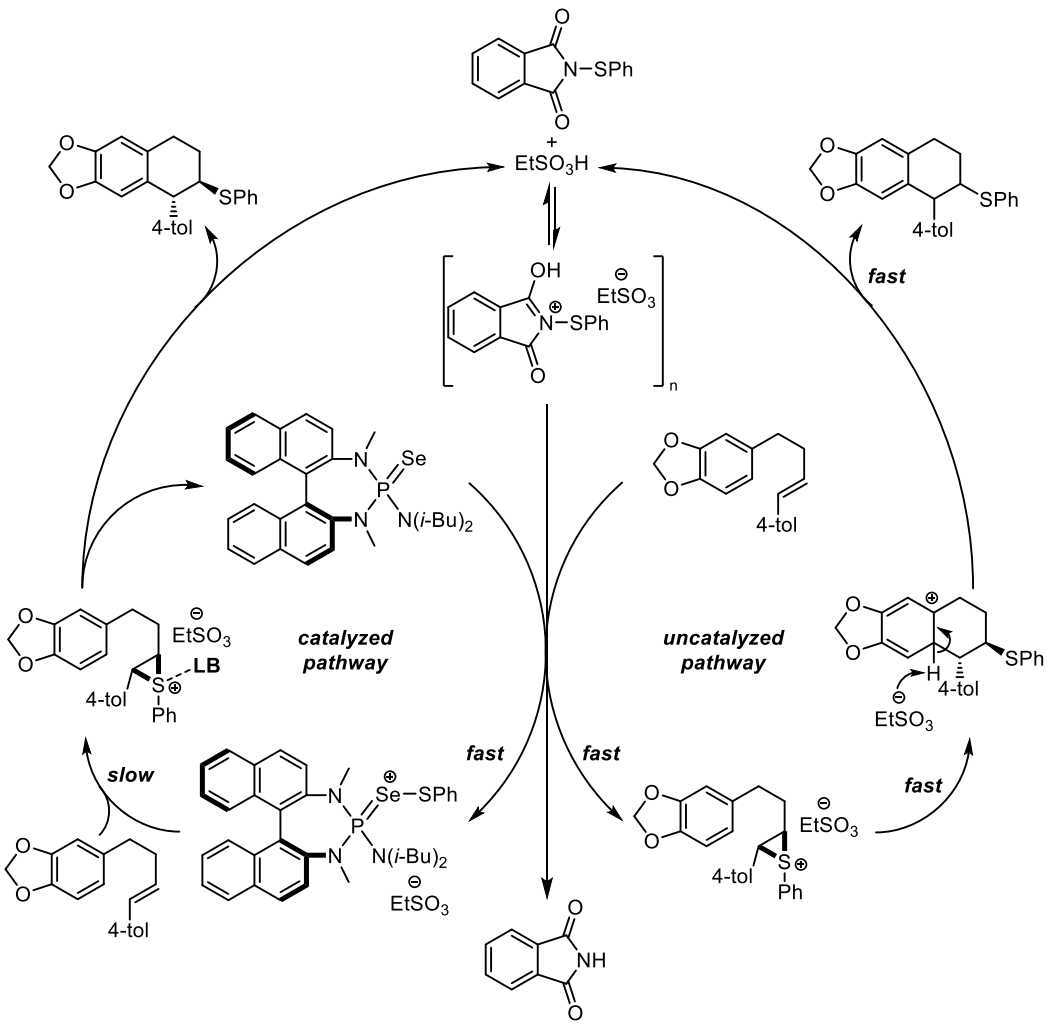

Figure 8. Proposed mechanism illustrating racemic background suppression in enantioselective sulfenocyclization.

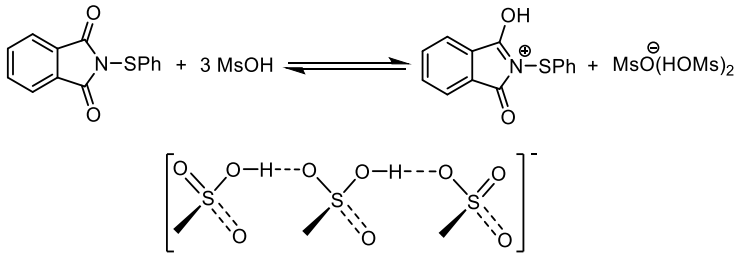

Scheme 23. Proposed mechanism for racemic background suppression via homoconjugation and triple ion complexation between sulfonic acid and sulfonate, which reduces acidity and inhibits non-selective sulfenylation — a representative case of negative catalysis.

1-4-4. Summary and Outlook

While the concept of negative catalysis has traditionally been discussed in the context of enzymatic selectivity or reaction suppression in small-molecule catalysis, its application to DKR of azlactones remains underexplored. In particular, nucleophilic ring-opening reactions involving nitrogen-based nucleophiles pose a unique challenge: unlike alcohols or thiols, nucleophiles such as hydrazine exhibit exceedingly high intrinsic reactivity (see the section 1-3-1), often leading to rapid, nonselective background reactions that outpace any meaningful catalyst-controlled discrimination.

To overcome this, a strategy grounded in *rate suppression rather than acceleration* becomes essential. Inspired by Jacobsen's approach in the Povarov reaction[61]—where selective stabilization of reactive intermediates by a chiral sulfinamidourea catalyst successfully attenuated background reactivity—it is envisioned that a similar network of noncovalent interactions could be leveraged to retard azlactone activation in the presence of strong nitrogen nucleophiles. Indeed, most successful examples of azlactone-based DKR, particularly in alcoholysis and thiolysis, have employed bifunctional organocatalysts bearing (thio)urea and cinchona alkaloid-derived frameworks, quinine-(thio)urea catalysts. These catalysts are known to engage the azlactone moiety through hydrogen bonding while simultaneously positioning the nucleophile in a stereochemically defined orientation. Such dual-site engagement is likely to be even more critical when applied to highly reactive nitrogen nucleophiles, as it may allow for modulation of the ground-state and transition-state energies in a way that selectively retards undesired pathways (Figure 9).

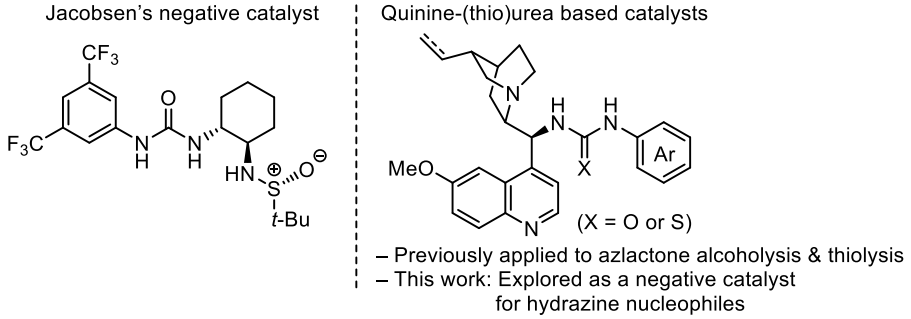

Figure 9. Representative bifunctional hydrogen bonding catalysts. Left: Jacobsen's urea catalyst designed to suppress background reaction in the Povarov reaction. Right: Quinine-derived (thio)urea catalyst widely used in azlactone alcoholysis and thiolysis reactions, explored herein for its potential as a negative catalyst.

1-5. Preferential Enrichment

In 1993, Tamura and co-workers serendipitously discovered a spontaneous enantiomeric enrichment phenomenon during the recrystallization of a racemic salt of suplatast tosylate, a chiral anti-allergic drug candidate (Figure 10).[63] This phenomenon, later termed preferential enrichment in 1998, was characterized by the recurring appearance of high ee in the solution phase after recrystallization, despite the absence of any external chiral influence. Over the following decades, Tamura's group conducted a comprehensive investigation into the mechanism of preferential enrichment, establishing that in certain racemic organic salts, a polymorphic transition between metastable and stable solid forms could trigger asymmetric redissolution of one enantiomer, leading to solution-phase enrichment. Based on these studies, preferential enrichment has been conceptualized as a nonequilibrium chiral symmetry-breaking event emerging during crystallization under high supersaturation conditions.

Since its discovery, preferential enrichment has been observed in a range of racemic compounds, including various amino acid salts and small chiral molecules, often under differing crystallization conditions. While the canonical mechanism proposed by Tamura involves a polymorphic transition and selective redissolution, not all cases adhere strictly to this model. In several reports, and occasionally in our own study, preferential enrichment has emerged unexpectedly during recrystallization trials, suggesting that the phenomenon may be more general than initially assumed. These findings underscore the value of investigating PE even in systems that lack clear polymorphic transitions or defined crystallization pathways.

In line with these observations, a spontaneous enantiomeric enrichment phenomenon was also incidentally observed during the recrystallization of an α-amino acid hydrazide derivative in this study. This unexpected behavior prompted further investigation, as described in the subsequent chapters.

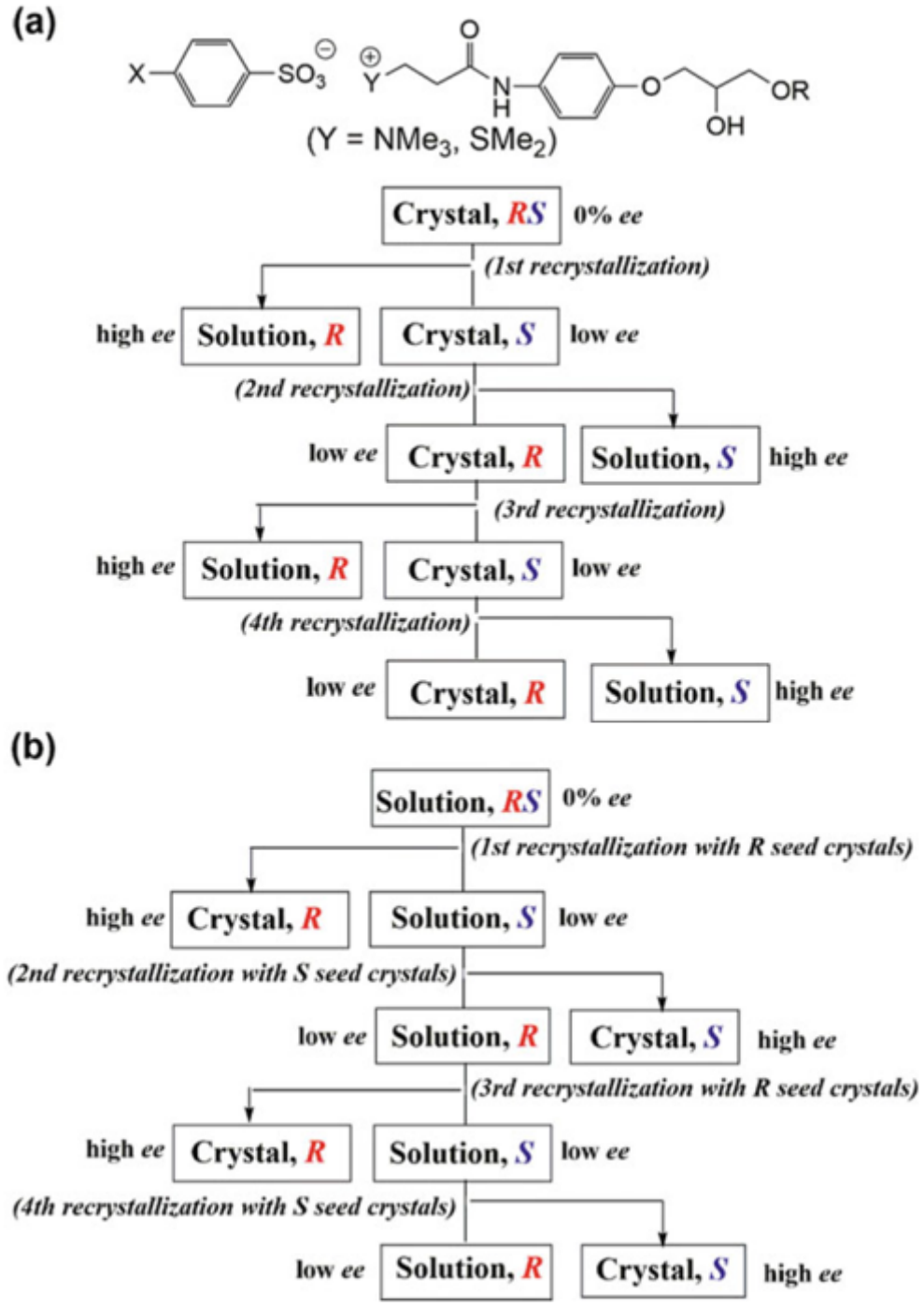

Figure 10. Schematic representation of preferential enrichment during repeated recrystallization of racemic organic salts. (a) Spontaneous solution-phase enantiomeric enrichment observed without any chiral bias. (b) Enhanced enantioselectivity induced by seeding with enantiopure crystals. (Reproduced figures from ref 63).

1-6. Research Objectives

In this study, a dynamic kinetic resolution (DKR) strategy was developed in which racemic azlactones were reacted with hydrazine nucleophiles to afford α-chiral amino acid hydrazides. Owing to the inherently high reactivity of hydrazines, rapid background reactions were encountered under uncatalyzed conditions, necessitating a mechanistic approach to suppress the undesired pathways. To address this challenge, a quinine-thiourea-based bifunctional organocatalyst was identified and employed as a negative catalyst, through which the nonselective background reaction was selectively inhibited (Figure 11).

To elucidate the underlying inhibition mechanism, the catalytic system was examined through kinetic studies and supported by computational analyses. The stereochemical outcome of the reaction was investigated by experimental comparison using a stereochemically defined congener, while the full catalytic pathway—including transition states and intermediates—was mapped using density functional theory (DFT) and noncovalent interaction analyses such as independent gradient model (IGM) calculations.

Additionally, a preferential enrichment phenomenon was observed in the recrystallization of selected hydrazide products. Although not central to the primary objectives, this behavior was characterized and discussed within the broader context of enantiomeric separation under crystallization conditions.

Through these investigations, the aim was to demonstrate that even highly reactive nucleophiles such as hydrazines can be subjected to catalytic stereocontrol via selective inhibition, and to provide deeper mechanistic insight into reaction pathway modulation by negative catalysis in asymmetric synthesis.

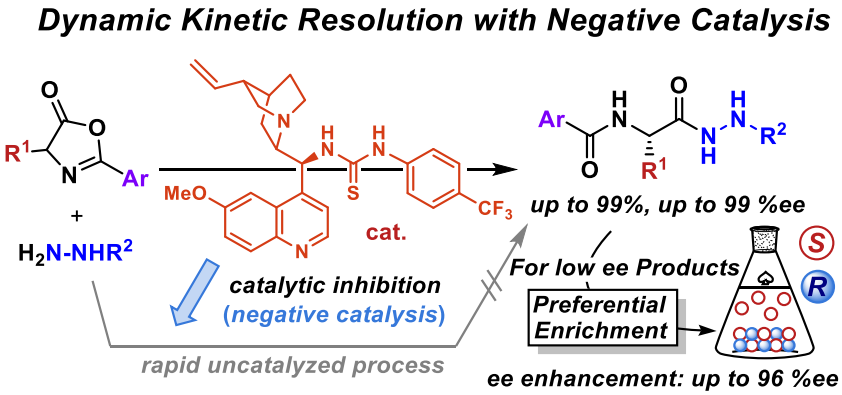

Figure 11. Overview of the DKR of azlactones with hydrazines under negative catalysis. The uncatalyzed background reaction proceeds rapidly due to the high reactivity of hydrazines. Catalytic inhibition by a bifunctional thiourea catalyst selectively suppresses this pathway, enabling enantioselective hydrazinolysis. Subsequent recrystallization of α-amino acid hydrazide products allows preferential enrichment, further enhancing enantiomeric purity.

1-7. References

[1] For selected reviews of amino acids, see: (a) Pecchini, P.; Fochi, M.; Bartoccini, F.; Piersanti, G.; Bernardi, L. *Chem. Sci.* **2024**, *15*, 5832–5868. (b) Zhang, Y.; Vanderghinste, J.; Wang, J.; Das, S. *Nat. Commun.* **2024**, *15*, 1474. (c) Hall, M. *RSC Chem. Biol.* **2021**, *2*, 958–989. (d) Narancic, T.; Almahboub, S. A.; O'Connor, K. E. *World J. Microbiol. Biotechnol.* **2019**, *35*, 67. (e) Xue, Y.-P.; Cao, C.-H.; Zheng, Y.-G. *Chem. Soc. Rev.* **2018**, *47*, 1516–1561. (f) Almhjell, P. J.; Boville, C. E.; Arnold, F. H. *Chem. Soc. Rev.* **2018**, *47*, 8980–8997. (g) Hönig, M.; Sondermann, P.; Turner, N. J.; Carreira, E. M. *Angew. Chem. Int. Ed.* **2017**, *56*, 8942–8973. (h) Hummel, W.; Gröger, H. Reductive Amination of Keto Acids. In *Enzyme Catalysis in Organic Synthesis*, 3rd ed.; Drauz, K.; Gröger, H.; May, O. Eds.; Wiley-VCH, Weinheim, **2012**, 1165–1203. (i) Zhu, D.; Hua, L. *Biotechnol. J.* **2009**, *4*, 1420–1431. (j) Bell, E. A.; Watson, A. A.; Nash, R. J. *Nat. Prod. Commun.* **2008**, *3*, 1, 93–110. (k) Leuchtenberger, W.; Huthmacher, K.; Drauz, K. *Appl. Microbiol. Biotechnol.* **2005**, *69*, 1–7.

[2] Hedges, J. B., Ryan, K. S**.** *Chemical Reviews* **2020**, *120*, 3161–3209.

[3] For selected reviews of azlactones, see: (a) Kushwaha, N., Kushwaha, S. *Biointerface Res. Appl. Chem.* **2022**, *12*, 6460–6486. (b) Wright, T. B.; Evans, P. A. *Chem. Rev.* **2021**, *121*, 9196–9242. (c) Jain, A., Rana, N. K. R. *Adv. Synth. Catal.* **2021**, *363*, 3879–3912. (d) Marra, I. F. S.; de Castro, P. P.; Amarante, G. W. *Eur. J. Org. Chem.* **2019**, 5830–5855. (e) de Castro, P. P., Batista, G. M. F., dos Santos, H. F., Amarante, G. W. *ACS Omega* **2018**, *3*, 3507–3512. (f) de Castro, P. P.; Carpanez, A. G.; Amarante, G. W. *Chem. Eur. J.* **2016**, *22*, 10294–10318.

[4] (a) Erlenmeyer, E. *Justus Liebigs Annalen der Chemie* **1893**, *275*, 1–8. (b) Plöchl, J. *Berichte der deutschen chemischen Gesellschaft* **1884**, *17*, 1616–1624.

[5] Sheehan, J. C.; Henery-Logan, K. R. *J. Am. Chem. Soc.* **1959**, *81*, 3089–3094.

[6] Goodman, M.; Levine, L. *J. Am. Chem. Soc.* **1964**, *86*, 2918–2922.

[7] de Jersey, J.; Zerner, B. *Biochemistry* **1969**, *8*, 5, 1967–1974.

[8] Slebioda, M.; St-Amand, M. A.; Chen, F. M. F.; Benoiton, N. L. *Can. J. Chem.* **1988**, *66*, 2540–2544.

[9] (a) Yamamoto, E.; Kobayashi, K.; Wakafuji, K.; Kamachi, T.; Tokunaga, M. *J. Org. Chem.* **2023**, *88*, 7748–7754. (b) Wakafuji, K.; Iwasa, S.; Ouchida, K. N.; Cho, H.; Dohi, H.; Yamamoto, E.; Kamachi, T.; Tokunaga, M. *ACS Catal.* **2021**, *11*, 14067–14075. (c) Yamamoto, E., Wakafuji, K., Furutachi, Y., Kobayashi, K., Kamachi, T., Tokunaga, M. *ACS Catalysis* **2018**, *8*, 5708–5713.

[10] (a) Liang, J.; Ruble, J. C.; Fu, G. C. *J. Org. Chem.* **1998**, *63*, 3154–3155. (b) Garrett, C. E.; Fu, G. C. *J. Am. Chem. Soc.* **1998**, *120*, 7479–7483.

[11] Berkessel, A.; Cleemann, F.; Mukherjee, S.; Müller, T. N.; Lex, J. *Angew. Chem. Int. Ed.* **2005**, *44*, 807–811.

[12] Berkessel, A.; Mukherjee, S.; Cleemann, F.; Müller, T. N.; Lex, J. *Chem. Commun.* **2005**, 1898–1900.

[13] Peschiulli, A.; Quigley, C.; Tallon, S.; Gun'ko, Y. K.; Connon, S. J. *J. Org. Chem.* **2008**, *73*, 6409–6412.

[14] Lee, J. W.; Ryu, T. H.; Oh, J. S.; Bae, H. Y.; Jang, H. B.; Song, C. E. *Chem. Commun.* **2009**, 7224–7226.

[15] Yang, X.; Lu, G.; Birman, V. B. *Org. Lett.* **2010**, *12*, 892–895.

[16] Lu, G.; Birman, V. B. *Org. Lett.* **2011**, *13*, 356–358.

[17] Quigley, C.; Rodríguez-Docampo, Z.; Connon, S. J. *Chem. Commun.* **2012**, *48*, 1443–1445.
[18] Metrano, A. J.; Miller, S. J. *J. Org. Chem.* **2014**, *79*, 1542–1554.
[19] Tallon, S.; Manoni, F.; Connon, S. J. *Angew. Chem. Int. Ed.* **2015**, *54*, 813–817.
[20] Mandai, H.; Hongo, K.; Fujiwara, T.; Fujii, K.; Mitsudo, K.; Suga, S. *Org. Lett.* **2018**, *20*, 4811–4814.
[21] (a) Kamachi, T.; Yoshizawa, K. *J. Chem. Inf. Model.* **2016**, *56*, 347−353. (b) Kamachi, T.; Yoshizawa, K. *Org. Lett.* **2014**, *16*, 472−475.
[22] Rodríguez-Docampo, Z.; Quigley, C.; Tallon, S.; Connon, S. J. *J. Org. Chem.* **2012**, *77*, 2407–2414.
[23] Palacio, C.; Connon, S. J. *Eur. J. Org. Chem.* **2013**, 5398–5413.
[24] Yu, K.; Liu, X.; Lin, X.; Lina, L.; Feng, X. *Chem. Commun.* **2015**, *51*, 14897–14900.
[25] Zhang, Y.-C.; Yang, Q.; Yang, X.; Zhu, Q.-N.; Shi, F. *Asian J. Org. Chem.* **2016**, *5*, 914–919.
[26] (a) Benoiton, N. L.; Kuroda, K.; Chen, F. M. F. *Int. J. Pept. Protein Res.* **1982**, *20*, 81–86. (b) Chen, F. M. F., Kuroda, K., Benoiton, N. L. *Synthesis* **1979**, *1979*, 230–232.
[27] (a) Zhou, L.; Shu, Z.-J.; Wang, Y.; Zhai, B.-S.; Wang, F.; Wei, G.-P.; Cui, S.-W.; Li, J.-G. CN 111196772 A, May 26, 2020. (b) Erdogan, B.; Filiatrault, T. D.; Kavanagh, M. A.; Krepski, L. R.; Gaddam, B. N. US 2011/0054115 A1, March 3, 2011. (c) Rasmussen, J. K.; Kipfke, C. A.; Hembre, R. A.; Wickert, P. D. WO 2010/117598 A2, October 14, 2010. (d) Lewandowski, K. M.; Fansler, D. D.; Wendland, M. S.; Heilmann, S. M.; Gaddam, B. N. U.S. Patent 6,762,257 B1, July 13, 2004.
[28] Barnes, D. K.; Campaigne, E.; Shriner, R. L. *J. Am. Chem. Soc.* **1948**, *70*, 1769–1772.
[29] Jones, M. W.; Richards, S.-J.; Haddleton, D. M.; Gibson, M. I. *Polym. Chem.* **2013**, *4*, 717–723.
[30] Ho, H. T.; Bénard, A.; Forcher, G.; Le Bohec, M.; Montembault, V.; Pascual, S.; Fontaine, L. *Org. Biomol. Chem.* **2018**, *16*, 7124–7128.
[31] Kumar, P.; Mukerjee, A. K. *Synthesis* **1979**, *1979*, 726–727.
[32] Pereira, A. A., de Castro, P. P., de Mello, A. C., Ferreira, B. R. V., Eberlin, M. N., Amarante, G. W. *Tetrahedron* **2014**, *70*, 3271–3275.
[33] (a) Mayr, H., Kempf, B., Ofial, A. R. *Acc. Chem. Res.* **2003**, *36*, 66–77. (b) Mayr, H., Patz, M. *Angew. Chem. Int. Ed. Engl.* **1994**, *33*, 938–957.
[34] Kumara, M. N., Nakahara, T., Kobayashi, S., Fujio, M., Mishima, M. *Bull. Chem. Soc. Jpn.* **2018**, *91*, 523–530.
[35] Minegishi, S., Kobayashi, S., Mayr, H. *J. Am. Chem. Soc.* **2004**, *126*, 5174–5181.
[36] Phan, T. B., Mayr, H. *Can. J. Chem.* **2005**, *83*, 1554–1560.
[37] Ammer, J., Nolte, C., Mayr, H. *J. Am. Chem. Soc.* **2012**, *134*, 13902–13911.
[38] Minegishi, S., Mayr, H. *J. Am. Chem. Soc.* **2003**, *125*, 286–295.
[39] Phan, T. B., Nolte, C., Kobayashi, S., Ofial, A. R., Mayr, H. *J. Am. Chem. Soc.* **2009**, *131*, 11392–11401.
[40] Mayer, R. J., Breugst, M., Hampel, N., Ofial, A. R., Mayr, H. *J. Org. Chem.* **2019**, *84*, 8837–8858.
[41] Maji, B., Duan, X.-H., Jüstel, P. M., Byrne, P. A., Ofial, A. R., Mayr, H. *Chem. Eur. J.* **2021**, *21*, 11367–11376.
[42] Jüstel, P. M., Pignot, C. D., Ofial, A. R. *J. Org. Chem.* **2021**, *86*, 5965–5972.
[43] Nigst, T. A., Antipova, A., Mayr, H. *J. Org. Chem.* **2012**, *77*, 8142–8155.

[44] Brotzel, F., Chu, Y. C., Mayr, H. *J. Org. Chem.* **2007**, *72*, 3679–3688.

[45] Kanzian, T., Nigst, T. A., Maier, A., Pichl, S., Mayr, H. *Eur. J. Org. Chem.* **2009**, 6379–6385.

[46] Ammer, J., Baidya, M., Kobayashi, S., Mayr, H. *J. Phys. Org. Chem.* **2010**, *23*, 1029–1035.

[47] An, F., Maji, B., Min, E., Ofial, A. R., Mayr, H. *J. Am. Chem. Soc.* **2020**, *142*, 1526–1547.

[48] Baidya, M., Kobayashi, S., Brotzel, F., Schmidhammer, U., Riedle, E., Mayr, H. *Angew. Chem. Int. Ed.* **2007**, *46*, 6176–6179.

[49] Follet, E., Zipse, H., Lakhdar, S., Ofial, A. R., Berionni, G. *Synthesis* **2017**, *49*, 3495–3504.

[50] Baidya, M., Horn, M., Zipse, H., Mayr, H. *J. Org. Chem.* **2009**, *74*, 7157–7164.

[51] Nigst, T. A., Ammer, J., Mayr, H. *Angew. Chem. Int. Ed.* **2012**, *51*, 1353–1356.

[52] Noor, E.; Flamholz, A. I.; Jayaraman, V.; Ross, B. L.; Cohen, Y.; Patrick, W. M.; Gruic-Sovulj, I.; Tawfik, D. S. *Protein Sci.* **2022**, *31*, e4381.

[53] Taylor, H. S. *J. Phys. Chem.* **1923**, *27*, 322–341.

[54] Christiansen, J. A. *J. Phys. Chem.* **1924**, *28*, 2, 145–148.

[55] Bäckström, H. L. J. *J. Am. Chem. Soc.* **1927**, *49*, 1460–1472.

[56] Tamaru, K. *Bull. Chem. Soc. Jpn.* **1950**, *23*, 180–184.

[57] Young, J. A., Malik, J. G. *J. Chem. Educ.* **1968**, *45*, 477–479.

[58] Singh, H.; Mittal, K. L. *J. Chem. Edu.* **1969**, *46*, 3, 185–186.

[59] Rétey, J. *Angew. Chem. Int. Ed.* **1990**, *29*, 355–361.

[60] Breslow, R. *Acc. Chem. Res.* **1991**, *24*, 11, 317–324.

[61] (a) Xu, H.; Zuend, S. J.; Woll, M. G.; Tao, Y.; Jacobsen, E. N. *Science* **2010**, *327*, 986–990. (b) Knowles, R. R.; Jacobsen, E. N. *Proc. Natl. Acad. Sci. U.S.A.* **2010**, *107*, 20678−20685.

[62] Denmark, S. E.; Chi, H. M. *J. Am. Chem. Soc.* **2014**, *136*, 3655–3663.

[63] Tamura, R.; Takahashi, H.; Coquerel, G. Twenty-Five Years' History, Mechanism, and Generality of Preferential Enrichment as a Complexity Phenomenon. In *Advances in Organic Crystal Chemistry*; Sakamoto, M.; Uekusa, H., Eds.; Springer: Singapore **2020**, 405–432.

2. Results and Discussion

2-1. Optimization of the Reaction and the Scope of Catalysts

To establish optimal conditions for enantioselective dynamic kinetic resolution (DKR), the electron-deficient azlactone **2a** bearing a trifluoromethyl substituent was selected as a model substrate and reacted with Boc-hydrazine using quinine-derived thiourea catalyst **1a** (Table 1). Initially, without any catalyst, the product **3a** was obtained in high yield (81%) in 12 reaction hours, confirming that the uncatalyzed background reaction proceeds rapidly under these conditions (entry 1). When 10 mol% of catalyst **1a** was employed, the product yield decreased to 53%, but a high level of enantioselectivity was achieved (83 %ee, entry 2). Prolonging the reaction time to 24 hours led to an improved yield of 83%, with 84 %ee (entry 3). However, when 10 mol% of *t*-butanol was introduced as an additive under otherwise identical conditions (entry 4), the yield dropped sharply to 45%, while the enantioselectivity remained unchanged. This suggests that the presence of an external proton donor may disrupt key interactions essential for efficient turnover. Extending the reaction time further to 40 hours (entry 5) restored the yield to 94%, again with no loss in enantioselectivity. These data suggest that catalyst **1a** plays a dual role by inducing chirality while also impeding the nonselective background pathway, consistent with the concept of enantioselective negative catalysis. Reducing the catalyst loading to 5 mol% caused a sharp decline in selectivity (entry 6: 91% yield, 4 %ee), highlighting the importance of sufficient catalyst concentration to suppress the inherent reactivity of hydrazine. Screening of solvents showed that nonpolar environments, particularly toluene, support both reactivity and selectivity, while polar solvents such as DCM and acetonitrile reduced both metrics (entries 7–11).

Table 1. Optimization of the reaction conditions

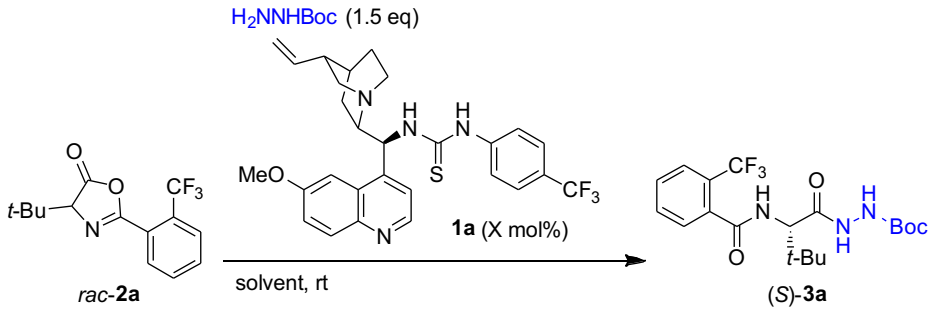

Entry	cat (X mol%)	solvent	additive	time (h)	Yield (%)[b]	ee (%ee)[c]
1	–	toluene	-	12	81	0
2	10	toluene	-	12	53	83
3	10	toluene	-	24	83	84
4	10	toluene	*t*-BuOH (10 mol%)	24	45	84
5	10	toluene	-	40	94	84
6	5	toluene	-	40	91	4
7	10	$CHCl_3$	-	40	56	72
8	10	THF	-	40	45	58
9	10	MeCN	-	40	22	38
10	10	DCM	-	40	66	74
11	10	Et_2O	-	40	58	82

[a]**2a** (0.1 mmol), Boc-hydrazine (1.5 equiv) and **1a** (10 mol%), in 1 mL of the solvent at rt (21–27 °C) under a N_2 atmosphere. [b]Isolated yield. [c]The ee was measured by HPLC.

Based on the Table 1 conditions, a series of catalyst screening experiments were conducted (Table 2). All catalysts were synthesized according to methods reported in the literature. The benchmark catalyst **1a** afforded the product in 94% yield with 84 %ee. Variants bearing electron-withdrawing substituents on the aryl group were then evaluated (**1b**, **1c**, and **1d**). Catalyst **1b** gave results comparable to **1a** (92%, 82 %ee), while **1c** showed a slight improvement in enantioselectivity (86 %ee), although the yield decreased to 76%. In the case of nitro-substituted **1d**, both yield and enantioselectivity declined to 78% and 72 %ee. A relatively electronically neutral aryl group in **1e** gave 76% yield and 81 %ee. Catalysts **1f**, **1g**, and **1h**, which possess electron-donating substituents at the *para*-position of the aryl group, exhibited slightly lower yields than the aforementioned catalysts, but comparable levels of enantioselectivity were observed (**1f**: 69%, 80 %ee; **1g**: 69%, 88 %ee; **1h**: 62%, 84 %ee). In catalyst **1i**, the aryl group was replaced with a 1-naphthyl moiety, resulting in a dramatic decrease in both reactivity and selectivity (34%, 60 %ee). In catalyst **1j**, the methoxy group on the quinoline ring was removed; in comparison with **1b**, a slight increase in yield was observed (94%, 82 %ee). Catalyst **1k**, which featured a squaramide moiety in place of the thiourea unit as reported by the Song group, showed a clear decrease in both yield and enantioselectivity relative to **1b** (56%, 68 %ee). Lastly, (*R*)-TRIP, a CPA catalyst previously employed by the Shi group for the DKR of azlactones with aniline nucleophiles, was tested.[1] Although it delivered the product in 99% yield within 20 hours, no

enantioselectivity was observed. Based on the data from Tables 1 and 2, catalyst **1a**, toluene (1 mL), and a reaction time of 40 hours at room temperature were selected as the optimal conditions for further studies.

Table 2. The catalyst scope of the reaction conditions[a]

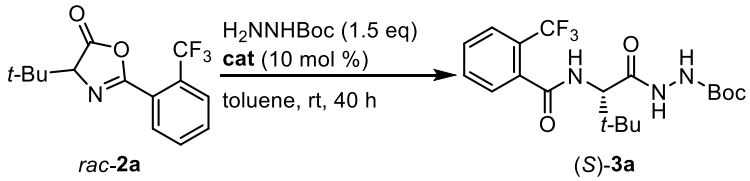

rac-**2a** (*S*)-**3a**

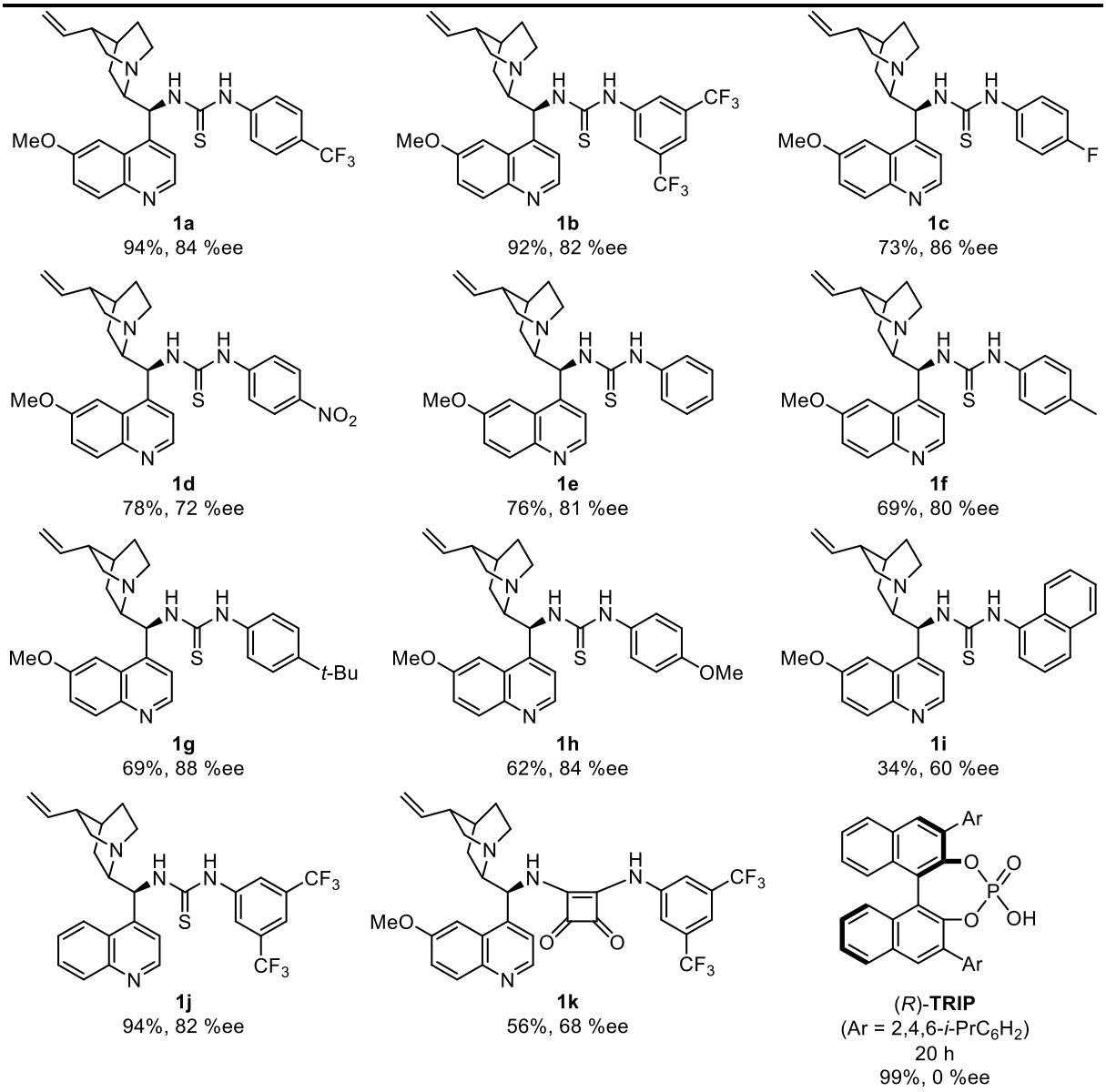

1a 94%, 84 %ee

1b 92%, 82 %ee

1c 73%, 86 %ee

1d 78%, 72 %ee

1e 76%, 81 %ee

1f 69%, 80 %ee

1g 69%, 88 %ee

1h 62%, 84 %ee

1i 34%, 60 %ee

1j 94%, 82 %ee

1k 56%, 68 %ee

(*R*)-**TRIP** (Ar = 2,4,6-*i*-PrC_6H_2) 20 h 99%, 0 %ee

[a]**2a** (0.1 mmol), Boc-hydrazine (1.5 equiv) and **1** (10 mol%), in 1 mL of toluene at rt (21–27 °C) under a N_2 atmosphere. Isolated yield. The ee was measured by HPLC.

2-2. Substrate Scope and Application

With the optimized reaction condition was established, a series of azlactone derivatives were evaluated to explore the substrate scope of the asymmetric ring-opening process (Table 3). In order to examine how trifluoromethyl substituents on the aryl ring influence stereoselectivity, azlactones **2b** to **2d**, each bearing CF_3 groups at distinct positions, were subjected to the standard conditions. When the CF_3 group was positioned at the *meta* or *para* site, a gradual reduction in enantioselectivity was observed (**3b**: 84%, 74 %ee; **3c**: 73%, 52 %ee). Furthermore, azlactone **2d**, featuring two CF_3 groups at the *meta* positions, also exhibited diminished selectivity compared to the unsubstituted variant (**3d**: 87%, 65 %ee). These findings collectively indicate that both the position and number of electron-withdrawing groups on the aromatic ring significantly influence the chiral induction during the reaction. In the case of azlactone **2e**, which contains a non-substituted phenyl moiety with no significant electronic perturbation, the product **3e** was obtained in moderate yield (60%) while maintaining a relatively high 80 %ee. Substrates **2f** and **2g**, which contain electron-donating groups on the aromatic ring, yielded the corresponding hydrazides **3f** and **3g** in lower chemical yields (48% and 45%, respectively), but the enantioselectivity remained in a comparable range to that of electron-deficient systems (76 %ee and 75 %ee, respectively). In addition, azlactone **2h**, bearing an *iso*-propyl tetrachlorobenzoate group that serves as a removable protecting group on the nitrogen atom, gave product **3h** in high yield and excellent selectivity (89%, 92 %ee).

Table 3. Substrate scope with variation of the azlactone aryl moiety[a]

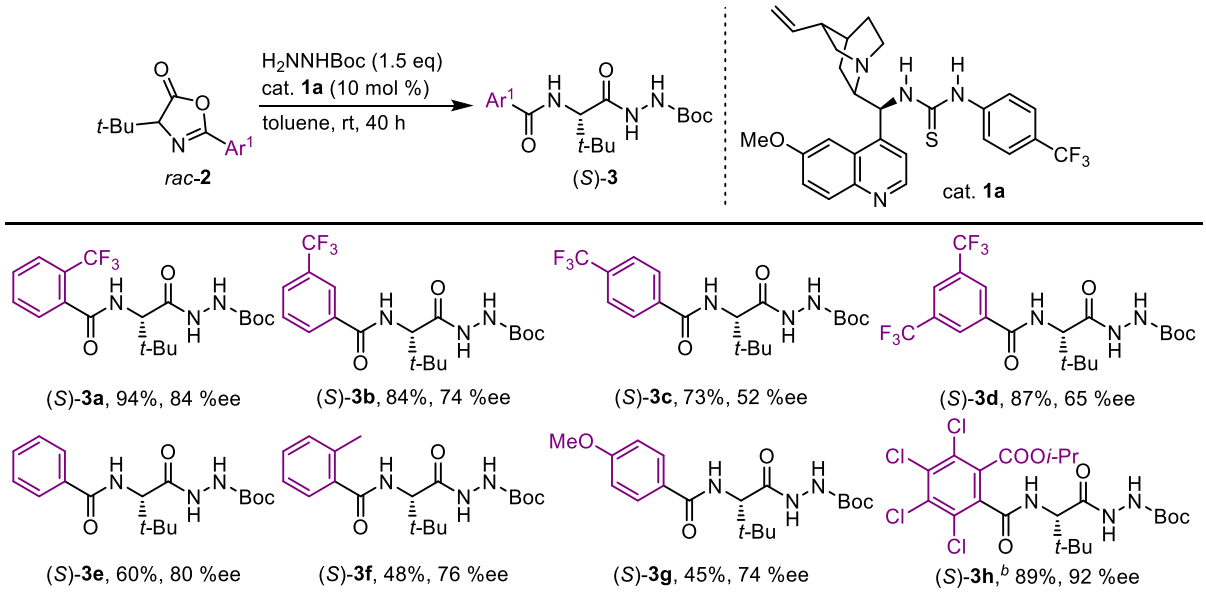

[a]**2** (0.1 mmol), Boc-hydrazine (1.5 equiv) and **1a** (10 mol%), in 1 mL of toluene at rt (21–27 °C) under a N_2 atmosphere. Isolated yield. The ee was measured by HPLC. [b]0.3 mmol scale, 41 h.

Modification of the α-substituent in the azlactone **2** led to notable changes in stereoselectivity (Table 4). When the substituent was ethyl (**2i**), the reaction afforded a high yield of 90% but with only moderate enantioselectivity (58 %ee). Replacing this with a benzyl group (**2j**) maintained excellent yield (99%) but

led to a further decrease in stereoselectivity (44 %ee). In contrast, introducing more sterically demanding groups, such as *iso*-propyl (**2k**) or 3-pentyl moieties (**2l**), resulted in better stereoselective control, reaching up to 70 %ee. Further increase in steric bulk using a trityl group (**2m**) provided a notable enhancement in enantioselectivity (88 %ee), although with a moderate yield (74%).

Table 4. Substrate scope with variation of the α-substituent of azlactone[a]

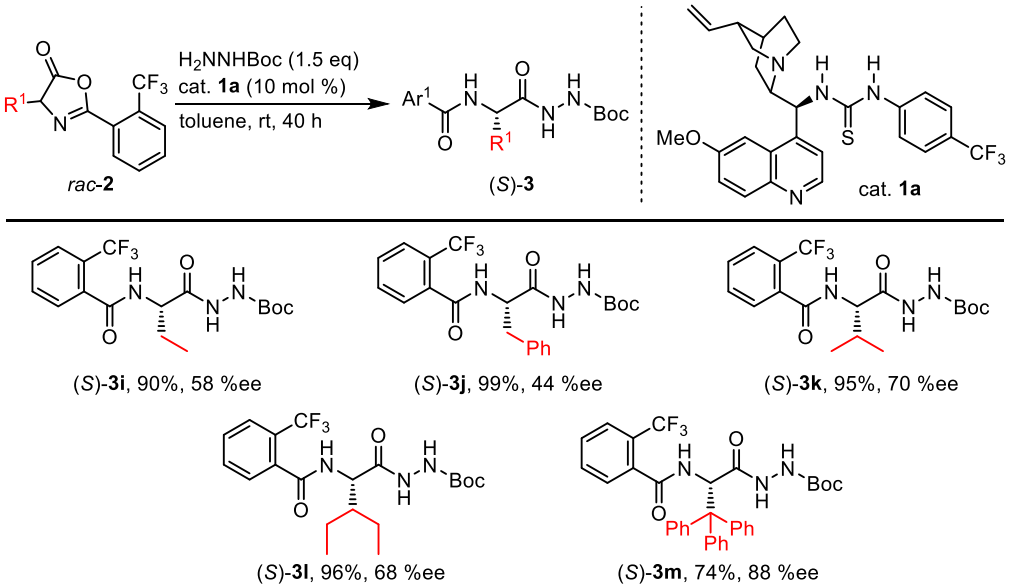

[a]**2** (0.1 mmol), Boc-hydrazine (1.5 equiv) and **1a** (10 mol%), in 1 mL of toluene at rt (21–27 °C) under a N_2 atmosphere. Isolated yield. The ee was measured by HPLC.

Further investigation focused on the influence of various hydrazine derivatives on the reaction outcome, while keeping azlactone **2a** as the fixed substrate (Table 5). Using simple hydrazine as the nucleophile resulted in high conversion, yet the enantioselectivity remained poor (**3n**: 97%, 16 %ee). Use of a Troc-protected hydrazine (Troc = 2,2,2-trichloroethoxycarbonyl) instead of Boc significantly reduced the reactivity, affording product **3o** in 21% yield with 70 %ee. Among arylhydrazines substituted at the *para* position, the unsubstituted phenylhydrazine afforded **3p** in moderate yield with excellent enantioselectivity (62%, >99 %ee) and extension of the reaction time to 71 hours led to the formation of the desired product in 81% yield, while maintaining an excellent >99 %ee. In contrast, electron-rich *para*-methoxyphenyl (PMP) substituted hydrazine led to **3q** in lower yield and moderate enantioselectivity (42%, 71 %ee). The *para*-trifluoromethyl analogue, bearing an electron-withdrawing group, delivered **3r** with even more diminished performance (39%, 29 %ee). These observations indicate a clear dependence of both conversion and stereocontrol on the electronic nature of the aryl ring in arylhydrazines. Benzoyl-substituted hydrazines bearing *para*-aryl groups were next evaluated (**3s**–**3u**). The phenyl-substituted one (**3s**) gave 71% outcome of and 80 %ee. The methoxy-derivative (**3t**), possessing an electron-donating group, offered a significant improvement in yield without altering the ee (97%, 80 %ee). In contrast, the CF_3-containing compound (**3u**) exhibited both slightly diminished yield and reduced enantioselectivity (69%, 70 %ee), highlighting the

sensitivity of the system to electronic effects even within this benzoyl-type scaffold. Carbazate-type hydrazines, bearing various alkyl groups, were also subjected to this reaction. The methyl-substituted carbazate gave **3v** with 81% and 74 %ee, while increasing the steric bulk to ethyl or benzyl groups led to a gradual decline in both yield and enantioselectivity (**3w**: 54%, 68 %ee; **3x**: 75%, 56 %ee). This trend suggests that steric hindrance near the hydrazine nitrogen adversely affects both reactivity and selectivity. Lastly, introducing a methyl group on the free NH of the hydrazine led to decreased stereocontrol and conversion (**3y**: 53%, 18 %ee), indicating that a free NH group may be essential for maintaining strong catalyst–nucleophile interaction and achieving high enantiocontrol.

Table 5. Hydrazine reagents scope[a]

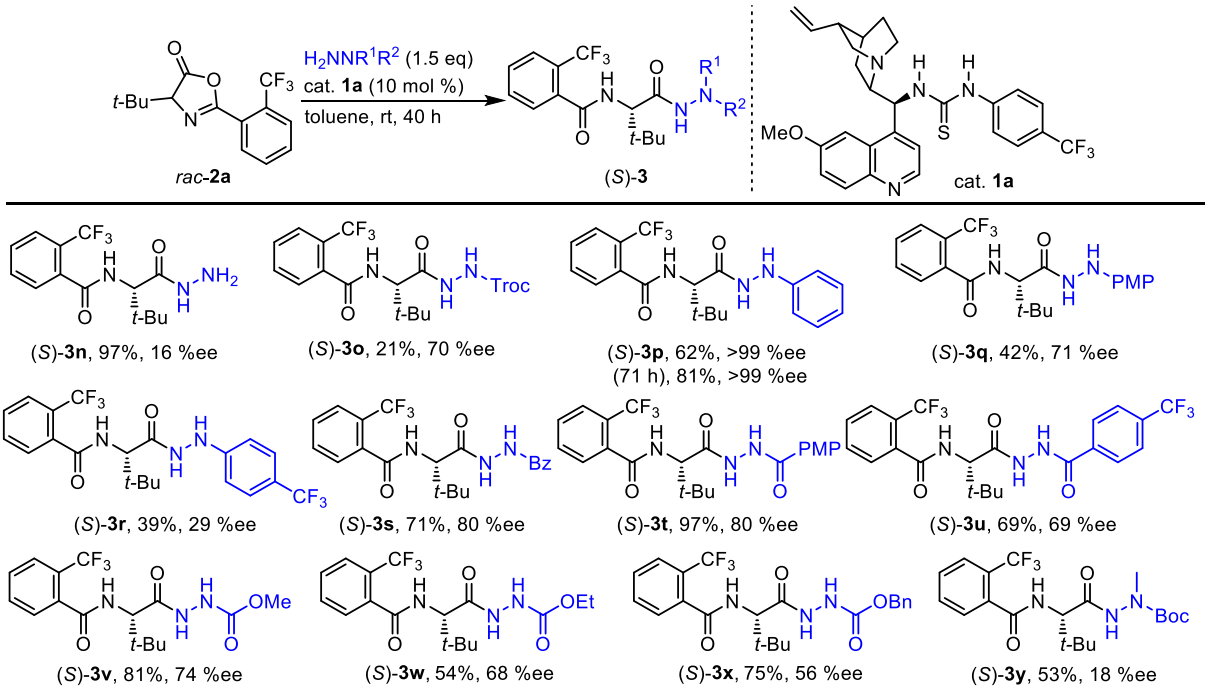

[a]**2a** (0.1 mmol), hydrazine reagent (1.5 equiv) and **1a** (10 mol%), in 1 mL of toluene at rt (21–27 °C) under a N_2 atmosphere. Isolated yield. The ee was measured by HPLC.

To evaluate the broader applicability of the developed methodology, the reaction of a phenylglycine-derived azlactone **2z** was also examined (Table 6). However, this substrate was found to undergo extremely rapid hydrolysis, even during routine handling such as chromatography and solvent removal. As a result, consistent selectivity could not be achieved, and reproducibility issues were encountered across independent runs (1st run, 58%, 40 %ee; 2nd run, 52%, 32 %ee). Despite the reaction being carried out without delay, the instability of the azlactone **2z** precluded reliable assessment of catalytic performance.

Table 6. Substrate scope: Phenylglycine-derived azlactone.[a]

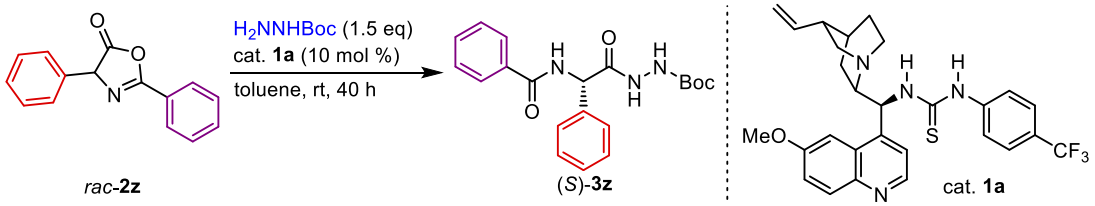

Run	Yield (%)[b]	ee (%ee)[c]
1	58	40
2	52	32

[a]**2z** (0.1 mmol), Boc-hydrazine (1.5 equiv) and **1a** (10 mol%), in 1 mL of toluene at rt (21–27 °C) under a N_2 atmosphere. [b]Isolated yield. [c]The ee was measured by HPLC.

To probe the scope of nitrogen nucleophiles beyond hydrazine, two representative nucleophiles with n values in the range of 14–16 were tested under the standard conditions using catalyst **1f**: morpholine and 2-amino-2-methyl-1-prpanol (Table 7). Unfortunately, enantioselectivity was not observed in either case. The reaction with morpholine proceeded efficiently to completion, yielding the product **4** in 98% yield, but without enantiomeric enrichment. In contrast, when the amino alcohol was employed, the reaction was significantly suppressed to generate **5** in 22%, likely due to intramolecular hydrogen bonding of amino alcohol itself interfering with nucleophilic attack.

Table 7. Evaluation of alternative nitrogen nucleophiles.[a]

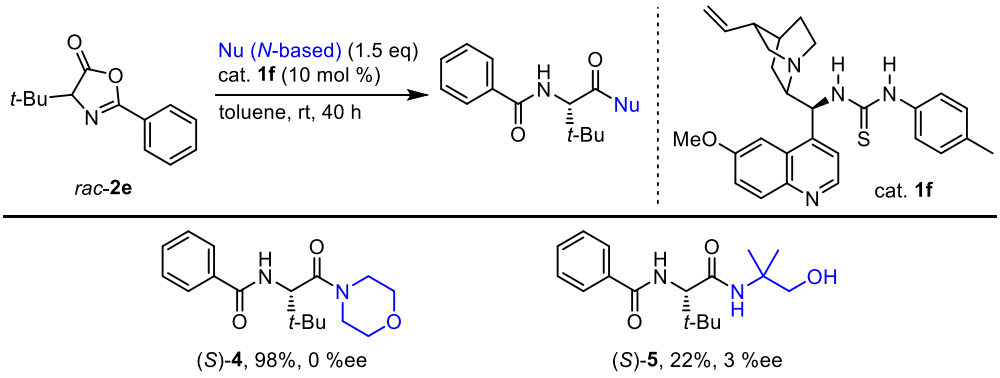

[a]**2e** (0.1 mmol), *N*-based nucleophile reagent (1.5 equiv) and **1f** (10 mol%), in 1 mL of toluene at rt (21–27 °C) under a N_2 atmosphere. Isolated yield. The ee was measured by HPLC.

The absolute configuration was confirmed by preparing (*S*)-**3e** from commercially available (*S*)-**S2e** under peptide coupling conditions with EDC/HOBt-mediated formations (Scheme 1). The identical optical rotation and spectroscopic data confirmed that the reaction system selectively affords the *S*-enantiomer.

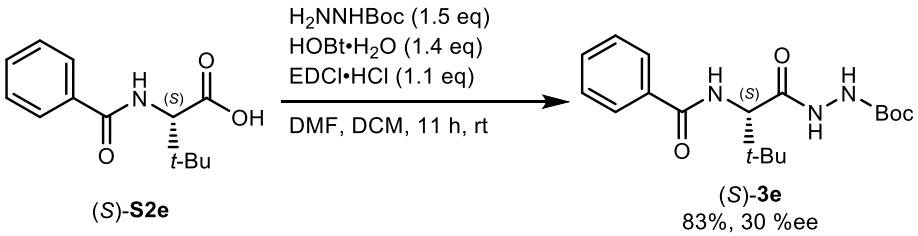

Scheme 1. Determination of absolute configuration by derivatization of (*S*)-**S2e**.

2-3. Investigation of Preferential Enrichment

2-3-1. Observation of Preferential Enrichment Phenomenon

At the early stage of this study, attempts were made to enhance the enantiomeric purity of the synthesized *α*-chiral amino acid hydrazide **3** by performing recrystallization. Unexpectedly, rather than simply increasing the enantiopurity of the isolated solids, a phenomenon known as *preferential enrichment* was observed (Table 8).[2] In this process, crystallization proceeded in a manner that favored the precipitation of a racemic solid phase, while the enantiomerically enriched component remained preferentially in the liquid phase. This behavior has been rarely reported and is atypical for most resolution processes.

Table 8. The preferential enrichment phenomenon of the *α*-chiral amino acid hydrazides **3**[a]

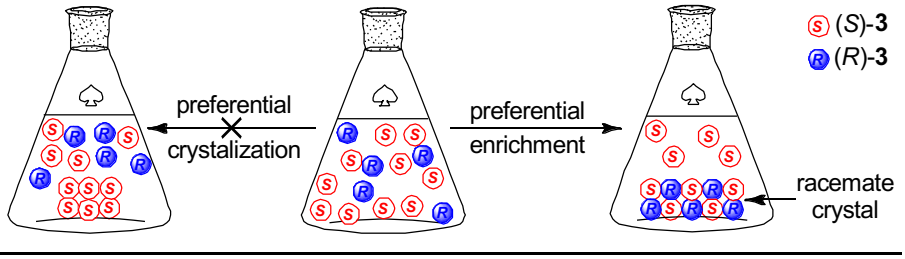

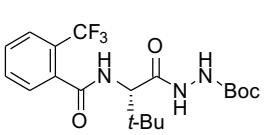

(*S*)-**3a**[b] from 84 %ee
liquid: 87%, 96 %ee (*S*)
solid: 13%, 9 %ee (*S*)

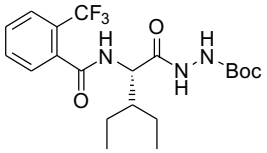

(*S*)-**3l**[c] from 68 %ee
liquid: 70%, 96 %ee (*S*)
solid: 30%, 6 %ee (*S*)

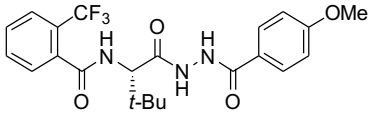

(*S*)-**3t**[c] from 80 %ee
liquid: 84%, 90 %ee (*S*)
solid: 16%, 34 %ee (*S*)

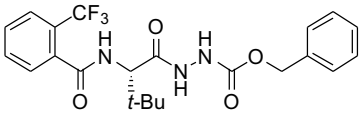

(*S*)-**3x**[c] from 56 %ee
liquid: 44%, 96 %ee (*S*)
solid: 56%, 50 %ee (*S*)

[a]Using product **3** from the substrate scope section. [b]Method A. [c]Method B.

Throughout the process of optimizing reaction conditions and exploring substrate scope, careful experimental procedures were implemented to avoid artificial elevation of enantiomeric ratios caused by this phenomenon. Special attention was given to the stages of work-up and sample preparation for HPLC analysis, ensuring that the recorded values accurately reflected the intrinsic enantioselectivity of the reactions rather than post-reaction enrichment artifacts.

To systematically examine the reproducibility and general applicability of the preferential enrichment phenomenon among the synthesized hydrazide products, two crystallization protocols were tested. **Method A** involved dissolving compound **3** in a mixed solvent of diethyl ether (10 mL) and hexane (5 mL), followed by crystallization at ambient temperature for 24 hours. In contrast, **Method B** consisted of dissolving **3** in a

small amount of EtOAc (1 mL) and hexane (0.05 mL), followed by heating to 70 °C to ensure complete dissolution, and then slowly cooling to –30 °C over 6 days to induce crystallization.

Both methods consistently led to the occurrence of preferential enrichment, not only for model compound **3a**, but also for structurally diverse substrates such as **3l**, **3s**, **3u**, and **3w**. Notably, during recrystallization, a significant drop in enantiomeric ratio was observed in the recovered solid, whereas the mother liquor was found to contain substantially enantioenriched material. For compound **3a**, which initially exhibited an enantiomeric excess of 84 %ee, recrystallization led to a clear separation: the supernatant was enriched to 96 %ee, while the recovered solid consisted of nearly racemic crystals (13% of the total, 9 %ee). In the case of **3l**, the enantiomeric excess improved from an initial 68 %ee to 96 %ee in the liquid phase after recrystallization. The remaining solid, comprising 30% of the total mass, showed 6 %ee consistent with racemate formation. For **3s**, which had an initial ee of 80%, recrystallization resulted in the liquid retaining 90 %ee, while the solid fraction (16%) showed diminished enantioenrichment (34 %ee), again indicating preferential enrichment phenomenon. Compound **3u** began with 74 %ee and underwent a similar transformation, with the mother liquor reaching 96 %ee. The solid phase, accounting for 26% of the total, exhibited a notably lower ee of 12%. In the case of **3w**, which initially displayed the lowest enantiomeric excess of 56%, the liquid fraction was successfully enriched to 96 %ee, while the solid, making up 56% of the total, retained a reduced ee of 50%. To the best of our knowledge, such behavior has not previously been documented for α-chiral amino acid hydrazide derivatives, suggesting that this class of compounds may represent a novel molecular system capable of undergoing preferential enrichment.

2-3-2. Crystal Structure Prediction (CSP) by CONFLEX via PXRD Analysis

The prediction of racemic and chiral crystal structures for **3a** was performed using the CONFLEX program,[3] primarily following three steps: generation of trial crystal structures, optimization of each trial structure, and selection of predicted structures based on energy comparison.[4] First, stable conformers of the (*S*)-**3a** in the gas phase were searched using the MMFF94 molecular force field.[5] The obtained stable *S*-conformer was used as the asymmetric unit (*Z*'=1). The molecule was systematically rotated around the x, y, and z axes to generate various initial orientations. Using this oriented *S*-enantiomer molecule as the asymmetric unit, trial crystal structures were generated by assuming specific space groups. For racemic crystal prediction, the space groups P-1, P21/c, Cc, C2/c, Pna21, Pbca, and Pnma were assumed. In the centrosymmetric space groups (P-1, P21/c, C2/c, Pbca, Pnma), the (*R*)-**3a** is generated from the (*S*)-**3a** in the asymmetric unit by the inversion symmetry operation, while in the non-centrosymmetric space groups (Cc, Pna21), the (*R*)-**3a** is generated by glide plane operations. For chiral crystal prediction, the chiral space groups P1, P2, $P2_1$, C2, P222, $P222_1$, $P2_12_12$, $P2_12_12_1$, $C222_1$, C222, F222, I222, and $I2_12_12_1$ were assumed.

Each generated trial crystal structure was subjected to crystal structure optimization. The optimization was performed using the MMFF94 molecular force field by minimizing the crystal energy, $E_{crystal}$.[4b] The crystal energy is calculated as the sum of the intramolecular interaction energy (E_{intra}) of the molecule in the asymmetric unit and the intermolecular interaction energy (E_{inter}) between the molecule in the asymmetric unit and those in the surrounding symmetry-related units. Intermolecular interactions were considered for

atom pairs within a specified cutoff radius of 20 Å. During the optimization, all degrees of freedom, including the intramolecular geometry (bond lengths, angles, torsions), the orientation and position of the molecule within the unit cell, and the unit cell parameters, were optimized simultaneously while maintaining the assumed space group symmetry. This allows for changes in the molecular conformation due to the crystal packing environment.

The optimization calculations resulted in 4595 unique stable structures for the racemic prediction and 4793 unique stable structures for the chiral prediction. Theoretical prediction of the crystal structure of a molecule remains a significant challenge, stemming partly from the difficulty in identifying the experimentally realized polymorph from a multitude of computationally generated candidates. Therefore, the structures obtained for **3a** represent plausible packing candidates rather than definitive predictions. Nevertheless, these predictions offer valuable structural insights. Notably, calculated powder X-ray diffraction (PXRD) patterns for some of the predicted low-energy structures showed reasonable correspondence with the experimental data (Figure 1), suggesting these models capture key structural features. Furthermore, the predicted low-energy racemic structures exhibit hydrogen bonding between the amide carbonyl oxygen and a hydrazine N-H group. This motif, involving amide group participation in hydrogen bonding networks, bears potential similarity to networks observed in related systems.[2]

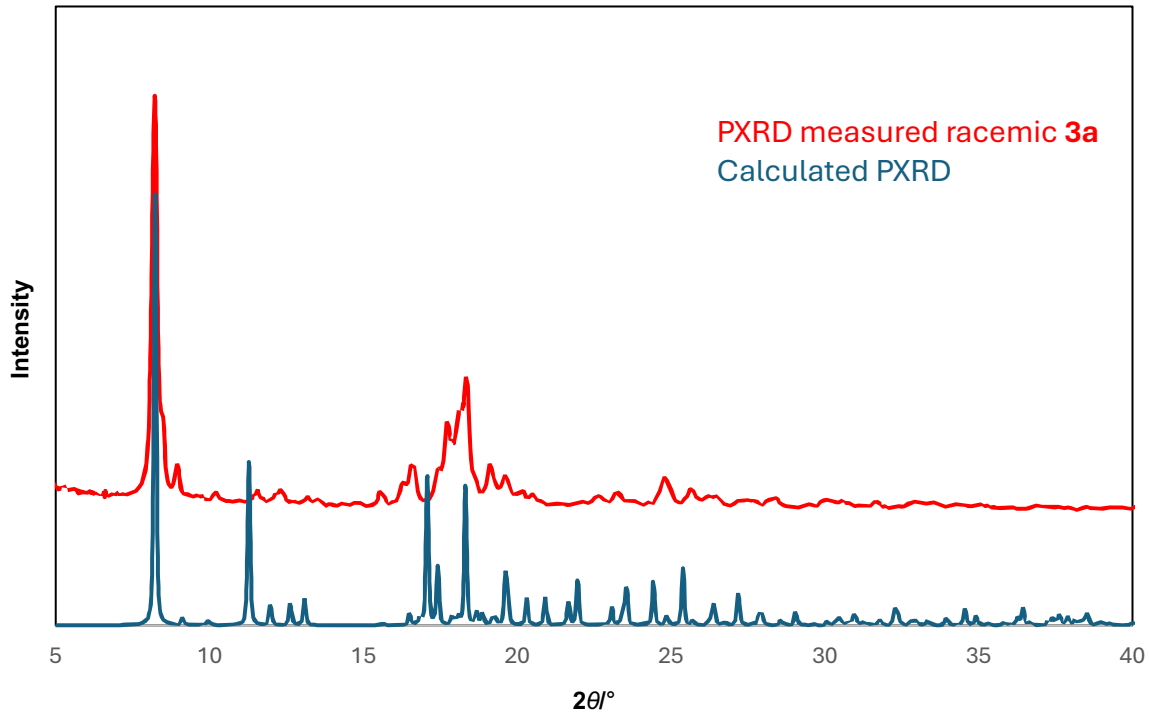

Figure 1. Powder XRD patterns of experimental and calculated (Similarity 0.652).

Among the low-energy structures predicted through crystal structure prediction (CSP) using CONFLX, a representative model showing extensive hydrogen-bonding interactions was selected and visualized (Figure 2). This model, identified as a racemic packing structure, demonstrates the presence of hydrogen-bonding networks formed between the amide carbonyl groups and hydrazine NH moieties. These interactions are

likely to play a crucial role in stabilizing the racemic crystal lattice and may account for the high similarity observed in the calculated PXRD patterns. Although the precise atomic arrangement awaits validation via single-crystal X-ray analysis, this computationally derived model offers a plausible hypothesis for the solid-state organization of compound **3a**.

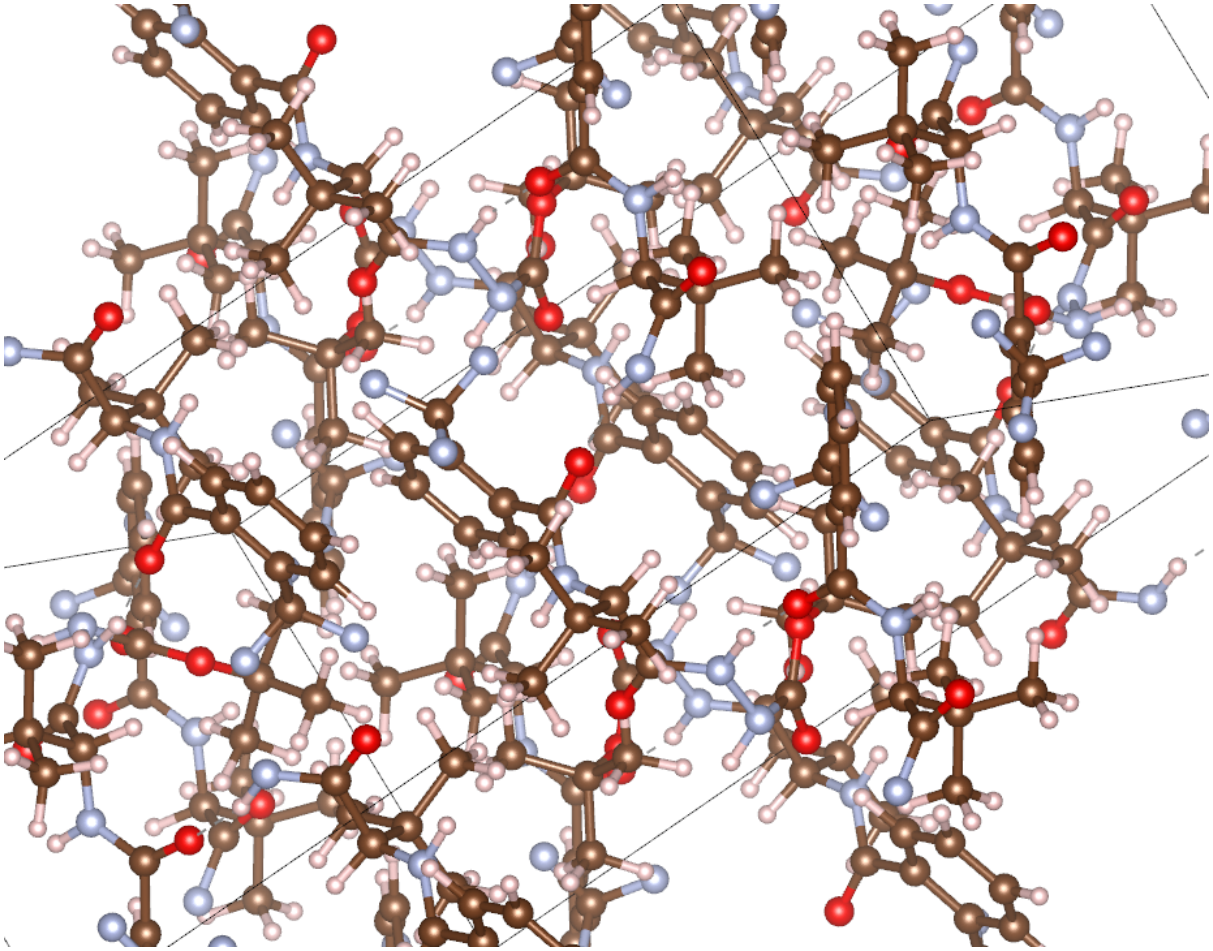

Figure 2. Hydrogen-bonding network in a low-energy racemic crystal structure of **3a** predicted by CSP. The model shows intermolecular hydrogen bonds (dashed lines) between the amide carbonyl oxygen and hydrazine N–H groups, suggesting a dense three-dimensional packing stabilized by directional noncovalent interactions.

In order to rationalize the PXRD pattern of **3a**, the CSP model was further analyzed in terms of its crystallographic parameters. The low-energy structure was assigned to the monoclinic space group P21/c with unit cell dimensions of a = 12.3608 Å, b = 10.1715 Å, c = 20.8318 Å, α = 90.0°, β = 119.76°, γ = 90.0°, and a calculated cell volume of 2273.6 Å³. These parameters are consistent with a dense hydrogen-bonding network that propagates along the crystallographic axes, as highlighted in Figure 2 and Figure 3. Notably, the intermolecular distances between amide carbonyl oxygens and hydrazine NH donors (ca. 10.5–12.1 Å) define repeating motifs that are in good agreement with the major diffraction peaks observed at low angles. In particular, the calculated packing shows an interlayer spacing of d = 10.73 Å, while the distance between equivalent enantiomeric chains is 20.83 Å, corresponding to a half-periodicity of ~10.4 Å. This value

matches closely with the experimental PXRD reflection at $2\theta = 8°$, which corresponds to a d-spacing of 11.1 Å with Cu Kα radiation (λ = 1.5418 Å). The close agreement between simulated and experimental values strongly supports the reliability of the CSP-derived racemic packing model. Although a definitive structural solution requires single-crystal X-ray diffraction, the consistency observed here validates the plausibility of the predicted lattice organization.

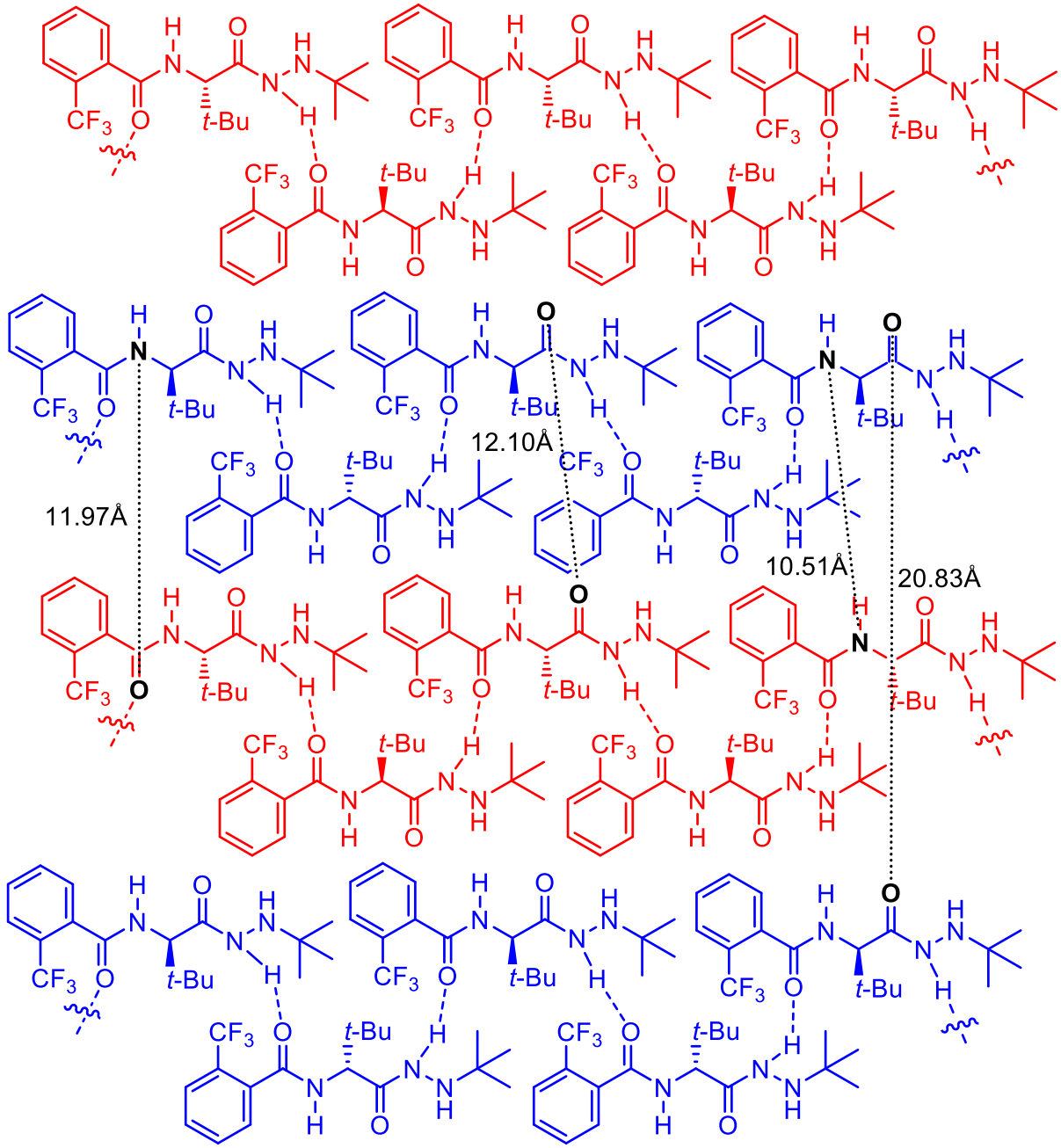

Figure 3. Simplified 2D representation of the CSP-predicted packing of **3a**, showing key hydrogen-bonding interactions and intermolecular distances (10.5–20.8 Å). This schematic complements Figure 2 by highlighting periodic spacing relevant to the PXRD analysis.

A simplified packing model was generated from the CSP output, illustrating the alternating arrangement of (*S*)-**3a** and (*R*)-**3a** in the predicted racemic crystal structure (Figure 5). This pattern is consistent with a

racemic compound-type packing.

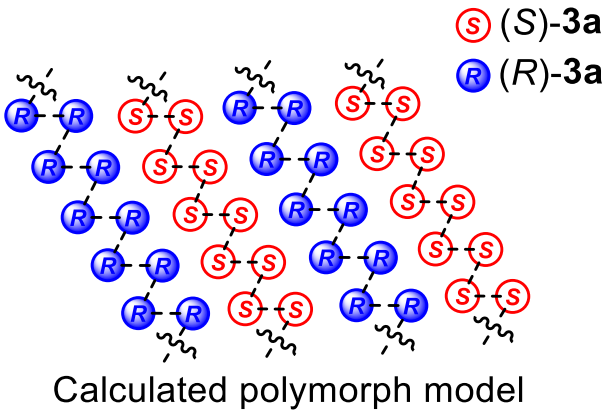

Figure 5. Simplified model showing alternating (*S*)-**3a** (red) and (*R*)-**3a** (blue) molecules in racemic packing.

2-4. Computational Study

2-4-1. Mechanistic Investigation via DFT Calculation

To gain insight into the transition state (TS) geometries relevant to this transformation, a conformational search was conducted utilizing the ConFinder program (Figure 5).[6] This methodology, which our group has previously applied to the DKR of azlactones through alcoholysis, proved effective for exploring the reaction landscape.[7] ConFinder performs a pseudo-transition state conformational search (PTSCS) by integrating low-mode conformational sampling with GFN2-xTB[8] calculations implemented in the xtb software package.[9] A model complex comprising azlactone **2a**, Boc-hydrazine, and catalyst **1a** was used for the search, where the distance between the carbonyl carbon of 1a and the terminal nitrogen atom of the hydrazine moiety was constrained to 1.8 Å to mimic the partially formed C–N bond characteristic of the nucleophilic attack TS.[6] Approximately 7700 conformers were generated and subjected to single-point energy evaluations and partial geometry optimizations. Among these, the lowest-energy structures corresponding to the enantiodivergent transition states (**TS1-S** and **TS1-R**) were identified and subsequently fully optimized at the M06-2X[10]/TZVP[11] level of theory. Based on these structures, further reaction intermediates were modeled, including the near-attack conformers (**NACs**), tetrahedral intermediates (**Int1**), transition states for proton transfer (**TS2**), ring-opened intermediates (**Int2**), and product-like complexes (**Int3**).

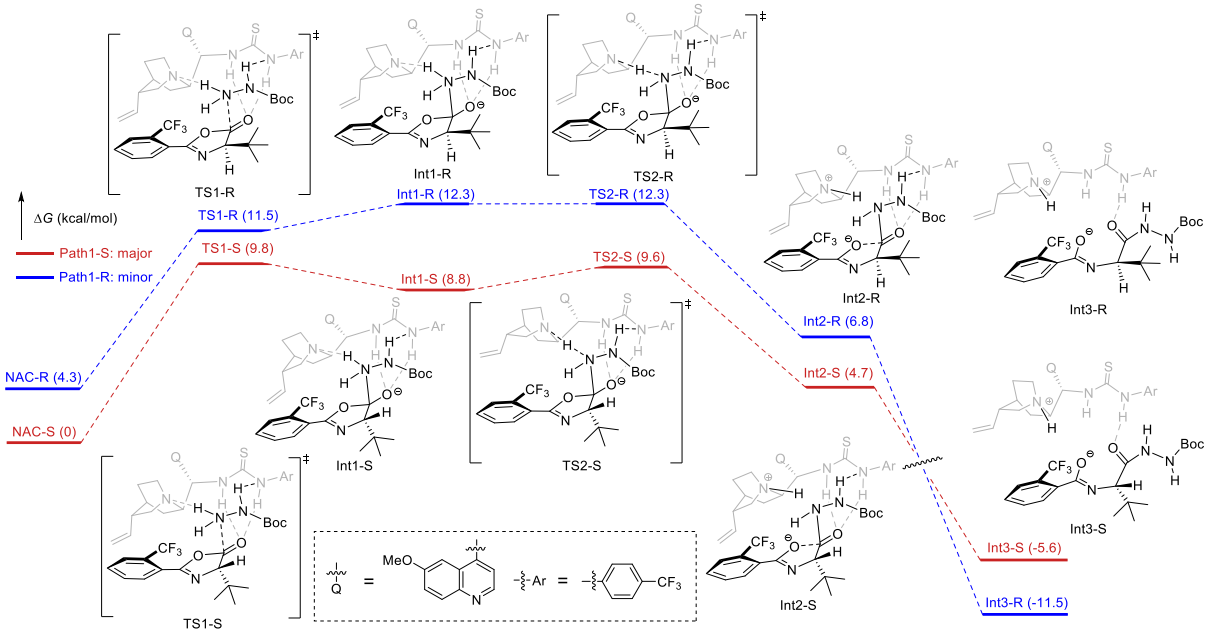

Figure 5. Density functional theory-calculated reaction energy diagram of the nucleophilic ring-opening of azlactone **2a** by Boc-hydrazine with catalyst **1a**. The relative free energy values were calculated at the M06-2X/TZVP level of theory.

Specifically, **NAC-S** and **NAC-R** structures were prepared by releasing all geometric constraints imposed during the **TS1** search and reoptimizing to simulate the pre-reaction configurations. To obtain the covalent adducts **Int1-S** and **Int1-R**, the distance between the carbonyl carbon of the azlactone and the terminal nitrogen of the hydrazine moiety was incrementally shortened, simulating bond formation. It is important to

note that proton migration from the hydrazine to the quinuclidine nitrogen atom did not occur spontaneously in these structures but emerged only in the following step.

For the localization of **TS2-S** and **TS2-R**, the proton-transfer coordinate (N–H···N) was gradually compressed starting from **Int1** geometries, resulting in structures that reflect the formation of ammonium–quinuclidine ion pairs. Transition-state searches based on these preorganized geometries afforded **TS2-S** and **TS2-R**, both characterized by a single imaginary frequency corresponding to proton transfer. Subsequently, the C–O bond in the azlactone ring was progressively elongated to generate **Int2-S** and **Int2-R**, which reflect the ring-opened intermediates. Further geometry optimizations without artificial constraints yielded the post-reaction hydrogen-bonded complexes (**Int3-S** and **Int3-R**), structurally representative of the product–catalyst assemblies.

All optimized geometries were verified through vibrational frequency analysis to confirm the absence of imaginary modes (except for TS structures) and to compute zero-point energy corrections along with thermal contributions to enthalpy and Gibbs free energy. These calculations were consistently performed at the M06-2X/TZVP level and evaluated under standard conditions (T = 300 K).

The calculated energy diagram of the reaction pathway was analyzed to gain insight into the mechanistic features of the reaction (Figure 4). In this analysis, relative Gibbs free energies (ΔG) were calculated using the most stable near attack conformation, **NAC-S**, as the reference point (ΔG = 0 kcal/mol). The **NACs**, representing the preorganized states poised for nucleophilic attack, were generated by relaxing the fixed C···N distance. The reaction proceeds through nucleophilic addition of the hydrazine to the azlactone, assisted by the quinuclidine moiety of catalyst **1a** acting as a Brønsted base. The resulting TS structures **TS1-S/R** lead to the tetrahedral intermediates **Int1-S/R**. A noteworthy point arises when comparing the relative energies of **TS1-R** and **Int1-R**. While the electronic energy (E_{elec}) profile shows the expected order with the transition state being higher than the intermediate (E_{elec} (**TS1-R**) > E_{elec} (**Int1-R**), see Figure 4), an inversion of this relative stability is observed in the Gibbs free energy profile, where ΔG of **TS1-R** (11.5 kcal/mol) is slightly lower than ΔG of **Int1-R** (12.3 kcal/mol). This inversion is likely attributed to the thermal corrections used to calculate Gibbs free energy. Specifically, the imaginary frequency in the transition state does not contribute to ZPE, but the corresponding real mode in the intermediate does contribute. Therefore, when electronic energies are similar, thermal corrections frequently cause the stability order to invert on the Gibbs free energy profile – a known phenomenon in computational studies. In **TS1**, the NH_2 group of the hydrazine forms a hydrogen bond with the quinuclidine nitrogen atom of the catalyst **1a**, while the proton of the Boc-NH group interacts with the aryl-proximal nitrogen atom of the thiourea moiety. Additionally, the two NH groups of the thiourea unit stabilize the transition-state via hydrogen bonding to the carbonyl oxygen atom in the azlactone. In the subsequent intermediate **Int1**, the nucleophilic NH_2 group of the hydrazine forms a covalent bond with the carbonyl carbon of the azlactone, while the proton transfer to the quinuclidine base occurs later at **TS2**. This proton transfer leads to the formation of the ammonium species and facilitates C–O bond cleavage, which led to **Int2**. The fully ring-opened **Int3** intermediates retain only one hydrogen bond between the aryl-proximal NH group of the catalyst and the substrate.

The enantioselectivity is effectively determined by the energy difference between **TS1-S** (ΔG = 9.8 kcal/mol) and **TS1-R** (ΔG = 11.5 kcal/mol) during the initial nucleophilic attack. This conclusion is supported by the close agreement between the calculated activation energy difference ($\Delta\Delta G = G$ (**TS1-R**) – G (**TS1-S**) = 1.7 kcal/mol) and the experimentally observed enantiomeric excess (84 %ee, corresponding to $\Delta\Delta G \approx 1.46$ kcal/mol). The subsequent transition state in the (*R*)-pathway, **TS2-R**, lies even higher in energy relative to the **NAC-S** reference state (ΔG = 12.3 kcal/mol), being 2.5 kcal/mol above **TS1-S**. The higher energy of **TS2** further reinforces the disfavored (*R*)-pathway but does not impact on the stereochemical outcome due to the irreversible nature of the initial attack. Overall, these results confirm the preference for the (*S*)-enantiomer.

2-4-2. IGM Analysis and the Control of Enantioselectivity

To gain deeper insight into the factors governing the observed enantioselectivity, independent gradient model (IGM) analyses were carried out on the transition state structures **TS1-S** and **TS1-R** (Figure 6).[7,12] This method enabled the visualization of noncovalent interactions that play a critical role in stereochemical discrimination. The most stable geometries of **TS1** were subjected to gain insight into the intermolecular noncovalent interactions that influence stereoselectivity. The IGM surfaces were generated using Multiwfn[13], and subsequent visualization was carried out with VMD.[14]

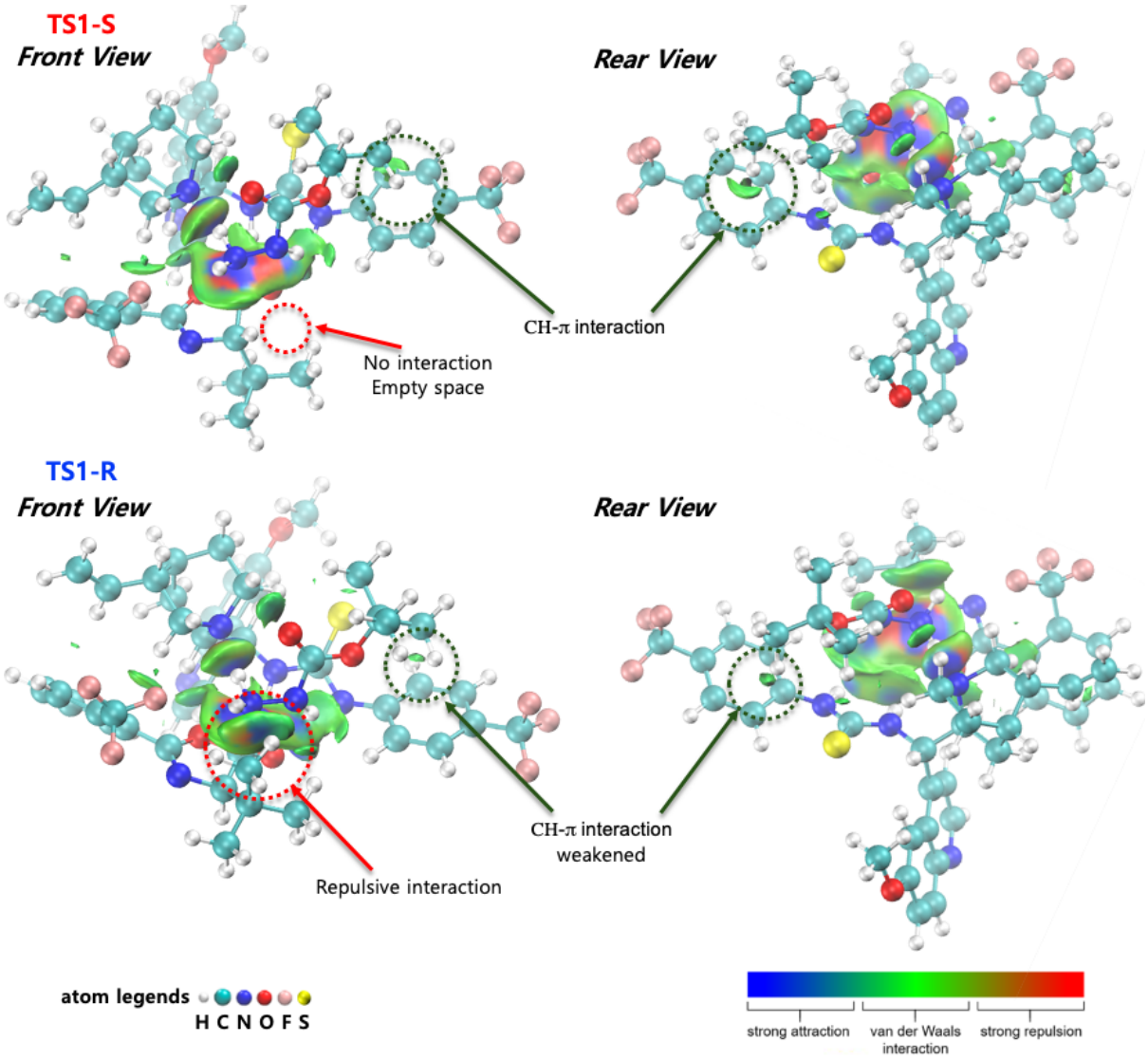

Figure 6. IGM analysis for the transition states of the nucleophilic addition of the hydrazine to azlactone **1a** (**TS1-S** and **TS1-R**) and the mechanism of the stereoselectivity. The blue, green, and red regions represent strongly attractive, attractive, and repulsive intermolecular interactions, respectively. The isovalue is 0.012.

In **TS1-S**, the hydrazine's terminal NH_2 group forms a strong hydrogen-bonding interaction with the quinuclidine nitrogen atom of catalyst **1a**, which appears as an intense blue-colored region in the IGM plot. Additionally, a CH–π interaction is present between the Boc hydrazine's C–H bond and the 4-

trifluoromethylphenyl ring of the thiourea moiety, indicated by a green isosurface.

By contrast, **TS1-R** exhibits notable steric repulsion involving the *tert*-butyl substituent of the azlactone scaffold, which disrupts the aforementioned CH–π interaction. This steric clash is represented by a red-colored repulsive region in the IGM map and contributes to the overall destabilization of the R-pathway. The cumulative effect of these interactions results in a 1.7 kcal/mol energy penalty for **TS1-R** relative to **TS1-S**, thereby rendering the R-pathway less favorable due to the relative instability of both **Int1-R** and **TS2-R** (Figure 7).

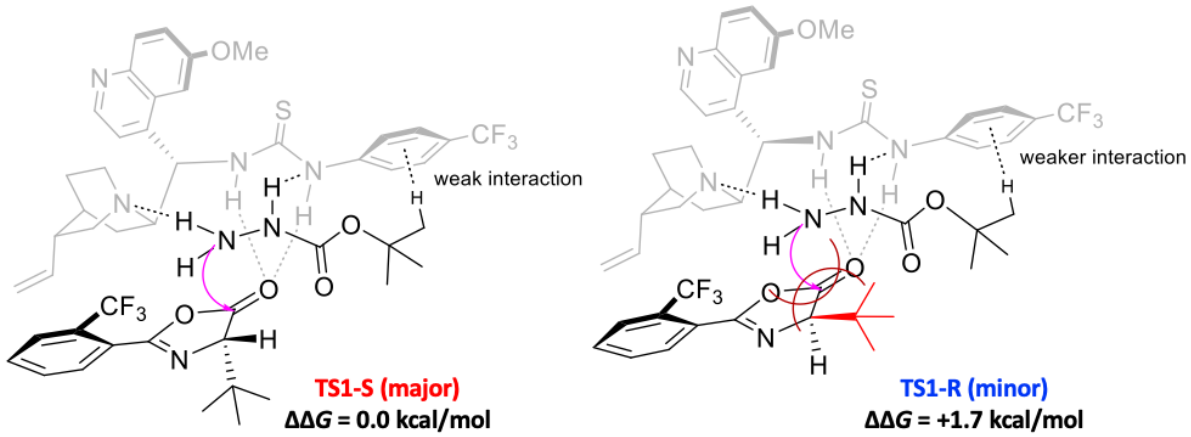

Figure 7. Contrasting noncovalent interactions in **TS1-S** and **TS1-R** as a mechanistic basis for enantioselectivity.

Further experimental support for the crucial role of hydrogen bonding was obtained using 1-Boc-1-methylhydrazine in place of Boc-hydrazine. In this case, the resulting product (*S*)-**3y** showed markedly diminished enantioselectivity, as illustrated in Table 5. Because the methylated hydrazine lacks an NH proton, it cannot engage in the key hydrogen-bonding interaction with the thiourea unit of the catalyst. This loss of interaction likely accounts for the decreased selectivity, reinforcing the importance of NH–thiourea hydrogen bonding in enantiodiscrimination.

2-5. NMR Study for Negative Catalysis via Catalyst-Hydrazine Interaction

To gain mechanistic insight into the suppression of undesired background reactivity by Boc-hydrazine, a series of NMR experiments were conducted in toluene-d_8 (Figure 8). The individual spectra of catalyst **1a** (brown) and Boc-hydrazine (green) were recorded, followed by the spectrum of their 1:15 mixture (blue) to assess interaction-induced spectral changes. Upon mixing, the NH_2 signals of Boc-hydrazine displayed marked upfield shifting and pronounced line broadening, consistent with rapid hydrogen-bonding dynamics or possible proton exchange processes. These spectral changes suggest that the thiourea moiety of catalyst **1a** likely donates a proton to the nucleophilic hydrazine and promotes the formation of an intermolecular hydrogen-bonding network among hydrazine molecules.[15] This aggregation effectively attenuates the nucleophilicity of unbound hydrazine, thereby diminishing its capacity to undergo non-selective background

reactions. Such inhibitory behavior is characteristic of negative catalysis. Analogous behavior was previously reported by Denmark and coworkers,[16] wherein sulfonate species suppressed racemic cyclizations by sequestering nucleophiles through ionic interactions. It is plausible that a related buffering interaction operates in our system, where reversible association between the catalyst and hydrazine reduces the concentration of free, reactive nucleophile and consequently promotes enantioselective turnover.

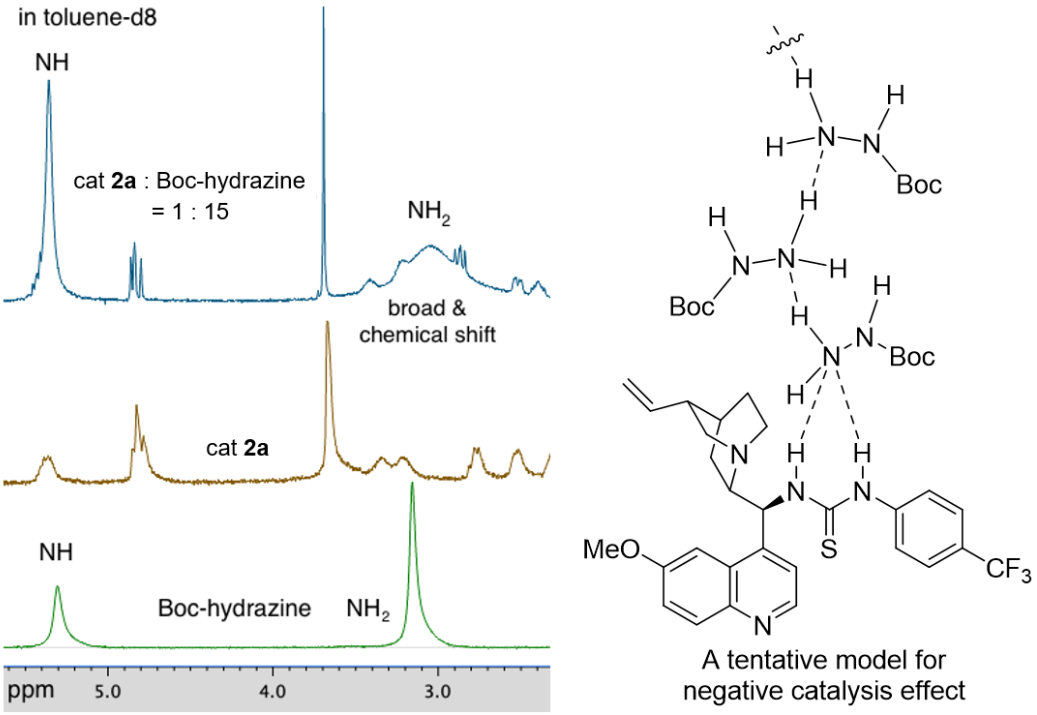

Figure 8. ^{1}H NMR investigation of the Interaction of the hydrazine with catalyst **1a**.

2-6. Conclusion

This study presents the development of a catalytic dynamic kinetic resolution (DKR) of azlactones using hydrazine derivatives as nucleophiles, furnishing α-chiral amino acid hydrazides with high enantioselectivity. A bifunctional quinine-thiourea catalyst was found to play a dual role—promoting asymmetric induction while concurrently tempering the inherent nucleophilicity of hydrazines. Detailed NMR spectroscopy and computational studies revealed that this dual function arises from a combination of Brønsted acid–base equilibrium and hydrogen-bond-mediated aggregation, which collectively attenuate background reactivity by limiting the concentration of free hydrazine. Remarkably, the optical purity of the product solution was further improved through preferential enrichment during recrystallization—a rare phenomenon previously unreported for α-amino acid hydrazides. These findings offer key mechanistic insight into the modulation of nucleophile reactivity under chiral catalysis and pave the way for extending enantioselective methodologies to other reactive nitrogen-based systems.

2-7. References

[1] Zhang, Y.-C.; Yang, Q.; Yang, X.; Zhu, Q.-N.; Shi, F. *Asian J. Org. Chem.* **2016**, *5*, 914–919.

[2] (a) Tamura, R.; Takahashi, H.; Coquerel, G. In *Advances in Organic Crystal Chemistry*; Sakamoto, M.; Uekusa, H., Eds.; Springer: Singapore **2020**, 405–432. (b) Tamura, R.; Iwama, S.; Gonnade, R. G. *CrystEngComm* **2011**, *13*, 5269–5280. (c) Tamura, R.; Iwama, S.; Takahashi, H. *Symmetry* **2010**, *2*, 112–135. (d) Tamura, R.; Takahashi, H.; Fujimoto, D.; Ushio, T. *Top. Curr. Chem.* **2007**, *269*, 53–82.

[3] Goto, H.; Obata, S.; Nakayama, N.; Ohta, K. CONFLEX 9. CONFLEX Corporation: Tokyo, Japan, 2021.

[4] (a) Obata, S.; Nakayama, N.; Goto, H. *J. Cryst. Soc. Jpn.* **2020**, *62*, 260–268. (b) Obata, S.; Miura, T.; Shimoi, Y. *Jpn. J. Appl. Phys.* **2014**, *53*, 01AD02.

[5] Halgren, T. A. *J. Comp. Chem.* **1996**, *17*, 490–519.

[6] (a) Kamachi, T.; Yoshizawa, K. *J. Chem. Inf. Model.* **2016**, *56*, 347−353. (b) Kamachi, T.; Yoshizawa, K. *Org. Lett.* **2014**, *16*, 472−475.

[7] Yamamoto, E.; Kobayashi, K.; Wakafuji, K.; Kamachi, T.; Tokunaga, M. *J. Org. Chem.* **2023**, *88*, 7748–7754.

[8] Bannwarth, C.; Ehlert, S.; Grimme, S. *J. Chem. Theory Comput.* **2019**, *15*, 1652–1671.

[9] Bannwarth, C.: Caldeweyher, E.; Ehlert, S.; Hansen, A.; Pracht, P.; Seibert, J.; Spicher, S.; Grimme, S. *WIREs Comput. Mol. Sci.* **2021**, *11*, e1493.

[10] Walker, M.; Harvey, A. J. A.; Sen, A.; Dessent, C. E. H. *J. Phys. Chem. A* **2013**, *117*, 12590–12600.

[11] Schäfer, A.; Huber, C.; Ahlrichs, R. *J. Chem. Phys.* **1994**, *100*, 5829–5835.

[12] Lefebvre, C.; Khartabil, H.; Boisson, J.-C.; Contreras-García, J.; Piquemal, J.-P.; Hénon, E. *ChemPhysChem* **2018**, *19*, 724–735.

[13] Lu, T.; Chen, F. *J. Comput. Chem.* **2012**, *33*, 580–592.

[14] Humphrey, W.; Dalke, A.; Schulten, K. *J. Mol. Graph.* **1996**, *14*, 33–38.

[15] (a) Ju, X.-H.; Xiao, H.-M. *J. Mol. Struct. (Theochem)* **2002**, *588*, 79–86. (b) Cabaleiro-Lago, E. M.; Ríos, M. A. *J. Phys. Chem. A* **1999**, *103*, 6468–6474.

[16] Denmark, S. E.; Chi, H. M. *J. Am. Chem. Soc.* **2014**, *136*, 3655–3663.

3. General Procedures and Experimental Data

3-1. General and Materials

Materials were purchased from commercial suppliers and used without further purification unless otherwise noted. All NMR spectra were measured with JEOL JNM-ECS400, JNM-ECS600 and Bruker AVANCE III HD 400 NanoBay spectrometers at room temperature. In ^{1}H NMR spectra, chemical shifts (ppm) referenced to tetramethylsilane (TMS) at 0.00 ppm in $CDCl_3$ or methanol at 3.31 ppm in methanol-d4. In ^{13}C {^{1}H} NMR spectra, chemical shift (ppm) referenced to the C signal of $CDCl_3$ at 77.16 ppm or the signal of methanol at 49.00 ppm. In ^{19}F NMR spectra, chemical shift (ppm) referenced to –62.61 ppm of trifluorotoluene as an internal standard in $CDCl_3$ or –64.24 ppm in methanol-d4. Multiplicity was indicated as follows: s (singlet), d (doublet), t (triplet), q (quartet), quin (quintet), sext (sextet), sep (septet), m (multiplet), br (broad). Enantiomeric ratio (er) was determined by high performance liquid chromatography (HPLC) analysis (GL-Sciences GL-7400 series and Hitachi Chromaster 5110), using various chiral columns described below in detail. Optical rotations were measured on JASCO DIP-1000 polarimeter. Elemental analysis was performed by the Service Centre of Elementary Analysis of Organic Compounds (Institute for Materials Chemistry and Engineering, Kyushu University). High-resolution mass spectrometry (HRMS) was measured on fast atom bombardment (FAB) ionization technique by the Network Joint Research Center for Materials and Devices (Institute for Materials Chemistry and Engineering, Kyushu University). Melting point was measured by Büchi Melting Point B-545. Flash column chromatography was performed with silica gel FUJIFILM Wako Pure Chemical Corporation (Wakosil HC-N, spherical; particle size 36-63 μm). All quinine-thiourea catalysts **1** (**1a**,[1b] **1b**,[1c,1h] **1c**,[1a] **1d**,[1d] **1e**,[1c,1f] **1f**,[1f] **1g**,[1g] **1h**,[1c] **1i**,[1b,1c] **1j**,[1h] **1k**[1e]) were prepared following previously reported methods. (*R*)**-TRIP** was purchased commercially and utilized without further purification.

3-2. General Procedure of Preparation of Azlactone 2

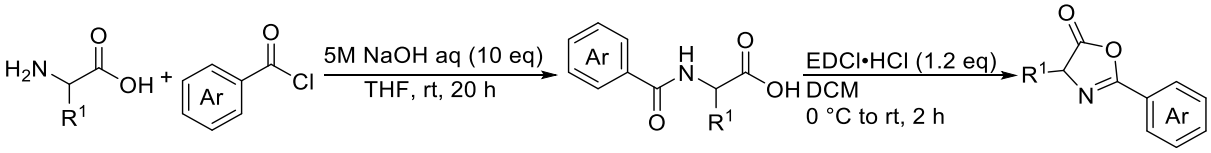

General Procedure A[2]: Initially, **S2** was synthesized via a Schotten-Baumann acylation with racemic amino acids (5 mmol) and aryl carbonyl chloride derivatives (1.1 equiv) in the presence of aqueous NaOH solution (10 equiv, 10 mL). The reaction was carried out in tetrahydrofuran (THF) (10 mL) at room temperature for 20 hours under nitrogen atmosphere. THF was evaporated under reduced pressure, and the resulting crude residue was used directly in the next step without purification. Subsequent intramolecular cyclization was performed under nitrogen atmosphere using 1-(3-dimethylaminopropyl)-3-ethylcarbodiimide hydrochloride (EDCl·HCl) mediated conditions. EDCl·HCl (1.2 equiv) was added to the reaction mixture in dichloromethane (DCM) (30 mL) at 0 °C, followed by gradual warming to room temperature and stirring for 2 hours. The crude product was then washed with water and brine and purified

via short flash column chromatography (hexane:EtOAc = 1:1) to afford azlactones **2**. Unless otherwise noted, azlactones **2** were synthesized according to this procedure.

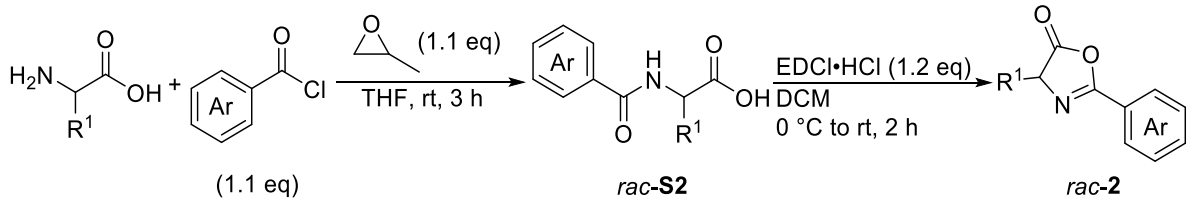

General Procedure B: Initially, **S2** was synthesized via the acylation with racemic amino acids (5 mmol) and aryl carbonyl chloride derivatives (1.1 equiv) under nitrogen atmosphere in the presence of propylene oxide (1.1 equiv, 0.4 mL), which was added dropwise over 15 minutes. The reaction was carried out in THF (30 mL) at room temperature for 3 hours under nitrogen atmosphere. THF was evaporated under reduced pressure, and the resulting crude residue was used directly in the next step without purification. Subsequent intramolecular cyclization was performed under nitrogen atmosphere using EDCl·HCl mediated conditions. EDCl·HCl (1.2 equiv) was added to the reaction mixture in DCM (30 mL) at 0 °C, followed by gradual warming to room temperature and stirring for 2 hours. The crude product was then washed with water and brine and purified via short flash column chromatography (hexane:EtOAc = 1:1) to afford azlactones **2**. Unless otherwise noted, azlactones **2** were synthesized according to this procedure.

4-(*t*-Butyl)-2-(2-(trifluoromethyl)phenyl)oxazol-5(4*H*)-one (**2a**)

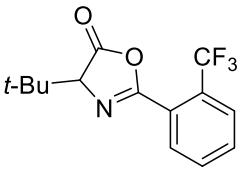

DL-*tert*-Leucine (655.9 mg, 5 mmol) was reacted with 2-(trifluoromethyl)benzoyl chloride (0.8 mL, 5.5 mmol) following the general procedure A, affording **2a** in 57% yield (813.0 mg, 2.85 mmol, white solid). mp = 47.3–49.1 °C. ^{1}H NMR (400 MHz, $CDCl_3$) δ = 7.92–7.86 (m, 1H), 7.85–7.80 (m, 1H), 7.69 (t, *J* = 3.8 Hz, 1H), 7.67 (t, *J* = 3.9 Hz, 1H), 4.12 (s, 1H), 1.17 (s, 9H). ^{13}C NMR (100 MHz, $CDCl_3$) δ = 176.4 (*C*O), 160.7 (*C*), 132.1 (*C*H), 131.9 (*C*H), 131.4 (*C*H), 129.4 (q, *J* = 31.5 Hz, *C*), 127.2 (q, *J* = 5.7 Hz, *C*H), 125.6 (*C*), 123.3 (q, *J* = 271.7 Hz, *C*), 74.5 (*C*), 36.2 (*C*), 26.3 (CH_3, 3C). ^{19}F NMR (376 MHz, $CDCl_3$) δ = –59.14. Elemental Analysis calcd for $C_{14}H_{14}F_3NO_2$: C, 58.95; H, 4.95; N, 4.91. Found: C, 58.85; H, 4.91; N, 4.91.

4-(*t*-Butyl)-2-(3-(trifluoromethyl)phenyl)oxazol-5(4*H*)-one (**2b**)

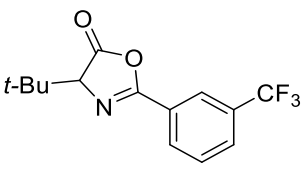

DL-*tert*-Leucine (655.9 mg, 5 mmol) was reacted with 3-(trifluoromethyl)benzoyl chloride (0.8 mL, 5.5 mmol) following the general procedure B, affording **2b** in 48% yield (684.6 mg, 2.40 mmol, white oil). ^{1}H

NMR (400 MHz, $CDCl_3$) δ = 8.30 (s, 1H), 8.20 (d, *J* = 7.8 Hz, 1H), 7.83 (d, *J* = 7.8 Hz, 1H), 7.64 (t, *J* = 7.8 Hz, 1H), 4.12 (s, 1H), 1.16 (s, 9H). ^{13}C NMR (100 MHz, $CDCl_3$) δ = 176.5 (*C*O), 160.3 (*C*), 131.6 (q, J = 32.9 Hz, *C*), 131.1 (*C*H), 129.6 (*C*H), 129.2 (q, *J* = 3.5 Hz, *C*H), 127.0 (*C*), 124.9 (q, *J* = 3.6 Hz, *C*H), 123.7 (q, *J* = 271.1 Hz, *C*), 74.3 (*C*H), 36.2 (*C*), 26.3 (*C*H_3, 3C). ^{19}F NMR (376 MHz, $CDCl_3$) δ = –62.78. HRMS-FAB (*m/z*): $[M+H]^+$ calcd for $C_{14}H_{14}F_3NO_2$: 285.0976; found 285.1038.

4-(*t*-Butyl)-2-(4-(trifluoromethyl)phenyl)oxazol-5(4*H*)-one (**2c**) [1508269-49-5][3a]

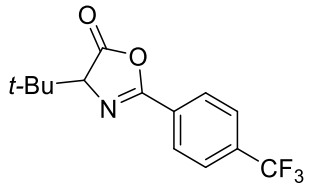

DL-*tert*-Leucine (655.9 mg, 5 mmol) was reacted with 4-(trifluoromethyl)benzoyl chloride (0.8 mL, 5.5 mmol) following the general procedure A, affording **2c** in 53% yield (755.9 mg, 2.65 mmol, white solid). mp = 60.7–61.5 °C. ^{1}H NMR (400 MHz, $CDCl_3$) δ = 8.15 (d, *J* = 7.8 Hz, 2H), 7.76 (d, *J* = 8.2 Hz, 2H), 4.12 (s, 1H), 1.15 (s, 9H). ^{13}C NMR (100 MHz, $CDCl_3$) δ = 176.5 (*C*O), 160.4 (*C*), 134.3 (q, *J* = 32.8 Hz, *C*), 129.4 (*C*), 128.4 (*C*H, 2C), 125.8 (d, *J* = 3.6 Hz, *C*H, 2C), 123.7 (q, *J* = 268.0 Hz, *C*), 74.4 (*C*H), 36.2 (*C*), 26.3 (*C*H_3, 3C). ^{19}F NMR (376 MHz, $CDCl_3$) δ = –62.19. HRMS-FAB (*m/z*): $[M+H]^+$ calcd for $C_{14}H_{14}F_3NO_2$: 285.0976; found 285.0891.

2-(3,5-Bis(trifluoromethyl)phenyl)-4-(*t*-butyl)oxazol-5(4*H*)-one (**2d**)

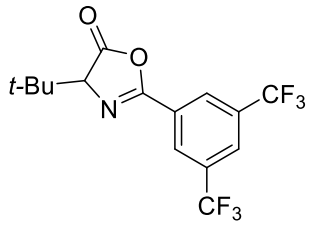

DL-*tert*-Leucine (655.9 mg, 5 mmol) was reacted with 3,5-bis(trifluoromethyl)benzoyl chloride (1.0 mL, 5.5 mmol) following the general procedure B. The subsequent intramolecular cyclization was carried out for 4.5 hours, affording **2d** in 82% (1148.3 mg, 4.10 mmol, white solid). mp = 60.4–61.2 °C. ^{1}H NMR (400 MHz, $CDCl_3$) δ = 8.47 (s, 2H), 8.08 (s, 1H), 4.16 (s, 1H), 1.17 (s, 9H). ^{13}C NMR (100 MHz, $CDCl_3$) δ = 175.7 (*C*O), 159.2 (*C*), 132.6 (q, *J* = 34.0 Hz, *C*, 2C), 128.3 (*C*), 128.0 (d, *J* = 2.9 Hz, *C*H, 2C), 126.1 (q, J = 3.5 Hz, *C*H), 122.9 (q, *J* = 271.7 Hz, *C*, 2C), 74.5 (*C*H), 36.4 (*C*), 26.3 (*C*H_3, 3C). ^{19}F NMR (376 MHz, $CDCl_3$) δ = –62.91. Elemental Analysis calcd for $C_{15}H_{13}F_6NO_2$: C, 51.00; H, 3.71; N, 3.97. Found: C, 51.15; H, 3.85; N, 4.11.

4-(*t*-Butyl)-2-phenyloxazol-5(4*H*)-one (**2e**) [71953-55-4][3]

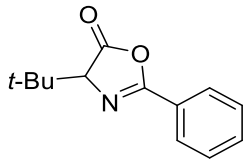

DL-*tert*-Leucine (655.9 mg, 5 mmol) was reacted with benzoyl chloride (0.7 mL, 6.0 mmol) following the general procedure A, affording **2e** in 67% yield (727.8 mg, 3.35 mmol, white solid). mp = 66.5–68.0 °C. ^{1}H NMR (600 MHz, $CDCl_3$) δ = 8.03–8.01 (m, 2H), 7.58 (t, *J* = 7.6 Hz, 1H), 7.49 (t, *J* = 7.6 Hz, 2H), 4.09 (s, 1H), 1.15 (s, 9H). ^{13}C NMR (100 MHz, $CDCl_3$) δ = 177.2 (*C*O), 161.4 (*C*), 132.8 (*C*H), 128.9 (*C*H, 2C), 128.0 (*C*H, 2C), 126.2 (*C*), 74.3 (*C*H), 36.1 (*C*), 26.4 (CH_3, 3C). Elemental Analysis calcd for $C_{13}H_{15}NO_2$: C, 71.87; H, 6.96; N, 6.45. Found: C, 71.72; H, 6.96; N, 6.35.

4-(*t*-Butyl)-2-(*o*-tolyl)oxazol-5(4*H*)-one (**2f**) [2907702-96-7][3a]

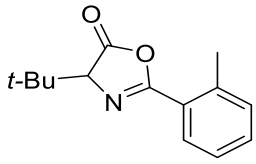

DL-*tert*-Leucine (655.9 mg, 5 mmol) was reacted with 2-methylbenzoyl chloride (1.0 mL, 5.5 mmol) following the general procedure B, affording **2f** in 78% yield (902.0 mg, 3.90 mmol, white solid). mp = 48.7–50.3 °C. ^{1}H NMR (400 MHz, $CDCl_3$) δ = 7.87–7.84 (m, 1H), 7.45-7.40 (m, 1H), 7.33–7.27 (m, 2H), 4.11 (s, 1H), 2.67 (s, 3H), 1.15 (s, 9H). ^{13}C NMR (100 MHz, $CDCl_3$) δ = 177.3 (*C*O), 161.5 (*C*), 139.8 (*C*), 131.92 (*C*H), 131.85 (*C*H), 130.0 (*C*H), 126.1 (*C*H), 125.0 (*C*), 74.5 (*C*H), 35.9 (*C*), 26.4 (CH_3, 3C), 22.3 (CH_3). HRMS-FAB (*m/z*): $[M+H]^+$ calcd for $C_{14}H_{17}NO_2$: 231.1259; found 231.1346

4-(*t*-Butyl)-2-(4-methoxyphenyl)oxazol-5(4*H*)-one (**2g**) [1836145-08-4][3a]

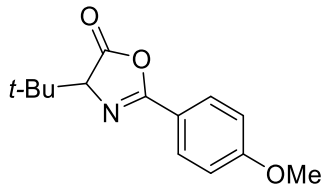

DL-*tert*-Leucine (655.9 mg, 5 mmol) was reacted with 4-methoxybenzoyl chloride (938.2 mg, 5.5 mmol) following the general procedure A, affording **2g** in 73% yield (903.8 mg, 3.65 mml, white solid). mp = 107.1–111.2 °C. ^{1}H NMR (400 MHz, $CDCl_3$) δ = 7.96 (d, *J* = 8.7 Hz, 2H), 6.98 (d, *J* = 8.7 Hz, 2H), 4.05 (s, 1H), 3.88 (s, 3H), 1.13 (s, 9H). ^{13}C NMR (100 MHz, $CDCl_3$) δ = 177.4 (*C*O), 163.3 (*C*), 161.1 (*C*), 129.9 (*C*H, 2C), 118.5 (*C*), 114.3 (*C*H, 2C), 74.1 (*C*H), 55.6 (CH_3), 36.0 (*C*), 26.3 (CH_3, 3C). Elemental Analysis calcd for $C_{14}H_{17}NO_3$: C, 68.00; H, 6.93; N, 5.66. Found: C, 67.60; H, 6.93; N, 5.56.

Isopropyl 2-(4-(*t*-butyl)-5-oxo-4,5-dihydrooxazol-2-yl)-3,4,5,6-tetrachlorobenzoate (2h)

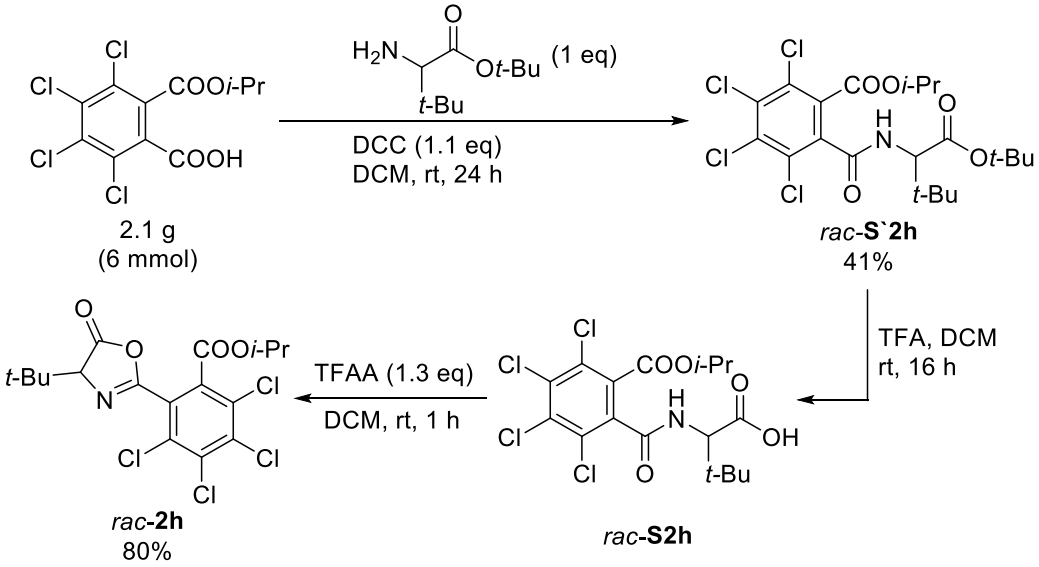

Under a nitrogen atmosphere, dry DCM (10 mL) was added to a reaction vessel containing *t*-butyl 2-amino-3,3-dimethylbutanoate (1.2 g, 6 mmol), followed by the addition of 2,3,4,5-tetrachloro-6-(isopropoxycarbonyl) benzoic acid (2.1 g, 6 mmol).[4] A solution of DCC (1.4 g, 6.6 mmol) in dry DCM (10 mL) was then introduced, and the reaction mixture was stirred at room temperature for 24 hours. Upon completion, the crude product was purified by flash column chromatography (hexane:EtOAc = 20:1) to afford **S`2h** 41% yield (1267.5 mg, 2.46 mmol). For deprotection, **S`2h** was dissolved in dry DCM (5 mL) under a nitrogen atmosphere, and trifluoroacetic acid (TFA) (5 mL, excess) was added. The reaction was stirred for 16 hours to afford **S2h**, which was subsequently subjected to intramolecular cyclization. To a solution of **S2h** in dry DCM (4 mL), trifluoroacetic anhydride (TFAA) (1.3 eq) was added, and the reaction was stirred at room temperature for 1 hour. After evaporation, the crude mixture was purified via short flash column chromatography (hexane:EtOAc = 1:1) to afford **2h** in 80% yield (868.1 mg, 1.97 mmol, white solid). mp = 88.3–91.9 °C. ^{1}H NMR (400 MHz, $CDCl_3$) δ = 5.25 (td, *J* = 12.5, 6.3 Hz, 1H), 4.00 (s, 1H), 1.35 (dd, *J* = 6.4, 2.3 Hz, 6H), 1.15 (s, 9H). ^{13}C NMR (100 MHz, $CDCl_3$) δ = 175.3 (*C*O), 163.2 (*C*), 157.9 (*C*O), 137.1 (*C*), 135.7 (*C*), 135.0 (*C*), 132.6 (*C*), 130.5 (*C*), 125.6 (*C*), 74.2 (*C*H), 71.5 (*C*H), 36.1 (*C*), 26.4 (*C*H_3, 3C), 21.74 (*C*H_3), 21.68 (*C*H_3). HRMS-FAB (*m/z*): $[M+H]^+$ calcd for $C_{17}H_{17}Cl_4NO_4$: 438.9911; found 438.9994.

4-Ethyl-2-(2-(trifluoromethyl)phenyl)oxazol-5(4*H*)-one (2i)

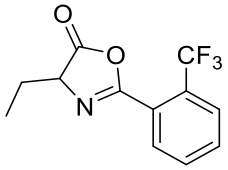

α-Aminobutyric acid (515.6 mg, 5 mmol) was reacted with 2-(trifluoromethyl)benzoyl chloride (0.8 mL, 5.5 mmol) following the general procedure B, affording **2i** in 23% (300.4 mg). White solid. ^{1}H NMR (400 MHz, $CDCl_3$) δ = 7.90–7.80 (m, 2H), 7.71–7.65 (m, 2H), 4.42 (dd, *J* = 6.4, 5.5 Hz, 1H), 2.18-2.07 (m, 1H),

2.03–1.91 (m, 1H), 1.08 (t, J = 7.3 Hz, 3H). ^{13}C NMR (100 MHz, $CDCl_3$) δ = 177.8 (*C*O), 161.1 (*C*), 132.1 (*C*H), 132.0 (*C*H), 131.2 (*C*H), 129.4 (q, J = 32.4 Hz, *C*), 127.1 (q, J = 5.1 Hz, *C*H), 125.6 (*C*), 123.3 (q, J = 272.0 Hz, *C*), 66.7 (*C*H), 24.8 (*C*H_3), 9.5 (*C*H_2).

4-Benzyl-2-(2-(trifluoromethyl)phenyl)oxazol-5(4*H*)-one (**2j**) [2648747-62-8][3b]

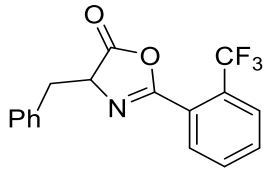

DL-Phenylalanine (826.0 mg, 5 mmol) was reacted with 2-(trifluoromethyl)benzoyl chloride (0.8 mL, 5.5 mmol) following the general procedure A, affording **2j** in 62% yield (991.3 mg, 3.10 mmol, white solid). mp = 114.7–117.5 °C. ^{1}H NMR (400 MHz, $CDCl_3$) δ = 7.80–7.74 (m, 1H), 7.67–7.55 (m, 3H), 7.33–7.23 (m, 5H), 4.71 (dd, J = 6.4, 5.0 Hz, 1H), 3.41 (dd, J = 14.2, 5.0 Hz, 1H), 3.23 (dd, J = 13.6, 6.4 Hz, 1H). ^{13}C NMR (100 MHz, $CDCl_3$) δ = 177.1 (*C*O), 161.1 (*C*), 135.1 (*C*), 132.0 (*C*H), 131.9 (*C*H), 131.2 (*C*H), 129.8 (*C*H, 2C), 129.2 (q, J = 35.0 Hz, *C*), 128.6 (*C*H, 2C), 127.5 (*C*H), 127.0, (q, J = 5.1 Hz, *C*H), 125.4 (*C*), 123.2 (q, J = 271.9 Hz, *C*), 66.8 (*C*H), 37.1 (*C*H_2). ^{19}F NMR (376 MHz, $CDCl_3$) δ = –59.33. HRMS-FAB (*m/z*): $[M+H]^+$ calcd for $C_{17}H_{12}F_3NO_2$: 319.0820; found 319.0896.

4-Isopropyl-2-(2-(trifluoromethyl)phenyl)oxazol-5(4*H*)-one (**2k**)

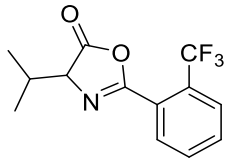

DL-Valine (585.8 mg, 5 mmol) was reacted with 2-methylbenzoyl chloride (1.0 mL, 5.5 mmol) following the general procedure B. The subsequent intramolecular cyclization was carried out for 3 hours, affording **2k** in 55% yield (741.4 mg, 2.75 mmol, white solid). mp = 124.1–127.6 °C. ^{1}H NMR (400 MHz, $CDCl_3$) δ = 7.90–7.85 (m, 1H), 7.84–7.81 (m, 1H), 7.69 (t, J = 3.9 Hz, 1H), 7.67 (t, J = 3.7 Hz, 1H), 4.32 (d, J = 4.6 Hz, 1H), 2.49–2.37 (m, 1H), 1.18 (d, J = 6.9 Hz, 3H), 1.05 (d, J = 6.9 Hz, 3H). ^{13}C NMR (100 MHz, $CDCl_3$) δ = 177.2 (*C*O), 161.2 (*C*), 132.1 (*C*H), 132.0 (*C*H), 131.4 (*C*H), 129.4 (q, J = 32.3 Hz, *C*), 127.1 (q, J = 5.1 Hz, *C*H), 125.6 (*C*), 123.3 (q, J = 271.7 Hz, *C*), 71.0 (*C*H), 31.3 (*C*H), 19.0 (*C*H_3), 17.6 (*C*H_3). ^{19}F NMR (376 MHz, $CDCl_3$) δ = –59.21. HRMS-FAB (*m/z*): $[M+H]^+$ calcd for $C_{13}H_{12}F_3NO_2$: 271.0820; found 271.0891.

4-(Pentan-3-yl)-2-(2-(trifluoromethyl)phenyl)oxazol-5(4*H*)-one (**2l**)

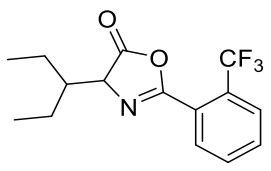

2-Amino-3-ethylpentanoic acid hydrochloride (908.3 mg, 5 mmol) was reacted with 2-(trifluoromethyl)

benzoyl chloride (0.8 mL, 5.5 mmol) following the general procedure A, with the acylation step requiring 36 hours. This afforded **2l** in 64% yield (953.9 mg, 3.20 mmol, white oil). ^{1}H NMR (400 MHz, $CDCl_3$) δ = 7.90–7.84 (m, 1H), 7.84–7.80 (m, 1H), 7.69 (t, *J* = 3.9 Hz, 1H), 7.66 (t, *J* = 3.9 Hz, 1H), 4.53 (d, *J* = 4.1 Hz, 1H), 2.01–1.92 (m, 1H), 1.63-1.53 (m, 2H), 1.49–1.34 (m, 2H), 1.04 (t, *J* = 7.3 Hz, 3H), 0.97 (t, *J* = 7.6 Hz, 3H). ^{13}C NMR (100 MHz, $CDCl_3$) δ = 178.2 (*C*O), 161.0 (*C*), 132.1 (*C*H), 131.9 (*C*H), 131.4 (*C*H), 129.4 (q, *J* = 32.4 Hz, *C*), 127.1 (q, *J* = 5.7 Hz, *C*H), 125.7 (*C*), 123.3 (q, *J* = 272.2 Hz, *C*), 67.8 (*C*H), 44.5 (*C*H), 23.2 (CH_2), 22.6 (CH_2), 11.9 (CH_3), 11.8 (CH_3). ^{19}F NMR (376 MHz, $CDCl_3$) δ = –59.17. HRMS-FAB (*m/z*): $[M+H]^+$ calcd for $C_{15}H_{16}F_3NO_2$: 299.2932; found 299.1201.

2-(2-(Trifluoromethyl)phenyl)-4-trityloxazol-5(4*H*)-one (2m)

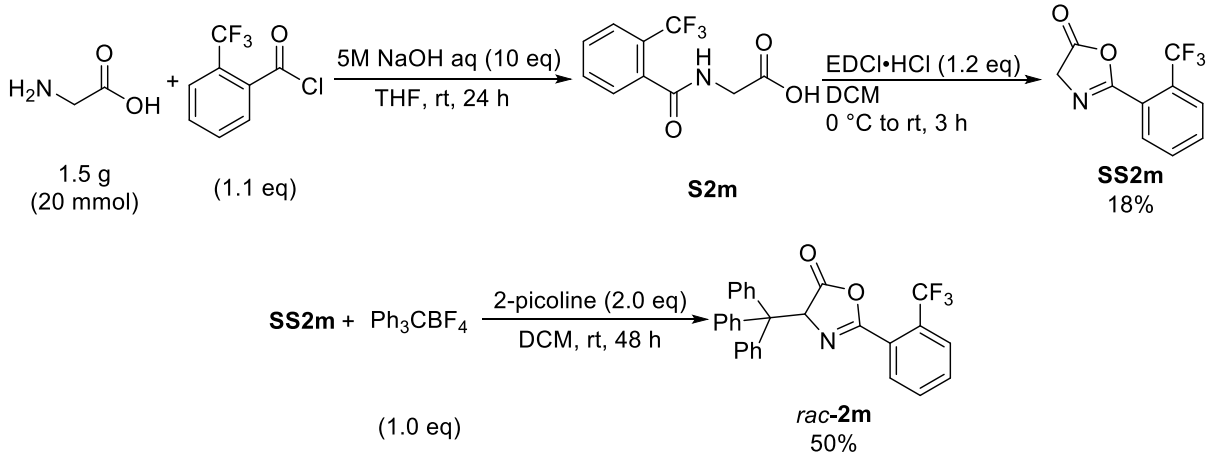

Glycine (1.5 g, 20 mmol) was reacted with 2-(trifluoromethyl)benzoyl chloride (3.2 mL, 22 mmol) following the general procedure A, with the first step requiring 24 hours, and 3 hours for the intramolecular cyclization. This afforded **SS2m** in 18% yield (824.9 mg, 3.6 mmol, white solid). Triphenylmethylium tetrafluoroborate (594.2 mg, 1.8 mmol) was placed in a reaction vessel under a nitrogen atmosphere, followed by the addition of dry DCM (4.5 mL) at 0 °C. 2-Picoline (0.35 mL, 3.60 mmol) was then added, and **SS2m** (412.5 mg, 1.8 mmol) in dry DCM (4.5 mL) was introduced. The reaction mixture was gradually warmed to room temperature and stirred for 48 hours. The reaction was quenched with 0.5 M HCl and extracted with DCM. The organic phase was washed with brine, dried over Na_2SO_4, filtered, and concentrated under reduced pressure. The crude mixture was purified via column chromatography (gradient elution from hexane to hexane:EtOAc = 5:1), affording the tritylated product **2m** in 50% yield (427.2 mg, 1.80 mmol, white solid). mp = 144.7–147.1 °C. ^{1}H NMR (400 MHz, $CDCl_3$) δ = 7.68 (d, J = 7.8 Hz, 1H), 7.55 (t, *J* = 7.8 Hz, 1H), 7.46 (t, *J* = 7.6 Hz, 1H), 7.39 (br s, 5H), 7.30 (t, *J* = 7.3 Hz, 7H), 7.25–7.21 (m, 3H), 7.07 (d, *J* = 7.8 Hz, 1H), 6.05 (s, 1H). ^{13}C NMR (100 MHz, $CDCl_3$) δ = 175.2 (*C*O), 160.9 (*C*), 131.8 (*C*H), 131.7 (*C*H), 131.1 (*C*H), 129.7 (*C*H, 6C), 129.2 (q, *J* = 32.5 Hz, *C*), 128.1 (*C*H, 6C), 127.0 (*C*H, 3C), 126.7 (q, *J* = 4.8 Hz, *C*H), 125.3 (*C*), 123.3 (q, *J* = 271.8 Hz, *C*), 70.5 (*C*H), 61.5 (*C*). ^{19}F NMR (376 MHz, $CDCl_3$) δ = –59.39. HRMS-FAB (*m/z*): $[M+H]^+$ calcd for $C_{29}H_{20}F_3NO_2$: 471.1446; found 471.1507.

3-3. General Procedure for the Asymmetric Ring-Opening Reaction of Azlactone via DKR

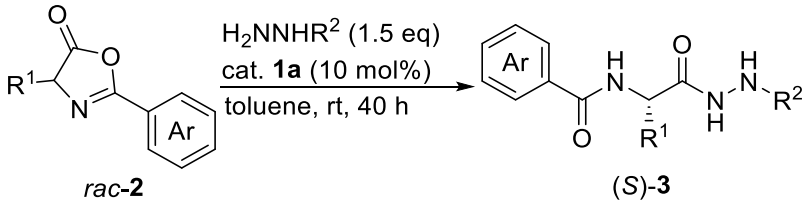

Azlactone **2** (0.1 mmol) was placed in a screw-capped test tube. Catalyst **1a** (5.3mg, 0.01 mmol) was then added, and the test tube was sealed with a rubber septum. The reaction vessel was subjected to three cycles of evacuation and nitrogen backfilling. Dry toluene (0.5 mL) was added, and the mixture was stirred at room temperature for 15 minutes. Under a nitrogen atmosphere, Boc-protected hydrazine (19.8 mg, 0.15 mmol) or hydrazine reagents (1.5 equiv), dissolved in dry toluene (0.5 mL), was added dropwise via cannula. The reaction mixture was stirred at room temperature for 40 hours or for the designated reaction time. After completion, the reaction mixture was directly subjected to flash column chromatography. Elution was performed with a hexane:EtOAc gradient, starting from a 3:1 ratio and gradually shifting to a 1:3 ratio. The ee of the isolated product **3** was determined by HPLC analysis.

Note 1: Azlactone **2** undergoes gradual hydrolysis over time and under certain temperature conditions to generate the precursor **S2**.[4] The presence of the precursor **S2** interferes with the activation of catalyst **1**, preventing the reaction from proceeding efficiently and affecting its reproducibility. The purity of azlactone **2** can be assessed easily by TLC analysis under hexane:EtOAc (3:1) condition. To minimize degradation, azlactone **2** was stored in a nitrogen-filled glovebox throughout the experiments.

Note 2: The products **3** exhibits preferential enrichment, necessitating complete dissolution in solution prior to HPLC analysis. Based on our observations, solid-state **3** displayed varying er values depending on the sampling location in a sample flask. This variation is attributed to preferential enrichment occurring during evaporation, leading to non-uniform er measurements. Therefore, for accurate and consistent er determination, complete dissolution of **3** in solution is required. The relative solubility of **3** in various solvents was observed as follows: MeOH > $CHCl_3$ > Acetone >> EtOAc >> DCM (with minimal solubility from EtOAc onward).

***t*-Butyl (*S*)-2-(3,3-dimethyl-2-(2-(trifluoromethyl)benzamido)butanoyl)hydrazine-1-carboxylate** ((*S*)-**3a**)

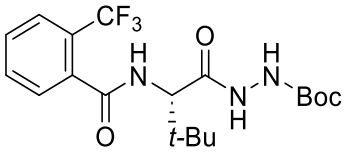

The title compound was synthesized from azlactone **2a** (28.5 mg, 0.1 mmol) following the general procedure and obtained in 94% yield with 84 %ee (39.2 mg, 0.094 mmol, white solid). The product **3a** (39.2

mg, 0.094 mmol) was subjected to preferential enrichment (method A, see Section 2-3-1), affording **3a** in 87% (34.1 mg, 0.082 mmol) recovery with 96 %ee from the supernatant and 13% (5.0 mg, 0.012 mmol) recovery with 9 %ee from the crystals. mp = 188.9–189.1 °C. ^{1}H NMR (400 MHz, Methanol-d4) δ = 7.75 (d, *J* = 7.3 Hz, 1H), 7.69 (t, *J* = 7.1 Hz, 1H), 7.63 (t, *J* = 7.3 Hz, 1H), 7.55 (d, *J* = 6.4 Hz, 1H), 4.50 (s, 1H), 1.48 (s, 9H), 1.12 (s, 9H). ^{13}C NMR (100 MHz, Methanol-d4) δ = 171.9 (*C*O), 170.4 (*C*O), 157.4 (*C*O), 136.9 (*C*), 133.3 (*C*H), 131.0 (*C*H), 129.9 (*C*H), 128.1 (q, *J* = 31.5 Hz, *C*), 127.3 (q, *J* = 4.8 Hz, *C*H), 125.1 (q, *J* = 271.8 Hz , *C*), 81.5 (*C*), 61.2 (*C*H), 35.8 (*C*), 28.6 (*C*H$_3$, 3C), 27.2 (*C*H$_3$, 3C). ^{19}F NMR (376 MHz, Methanol-d4) δ = –59.6. Elemental Analysis calcd for $C_{19}H_{26}F_3N_3O_4$: C, 54.67; H, 6.28; N, 10.07. Found: C, 54.88; H, 6.31; N, 10.07. HPLC analysis: CHIRALPAK IB column [conditions, hexane:*i*PrOH = 96:4, flow rate = 1 mL/min, rt, Rt (minor) = 15.74 min, Rt (major) = 23.60 min] , or CHIRALCEL OD-3 column [conditions, hexane:*i*PrOH = 95:5, flow rate = 1 mL/min, rt, Rt (minor) = 8.16 min, Rt (major) = 16.58 min]. For 84 %ee, $[\alpha]_D^{21.9}$ = –19.5 (c = 1.0, $CHCl_3$).

***t*-Butyl (*S*)-2-(3,3-dimethyl-2-(3-(trifluoromethyl)benzamido)butanoyl)hydrazine-1-carboxylate** ((*S*)-**3b**)

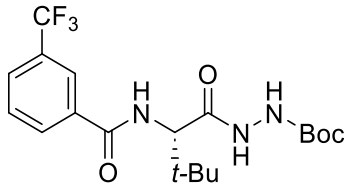

The title compound was synthesized from azlactone **2b** (28.5 mg, 0.1 mmol) following the general procedure and obtained in 84% yield with 74 %ee (35.0 mg, 0.084 mmol, white solid). mp = 182.5–183.7 °C. ^{1}H NMR (400 MHz, Methanol-d4) δ = 8.13 (s, 1H), 8.09 (d, *J* = 7.8 Hz, 1H), 7.86 (d, *J* = 7.8 Hz, 1H), 7.69 (t, *J* = 8.0 Hz, 1H), 4.60 (s, 1H), 1.46 (s, 9H), 1.12 (s, 9H). ^{13}C NMR (100 MHz, Methanol-d4) δ = 172.2 (*C*O), 168.6 (*C*O), 157.4 (*C*O), 136.6 (*C*), 132.4 (*C*H), 131.9 (q, *J* = 32.4 Hz, *C*), 130.6 (*C*H), 129.3 (d, *J* = 3.8 Hz, *C*H), 125.5 (d, *J* = 2.8 Hz, *C*H), 125.3 (q, *J* = 270.3 Hz, *C*), 81.7 (*C*), 61.0 (*C*H), 36.1 (*C*), 28.5 (*C*H$_3$, 3C), 27.2 (*C*H$_3$, 3C). ^{19}F NMR (376 MHz, Methanol-d4) δ = –64.2. HRMS-FAB (*m/z*): $[M+H]^+$ calcd for $C_{19}H_{26}F_3N_3O_4$: 417.1875; found 417.1952. HPLC analysis: CHIRALPAK IF column [conditions, hexane:*i*PrOH = 8:2, flow rate = 1 mL/min, rt, Rt (minor) = 10.43 min, Rt (major) = 12.03 min]. $[\alpha]_D^{24.5}$ = –17.7 (c = 3.2, $CHCl_3$).

***t*-Butyl (*S*)-2-(3,3-dimethyl-2-(4-(trifluoromethyl)benzamido)butanoyl)hydrazine-1-carboxylate** ((*S*)-**3c**)

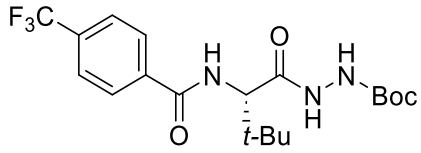

The title compound was synthesized from azlactone **2c** (28.5 mg, 0.1 mmol) following the general procedure and obtained in 73% yield with 52 %ee (30.5 mg, 0.073 mmol, white solid). mp = 160.9–162.4 °C.

^{1}H NMR (400 MHz, Methanol-d4) δ = 7.99 (d, *J* = 8.2 Hz, 2H), 7.79 (d, *J* = 8.2 Hz, 2H), 4.60 (d, *J* = 16.0 Hz, 1H), 1.46 (s, 9H), 1.12 (s, 9H). ^{13}C NMR (100 MHz, Methanol-d4) δ = 172.1 (*C*O), 168.8 (*C*O), 157.4 (*C*O), 139.3 (*C*), 134.2 (q, *J* = 32.4 Hz, *C*), 129.3 (*C*H, 2C), 126.5 (d, *J* = 3.8 Hz, *C*H, 2C), 125.3 (q, *J* = 270.3 Hz, *C*), 81.6 (*C*), 61.0 (*C*H), 36.1 (*C*), 28.6 (*C*H$_3$, 3C), 27.2 (*C*H$_3$, 3C). ; ^{19}F NMR (376 MHz, Methanol-d4) δ = –59.1. HRMS-FAB (*m/z*): $[M+H]^+$ calcd for $C_{19}H_{26}F_3N_3O_4$: 417.1875; found 417.1951. HPLC analysis: CHIRALCEL OD-3 column [conditions, hexane:*i*PrOH = 95:5, flow rate = 1 mL/min, rt, Rt (minor) = 6.28 min, Rt (major) = 11.19 min]. $[\alpha]_D^{22.9}$ = –19.0 (c = 1.8, $CHCl_3$).

***t*-Butyl (*S*)-2-(2-(3,5-bis(trifluoromethyl)benzamido)-3,3-dimethylbutanoyl)hydrazine-1-carboxylate ((*S*)-3d)**

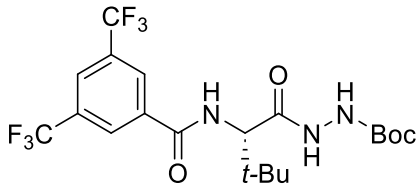

The title compound was synthesized from azlactone **2d** (35.3 mg, 0.1 mmol) following the general procedure and obtained in 87% yield with 65 %ee (42.2 mg, 0.087 mmol, white solid). mp = 175.9–179.2 °C. ^{1}H NMR (400 MHz, Methanol-d4) δ = 8.42 (s, 2H), 8.15 (s, 1H), 4.63 (s, 1H), 1.46 (s, 9H), 1.13 (s, 9H). ^{13}C NMR (100 MHz, Methanol-d4) δ = 172.1 (*C*O), 167.1 (*C*O), 157.4 (*C*O), 138.1 (*C*), 132.9 (q, *J* = 22.1 Hz, *C*, 2C), 129.4 (*C*H, 2C), 126.0 (*C*H), 124.6 (q, *J* = 180.0 Hz, *C*), 81.7 (*C*), 61.4 (*C*H), 36.0 (*C*), 28.6 (*C*H$_3$, 3C), 27.2 (*C*H$_3$, 3C). ^{19}F NMR (376 MHz, Methanol-d4) δ = –64.2. HRMS-FAB (*m/z*): $[M+H]^+$ calcd for $C_{20}H_{25}F_6N_3O_4$: 485.1749; found 485.1788. HPLC analysis: CHIRALCEL OD-3 column [conditions, hexane:*i*PrOH = 95:5, flow rate = 1 mL/min, rt, Rt (minor) = 4.71 min, Rt (major) = 5.25 min]. $[\alpha]_D^{22.8}$ = –17.9 (c = 1.2, MeOH).

***t*-Butyl (*S*)-2-(2-benzamido-3,3-dimethylbutanoyl)hydrazine-1-carboxylate ((*S*)-3e)**

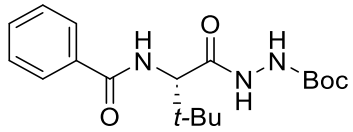

The title compound was synthesized from azlactone **2e** (21.7 mg, 0.1 mmol) following the general procedure and obtained in 60% with 80 %ee (21.0 mg, 0.060 mmol, white solid). mp = 164.6–165.8 °C. ^{1}H NMR (400 MHz, Methanol-d4) δ = 7.84–7.72 (m, 2H), 7.58–7.52 (m, 1H), 7.50–7.42 (m, 2H), 4.57 (s, 1H), 1.45 (s, 9H), 1.11 (s, 9H). ^{13}C NMR (100 MHz, Methanol-d4) δ = 172.3 (*C*O), 169.9 (*C*O), 157.3 (*C*O), 135.5 (*C*), 132.9 (*C*H), 129.6 (*C*H, 2C), 128.4 (*C*H, 2C), 81.6 (*C*), 60.7 (*C*H), 36.1 (*C*), 28.6 (*C*H$_3$, 3C), 27.2 (*C*H$_3$, 3C). HRMS-FAB (*m/z*): $[M+H]^+$ calcd for $C_{18}H_{27}N_3O_4$: 349.2001; found 349.2082. HPLC analysis: CHIRALPAK IA column [conditions, hexane:*i*PrOH = 92:8, flow rate = 1 mL/min, rt, Rt (minor) = 12.78 min, Rt (major) = 23.30 min]. $[\alpha]_D^{24.4}$ = –4.0 (c = 1.3, MeOH).

***t*-Butyl (*S*)-2-(3,3-dimethyl-2-(2-methylbenzamido)butanoyl)hydrazine-1-carboxylate** ((*S*)-**3f**)

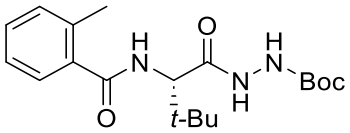

The title compound was synthesized from azlactone **2f** (23.1 mg, 0.1 mmol) following the general procedure and obtained in 48% yield with 76 %ee (17.4 mg, 0.048 mmol, white solid). mp = 171.7–173.6 °C. ^{1}H NMR (400 MHz, Methanol-d4) δ = 7.36–7.32 (m, 2H), 7.26–7.22 (m, 2H), 4.53 (s, 1H), 2.39 (s, 3H), 1.47 (s, 9H), 1.12 (s, 9H). ^{13}C NMR (100 MHz, Methanol-d4) δ = 172.8 (*C*O), 172.2 (*C*O), 157.3 (*C*O), 137.8 (*C*), 136.8 (*C*), 131.7 (*C*H), 130.9 (*C*H), 128.1 (*C*H), 126.7 (*C*H), 81.6 (*C*), 60.8 (*C*H), 35.8 (*C*), 28.6 (*C*H$_3$, 3C), 27.2 (*C*H$_3$, 3C), 19.8 (*C*H$_3$). HRMS-FAB (*m/z*): [M+H]$^+$ calcd for $C_{19}H_{29}N_3O_4$: 363.2158; found 363.2238. HPLC analysis: CHIRALCEL OD-3 column [conditions, hexane:*i*PrOH = 95:5, flow rate = 1 mL/min, rt, Rt (minor) = 9.52 min, Rt (major) = 13.63 min]. $[\alpha]_D^{23.9}$ = –46.0 (c = 0.9, MeOH).

***t*-Butyl (*S*)-2-(2-(4-methoxybenzamido)-3,3-dimethylbutanoyl)hydrazine-1-carboxylate** ((*S*)-**3g**)

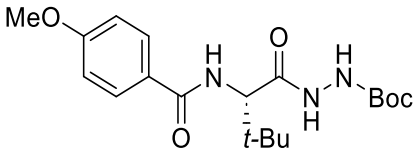

The title compound was synthesized from azlactone **2g** (24.7 mg, 0.1 mmol) following the general procedure and obtained in 45% yield with 74 %ee (17.1 mg, 0.045 mmol, white solid). mp = 182.6–185.2 °C. ^{1}H NMR (400 MHz, Methanol-d4) δ = 7.81 (d, *J* = 8.2 Hz, 2H), 7.00 (d, *J* = 8.2 Hz, 2H), 4.56 (s, 1H), 3.85 (s, 3H), 1.45 (s, 9H), 1.10 (s, 9H). ^{13}C NMR (100 MHz, Methanol-d4) δ = 172.4 (*C*O), 169.4 (*C*O), 164.1 (*C*), 157.3 (*C*O), 130.3 (*C*H, 2C), 127.4 (*C*), 114.8 (*C*H, 2C), 80.8 (*C*), 60.6 (*C*H), 56.0 (*C*H$_3$), 36.1 (*C*), 28.6 (*C*H$_3$, 3C), 27.2 (*C*H$_3$, 3C). HRMS-FAB (*m/z*): [M+H]$^+$ calcd for $C_{19}H_{29}N_3O_5$: 379.2107; found 379.2185. HPLC analysis: CHIRALPAK AD-H column [conditions, hexane:*i*PrOH = 8:2, flow rate = 1 mL/min, rt, Rt (minor) = 15.70 min, Rt (major) = 25.93 min]. $[\alpha]_D^{23.4}$ = –7.2 (c = 0.4, MeOH).

***t*-Butyl (*S*)-2-(3,3-dimethyl-2-(2,3,4,5-tetrachloro-6-(isopropoxycarbonyl)benzamido)butanoyl) hydrazine-1-carboxylate** ((*S*)-**3h**)

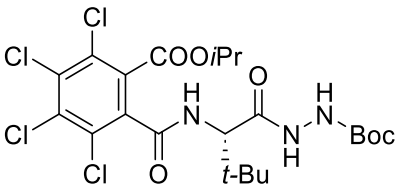

The title compound was synthesized from azlactone **2h** (132.3 mg, 0.3 mmol) following the general procedure within 41 reaction hours and obtained in 89% yield with 92 %ee (153.0 mg, 0.27 mmol, white solid). mp = 183.2–186.4 °C. ^{1}H NMR (400 MHz, Methanol-d4) δ = 5.24–5.14 (m, 1H), 4.42 (s, 1H), 1.47 (s, 9H), 1.35 (dd, *J* = 6.2, 3.9 Hz, 6H), 1.11 (s, 9H). ^{13}C NMR (100 MHz, Methanol-d4) δ = 171.1 (*C*O), 165.5 (*C*O), 164.7 (*C*O), 157.2 (*C*O), 136.7 (*C*), 135.6 (*C*), 135.2 (*C*), 133.9 (*C*), 131.6 (*C*), 130.6 (*C*), 81.5

(*C*), 72.7 (*C*H), 61.3 (*C*H), 36.0 (*C*), 28.6 (*C*H$_3$, 3C), 27.3 (*C*H$_3$, 3C), 21.8 (*C*H$_3$, 2C). HRMS-FAB (*m/z*): [M+H]$^+$ calcd for $C_{22}H_{29}Cl_4N_3O_6$: 571.0810; found 571.0890. HPLC analysis: CHIRALPAK IA column [conditions, hexane:*i*PrOH = 1:1, flow rate = 1 mL/min, rt, Rt (minor) = 3.91 min, Rt (major) = 5.62 min]. $[\alpha]_D^{26.8}$ = –46.1 (c = 1.0, MeOH).

***t*-Butyl (*S*)-2-(2-(2-(trifluoromethyl)benzamido)butanoyl)hydrazine-1-carboxylate** ((*S*)-**3i**)

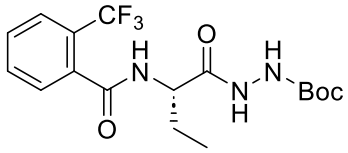

The title compound was synthesized from azlactone **2i** (25.7 mg, 0.1 mmol) following the general procedure and obtained in 90% yield with 58 %ee (35.0 mg, 0.090 mmol, white solid). mp = 115.9–118.6 °C. ^{1}H NMR (400 MHz, Methanol-d4) δ = 7.76 (d, *J* = 7.8 Hz, 1H), 7.71–7.59 (m, 3H), 4.48 (t, *J* = 6.2 Hz, 1H), 1.99–1.89 (m, 1H), 1.84–1.73 (m, 1H), 1.48 (s, 9H), 1.07 (t, *J* = 7.3 Hz, 3H). ^{13}C NMR (100 MHz, Methanol-d4) δ = 173.6 (*C*O), 170.5 (*C*O), 157.5 (*C*O), 136.8 (*C*), 133.3 (*C*H), 131.1 (*C*H), 129.9 (*C*H), 128.3 (q, *J* = 31.4 Hz, *C*), 127.4 (q, *J* = 4.8 Hz, *C*H), 125.0 (q, *J* = 271.8 Hz, *C*), 81.7 (*C*), 55.1 (*C*H), 28.5 (*C*H$_3$, 3C), 26.5 (*C*H$_2$), 10.6 (*C*H$_3$). ^{19}F NMR (376 MHz, Methanol-d4) δ = –59.7. Elemental Analysis calcd for $C_{17}H_{22}F_3N_3O_4$: C, 52.44; H, 5.70; N, 10.79. Found: C, 52.45; H, 5.92; N, 10.49. HPLC analysis: CHIRALCEL OD-3 column [conditions, hexane:*i*PrOH = 95:5, flow rate = 1 mL/min, rt, Rt (minor) = 11.06 min, Rt (major) = 22.45 min]. $[\alpha]_D^{23.7}$ = –26.7 (c = 0.8, MeOH), $[\alpha]_D^{19.7}$ = –17.4 (c = 1.0, $CHCl_3$).

***t*-Butyl 2-((2-(trifluoromethyl)benzoyl)-*L*-phenylalanyl)hydrazine-1-carboxylate** ((*S*)-**3j**)

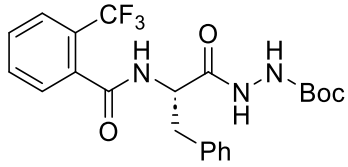

The title compound was synthesized from azlactone **2j** (31.9 mg, 0.1 mmol) following the general procedure and obtained in 99% yield with 44 %ee (44.7 mg, 0.099 mmol, white solid). mp = 190.5–197.3 °C. ^{1}H NMR (400 MHz, Methanol-d4) δ = δ 7.71–7.66 (m, 1H), 7.63–7.55 (m, 2H), 7.36–7.20 (m, 6H), 4.93–4.88 (m, 1H), 3.31–3.22 (m, 1H), 3.04–2.97 (m, 1H), 1.48 (s, 9H). ^{13}C NMR (100 MHz, Methanol-d4) δ = 173.0 (*C*O), 170.3 (*C*O), 157.5 (*C*O), 138.3 (*C*), 136.5 (*C*H), 133.1 (*C*H), 131.1 (*C*H), 130.4 (*C*H, 2C), 129.7 (*C*H), 129.4 (*C*H, 2C), 128.3 (q, *J* = 32.4 Hz, *C*), 127.8 (*C*), 127.3 (q, *J* = 4.7 Hz, *C*H), 124.9 (q, *J* = 271.7 Hz, *C*), 81.8 (*C*), 54.6 (*C*H), 38.8 (*C*H$_2$), 28.5 (*C*H$_3$, 3C). ^{19}F NMR (376 MHz, Methanol-d4) δ = –60.3. Elemental Analysis calcd for $C_{22}H_{24}F_3N_3O_4$: C, 58.53; H, 5.36; N, 9.31. Found: C, 58.35; H, 5.46; N, 9.18. HPLC analysis: CHIRALPAK IF column [conditions, hexane:*i*PrOH = 7:3, flow rate = 1 mL/min, rt, Rt (minor) = 4.99 min, Rt (major) = 6.17 min]. $[\alpha]_D^{20.2}$ = –13.1 (c = 1.0, $CHCl_3$).

***t*-Butyl 2-((2-(trifluoromethyl)benzoyl)-*L*-valyl)hydrazine-1-carboxylate** ((*S*)-**3k**)

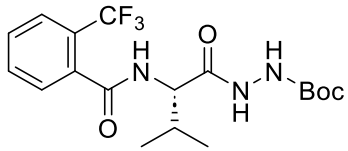

The title compound was synthesized from azlactone **2k** (27.1 mg, 0.1 mmol) following the general procedure and obtained in 95% yield with 70 %ee (38.3 mg, 0.095 mmol, white solid). mp = 174.2–176.4 °C. ^{1}H NMR (400 MHz, Methanol-d4) δ = 7.76 (d, *J* = 8.2 Hz, 1H), 7.69 (t, *J* = 7.1 Hz, 1H), 7.63 (t, *J* = 7.8 Hz, 1H), 7.58–7.52 (m, 1H), 4.37 (d, *J* = 7.8 Hz, 1H), 2.20–2.10 (m, 1H), 1.47 (s, 9H), 1.09 (d, *J* = 6.4 Hz, 2H), 1.05 (d, *J* = 6.9 Hz, 3H). ^{13}C NMR (150 MHz, Methanol-d4) δ = 173.0 (*C*O), 170.5 (*C*O), 157.3 (*C*O), 136.9 (*C*), 133.3 (*C*H), 131.1 (*C*H), 129.9 (*C*H), 128.3 (q, *J* = 31.7 Hz, *C*), 127.4 (d, *J* = 4.4 Hz, *C*H), 125.1 (q, *J* = 271.4 Hz, *C*), 81.6 (*C*), 59.2 (*C*H), 32.1 (*C*H), 28.6 (*C*H$_3$, 3C), 19.8 (*C*H$_3$, C), 18.9 (*C*H$_3$, C). ^{19}F NMR (376 MHz, Methanol-d4) δ = –60.3. HRMS-FAB (*m/z*): [M+H]$^+$ calcd for $C_{18}H_{24}F_3N_3O_4$: 403.1718; found 403.1795. HPLC analysis: CHIRALPAK IF column [conditions, hexane:*i*PrOH = 9:1, flow rate = 1 mL/min, rt, Rt (minor) = 10.60 min, Rt (major) = 18.57 min]. $[\alpha]_D^{19.8}$ = –22.4 (c = 1.0, $CHCl_3$).

***t*-Butyl (*S*)-2-(3-ethyl-2-(2-(trifluoromethyl)benzamido)pentanoyl)hydrazine-1-carboxylate** ((*S*)-**3l**)

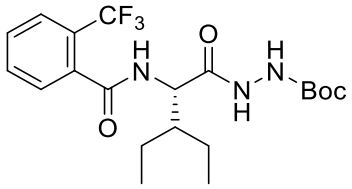

The title compound was synthesized from azlactone **2l** (29.9 mg, 0.1 mmol) following the general procedure and obtained in 96% yield with 68 %ee (41.4 mg, 0.096 mmol, white solid). The product **3l** (41.4 mg, 0.096 mmol) was subjected to preferential enrichment (method B, see Section 2-3-1), affording **3l** in 70% (28.9 mg, 0.067 mmol) recovery with 96 %ee from the supernatant and 30% (12.4 mg, 0.029 mmol) recovery with 6 %ee from the crystals. mp = 176.2–179.3 °C. ^{1}H NMR (400 MHz, Methanol-d4) δ = 7.75 (d, *J* = 7.8 Hz, 1H), 7.68 (t, *J* = 1.9 Hz, 1H), 7.62 (t. *J* = 1.9 Hz, 1H), 7.59–7.54 (m, 1H), 4.67 (d, *J* = 7.3 Hz, 1H), 1.87–1.79 (m, 1H), 1.67–1.50 (m, 5H), 1.47 (s, 9H), 1.43–1.39 (m, 1H), 0.99 (t, *J* = 7.3 Hz, 3H), 0.93 (t, *J* = 7.3 Hz, 3H). ^{13}C NMR (100 MHz, Methanol-d4) δ = 173.5 (*C*O), 170.5 (*C*O), 157.3 (*C*O), 136.9 (*C*), 133.2 (*C*H), 131.0 (*C*H), 129.9 (*C*H), 128.2 (q, *J* = 31.5 Hz, *C*), 127.3 (d or q, *J* = 4.8 Hz, *C*H), 125.2 (q, *J* = 271.8 Hz, *C*), 81.6 (*C*), 55.2 (*C*H), 43.9 (*C*H), 28.6 (*C*H$_3$, 3C), 22.6 (*C*H$_2$), 21.7 (*C*H$_2$), 11.5 (*C*H$_3$), 10.5 (*C*H$_3$). ^{19}F NMR (376 MHz, Methanol-d4) δ = –60.2. HRMS-FAB (*m/z*): [M+H]+ calcd for $C_{20}H_{28}F_3N_3O_4$: 431.4562; found 431.2095. HPLC analysis: CHIRALPAK IF column [conditions, hexane:*i*PrOH = 9:1, flow rate = 1 mL/min, rt, Rt (minor) = 9.87 min, Rt (major) = 14.75 min] , or CHIRALCEL OD-3 column [conditions, hexane:*i*PrOH = 95:5, flow rate = 1 mL/min, rt, Rt (minor) = 8.02 min, Rt (major) = 10.24 min]. For 68 %ee. $[\alpha]_D^{19.8}$ = –23.5 (c = 1.0, $CHCl_3$).

***t*-Butyl (*S*)-2-(3,3,3-triphenyl-2-(2-(trifluoromethyl)benzamido)propanoyl)hydrazine-1-carboxylate** ((*S*)-**3m**)

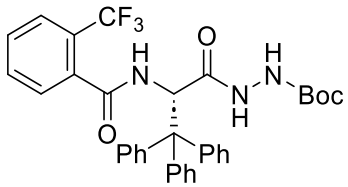

The title compound was synthesized from azlactone **2m** (47.1 mg, 0.1 mmol) following the general procedure and obtained in 74% yield with 88 %ee (44.7 mg, 0.074 mmol, white solid). mp = 165.7–168.6 °C. ^{1}H NMR (400 MHz, Methanol-d4) δ = 7.70 (d, *J* = 7.3 Hz, 1H), 7.60–7.51 (m, 2H), 7.46–7.42 (m, 6H), 7.30–7.23 (m, 7H), 7.23–7.17 (m, 3H), 6.47 (s, 1H), 1.41 (s, 9H). ^{13}C NMR (100 MHz, Methanol-d4) δ = 170.8 (*C*O), 169.5 (*C*O), 156.9 (*C*O), 145.0 (*C*, 3C), 136.3 (*C*), 133.3 (*C*H), 131.6 (*C*H), 131.1 (*C*H, 6C), 129.6 (*C*H), 129.0 (*C*H, 6C), 128.4 (q, J = 32.4 Hz, C), 127.8 (*C*H, 3C), 127.6 (d, *J* = 3.9 Hz, *C*H), 124.9 (q, *J* = 271.8 Hz, *C*), 81.6 (*C*), 62.4 (*C*), 57.8 (*C*H), 28.5 (*C*H$_3$, 3C). ^{19}F NMR (376 MHz, Methanol-d4) δ = –60.0. Elemental Analysis calcd for $C_{34}H_{32}F_3N_3O_4$: C, 67.65; H, 5.34; N, 9.44. Found: C, 67.82; H, 5.67; N, 6.70. HPLC analysis: CHIRALPAK AD-H column [conditions, hexane:*i*PrOH = 7:3, flow rate = 1 mL/min, rt, Rt (minor) = 6.21 min, Rt (major) = 11.96 min]. $[\alpha]_D^{20.4}$ = +36.3 (c = 1.0, $CHCl_3$).

(*S*)-*N*-(1-hydrazineyl-3,3-dimethyl-1-oxobutan-2-yl)-2-(trifluoromethyl)benzamide ((S)-**3n**)

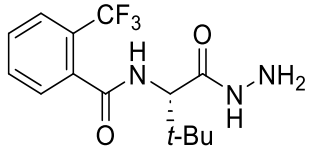

The title compound was synthesized from azlactone **2a** (28.5 mg, 0.1 mmol) and hydrazine (4.8 mg, 0.15mmol) following the general procedure and obtained in 97% yield with 16 %ee (30.7 mg, 0.097 mmol, white solid). mp = 192.4–200.4 °C. ^{1}H NMR (400 MHz, Methanol-d4) δ = 7.76 (d, *J* = 7.8 Hz, 1H), 7.69 (t, *J* = 7.1 Hz, 1H), 7.63 (t, *J* = 7.3 Hz, 1H), 7.52 (d, *J* = 7.8 Hz, 1H), 4.41 (s, 1H), 1.06 (s, 9H). ^{13}C NMR (100 MHz, Methanol-d4) δ = 170.7 (*C*O), 168.9 (*C*O), 137.0 (*C*), 133.3 (*C*H), 131.0 (*C*H), 129.7 (*C*H), 128.2 (q, *J* = 31.3 Hz, *C*), 127.4 (d or q, *J* = 4.8 Hz, *C*H), 125.2 (q, *J* = 271.2 Hz, *C*), 61.2 (*C*H), 35.7 (*C*), 27.1 (*C*H$_3$, 3C). ^{19}F NMR (376 MHz, Methanol-d4) δ = –60.3. HRMS-FAB (*m/z*): $[M+H]^+$ calcd for $C_{14}H_{18}F_3N_3O_2$: 317.3122; found 317.1423. HPLC analysis: CHIRALCEL OD-3 column [conditions, hexane:*i*PrOH = 85:15, flow rate = 1 mL/min, rt, Rt (minor) = 10.38 min, Rt (major) = 13.55 min]. $[\alpha]_D^{24.3}$ = +2.8 (c = 1.0, MeOH).

2,2,2-Trichloroethyl (*S*)-2-(3,3-dimethyl-2-(2-(trifluoromethyl)benzamido)butanoyl)hydrazine-1-carboxylate ((*S*)-**3o**)

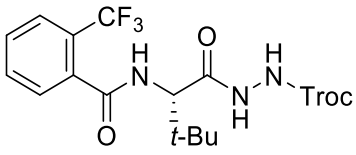

The title compound was synthesized from azlactone **2a** (28.5 mg, 0.1 mmol) and Troc-hydrazine[5] (31.1

mg, 0.15mmol) following the general procedure and obtained in 21% yield with 70 %ee (10.5 mg, 0.021 mmol, colorless oil). ^{1}H NMR (400 MHz, Methanol-d4) δ = 7.76 (d, *J* = 7.8 Hz, 1H), 7.69 (t, *J* = 7.3 Hz, 1H), 7.63 (t, *J* = 7.1 Hz, 1H), 7.54 (d, *J* = 7.3 Hz, 1H), 4.80 (s, 2H), 4.51 (s, 1H), 1.12 (s, 9H). ^{13}C NMR (100 MHz, Methanol-d4) δ = 171.9 (CO), 170.5 (CO), 158.6 (CO), 136.9 (C), 133.3 (CH), 131.1 (CH), 129.9 (CH), 128.4 (s or q, unresolved *J*, C), 127.4 (d or q, *J* = 3.8 Hz, CH), 125.1 (q, *J* = 271.7 Hz, C), 97.0 (C), 75.6 (CH2), 61.2 (CH), 35.7 (C), 27.1 (CH3, 3C). ^{19}F NMR (376 MHz, Methanol-d4) δ = –60.2. HRMS-FAB (m/z): $[M+H]^+$ calcd for $C_{17}H_{19}C_{l3}F_3N_3O_4$: 491.0393; found 491.0471. HPLC analysis: CHIRALPAK IB column [conditions, hexane:iPrOH = 8:2, flow rate = 1 mL/min, rt, Rt (minor) = 4.36 min, Rt (major) = 5.27 min]. $[\alpha]_D^{26.4}$ = –6.6 (c = 0.7, MeOH).

(*S*)-*N*-(3,3-Dimethyl-1-oxo-1-(2-phenylhydrazineyl)butan-2-yl)-2-(trifluoromethyl)benzamide ((*S*)-**3p**)

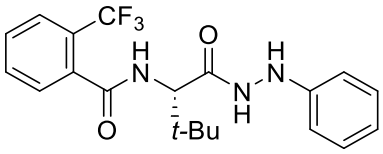

The title compound was synthesized from azlactone **2a** (28.5 mg, 0.1 mmol) and phenylhydrazine (16.2 mg, 0.15mmol) following the general procedure and obtained in 62% yield with over 99 %ee (24.4 mg, 0.062 mmol, yellow solid). mp = 250.3–253.1 °C. ^{1}H NMR (400 MHz, Methanol-d4) δ = 7.77 (dd, *J* = 7.8, 0.9 Hz, 1H), 7.71–7.67 (m, 1H), 7.65-7.62 (m, 1H), 7.53–7.52 (m, 1H), 7.20–7.15 (m, 2H), 6.88–6.84 (m, 2H), 6.80 (tt, *J* = 7.3, 1.1 Hz, 1H), 4.56 (s, 1H), 1.13 (s, 9H). ^{13}C NMR (100 MHz, Methanol-d4) δ = 172.4 (*C*O), 170.7 (*C*O), 149.8 (*C*), 137.0 (*C*), 133.3 (*C*H), 131.0 (*C*H), 129.9 (*C*H), 129.7 (*C*H), 128.2 (q, *J* = 31.4 Hz, *C*), 127.6 (q, *J* = 4.6 Hz, *C*H), 125.2 (q, *J* = 271.2 Hz, *C*), 121.1 (*C*H, 2C), 114.3 (*C*H, 2C), 61.5 (*C*H), 35.4 (*C*), 27.2 (*C*H$_3$, 3C). ^{19}F NMR (376 MHz, Methanol-d4) δ = –60.2. HRMS-FAB (*m/z*): $[M+H]^+$ calcd for $C_{20}H_{22}F_3N_3O_2$: 393.1664; found 393.1682. HPLC analysis: CHIRALCEL OD-3 column [conditions, hexane:*i*PrOH = 95:5, flow rate = 1 mL/min, rt, Rt (major) = 10.51 min, Rt (minor) = 15.17 min]. $[\alpha]_D^{20.4}$ = +27.9 (c = 1.0, $CHCl_3$).

(*S*)-*N*-(1-(2-(4-methoxyphenyl)hydrazineyl)-3,3-dimethyl-1-oxobutan-2-yl)-2-(trifluoromethyl) benzamide ((*S*)-**3q**)

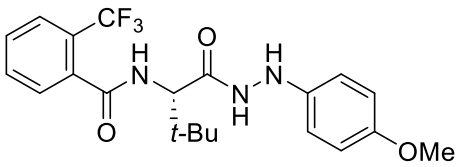

The title compound was synthesized from azlactone **2a** (28.5 mg, 0.1 mmol) and (4-methoxyphenyl) hydrazine (20.7 mg, 0.15mmol) following the general procedure and obtained in 42% yield with 71 %ee (17.8 mg, 0.042 mmol, yellow solid). mp = 176.3–182.2 °C. ^{1}H NMR (400 MHz, Methanol-d4) δ = 7.77 (d, *J* = 7.3 Hz, 1H), 7.69 (t, *J* = 7.1 Hz, 1H), 7.63 (t, *J* = 7.3 Hz, 1H), 7.53–7.51 (m, 1H), 6.84 (dt, *J* = 9.3, 2.6 Hz, 2H), 6.79 (td, *J* = 6.1, 3.4 Hz, 2H), 4.52 (s, 1H), 3.72 (s, 3H), 1.12 (s, 9H). ^{13}C NMR (100 MHz, Methanol-d4) δ = 172.2 (*C*O), 170.7 (*C*O), 155.6 (*C*), 143.4 (*C*), 137.0 (*C*), 133.3 (*C*H), 131.0 (*C*H), 129.7

(*C*H), 128.2 (q, *J* = 31.3 Hz, *C*), 127.4 (q, *J* = 4.6 Hz, *C*H), 125.2 (q, *J* = 268.1 Hz, *C*), 116.2 (*C*H, 2C), 115.4 (*C*H, 2C), 61.6 (*C*H), 56.1 (*C*H$_3$), 35.4 (*C*), 30.7 (*C*H$_3$, 3C). ^{19}F NMR (376 MHz, Methanol-d4) δ = –60.2. HRMS-FAB (*m/z*): $[M+H]^+$ calcd for $C_{21}H_{24}F_3N_3O_3$: 423.4362; found 423.1765. HPLC analysis: CHIRALCEL AD-3 column [conditions, hexane:*i*PrOH = 8:2, flow rate = 1 mL/min, rt, Rt (minor) = 10.13 min, Rt (major) = 12.26 min]. $[\alpha]_D^{25.0}$ = +27.9 (c = 0.5, MeOH).

(*S*)-*N*-(3,3-dimethyl-1-oxo-1-(2-(4-(trifluoromethyl)phenyl)hydrazineyl)butan-2-yl)-2-(trifluoro methyl)benzamide ((S)-**3r**)

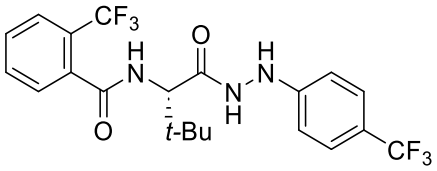

The title compound was synthesized from azlactone **2a** (28.5 mg, 0.1 mmol) and 4-(trifluoromethyl)phenyl hydrazine (26.4 mg, 0.15mmol) following the general procedure and obtained in 39% yield with 29 %ee (17.9 mg, 0.039 mmol, white solid). mp = 247.9–249.0 °C. ^{1}H NMR (400 MHz, Methanol-d4) δ = 7.77 (d, *J* = 7.8 Hz, 1H), 7.69 (t, *J* = 7.6 Hz, 1H), 7.63 (t, *J* = 7.3 Hz, 1H), 7.52 (d, *J* = 7.8 Hz, 1H), 7.43 (d, *J* = 8.7 Hz, 2H), 6.93 (d, *J* = 8.2 Hz, 2H), 4.53 (s, 1H), 1.14 (s, 9H). ^{13}C NMR (100 MHz, Methanol-d4) δ = 172.6 (*C*O), 170.9 (*C*O), 153.1 (*C*), 136.9 (*C*), 133.3 (*C*H), 131.1 (*C*H), 129.7 (*C*H), 128.2 (q, *J* = 31.4 Hz, *C*), 127.4 (q, *J* = 4.8 Hz, *C*H), 127.2 (q, *J* = 3.8 Hz, *C*H), 126.3 (q, *J* = 268.9 Hz, *C*), 125.2 (q, *J* = 271.7 Hz, *C*), 122.0 (q, *J* = 32.4 Hz, *C*), 113.3 (*C*H, 2C), 61.7 (*C*H), 35.2 (*C*), 27.2 (*C*H$_3$, 3C). ^{19}F NMR (376 MHz, Methanol-d4) δ = –60.2, –62.7. HRMS-FAB (*m/z*): $[M+H]^+$ calcd for $C_{21}H_{21}F_6N_3O_2$: 461.1538; found 461.1538. HPLC analysis: CHIRALPAK AD-H column [conditions, hexane:*i*PrOH = 95:5, flow rate = 1 mL/min, rt, Rt (minor) = 39.49 min, Rt (major) = 44.48 min]. $[\alpha]_D^{24.2}$ = +1.4 (c = 0.1, MeOH).

(*S*)-*N*-(1-(2-Benzoylhydrazineyl)-3,3-dimethyl-1-oxobutan-2-yl)-2-(trifluoromethyl)benzamide ((*S*)-**3s**)

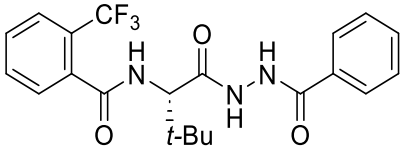

The title compound was synthesized from azlactone **2a** (28.5 mg, 0.1 mmol) and benzoylhydrazine (20.4 mg, 0.15mmol) following the general procedure and obtained in 71% yield with 80 %ee (29.9 mg, 0.071 mmol, white solid). mp = 219.2–222.5 °C. ^{1}H NMR (400 MHz, Methanol-d4) δ = 7.92–7.85 (m, 2H), 7.77 (d, *J* = 7.8 Hz, 1H), 7.70 (t, *J* = 7.1 Hz, 1H), 7.63 (t, *J* = 7.3 Hz, 1H), 7.61–7.53 (m, 2H), 7.53–7.44 (m, 2H), 4.62 (s, 1H), 1.18 (s, 9H). ^{13}C NMR (100 MHz, Methanol-d4) δ = 171.5 (*C*O), 170.5 (*C*O), 168.9 (*C*O), 137.0 (*C*), 133.7 (*C*), 133.3 (*C*H), 133.2 (*C*H), 131.0 (*C*H), 129.9 (*C*H), 129.6 (*C*H, 2C), 128.7 (*C*H, 2C), 128.2 (q, *J* = 32.1 Hz, *C*), 127.4 (q, *J* = 4.9 Hz, *C*H), 125.2 (q, *J* = 271.1 Hz, *C*), 61.4 (*C*H), 35.7 (*C*), 27.2 (*C*H$_3$, 3C). ^{19}F NMR (376 MHz, Methanol-d4) δ = –60.3. HRMS-FAB (*m/z*): $[M+H]^+$ calcd for $C_{21}H_{22}F_3N_3O_3$: 421.1613; found 421.1681. HPLC analysis: CHIRALPAK IA column [conditions,

hexane:*i*PrOH = 85:15, flow rate = 1 mL/min, rt, Rt (major) = 10.30 min, Rt (minor) = 12.85 min]. $[\alpha]_D^{24.1}$ = –24.6 (c = 1.2, MeOH).

(*S*)-*N*-(1-(2-(4-Methoxybenzoyl)hydrazineyl)-3,3-dimethyl-1-oxobutan-2-yl)-2-(trifluoromethyl) benzamide ((*S*)-**3t**)

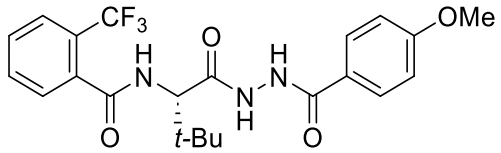

The title compound was synthesized from azlactone **2a** (28.5 mg, 0.1 mmol) and *p*-anisoylhydrazine (24.9 mg, 0.15mmol) following the general procedure and obtained in 97% yield with 80 %ee (43.8 mg, 0.097 mmol, white solid). The product **3t** (43.8 mg, 0.097 mmol) was subjected to preferential enrichment (method B, see Section 2-3-1), affording **3t** in 84% (36.7 mg, 0.081 mmol) recovery with 90 %ee from the supernatant and 16% (7.0 mg, 0.016 mmol) recovery with 34 %ee from the crystals. mp = 240.4–244.1 °C. ^{1}H NMR (400 MHz, Methanol-d4) δ = 7.90–7.83 (m, 2H), 7.76 (d, *J* = 7.3 Hz, 1H), 7.70 (t, *J* = 7.3 Hz, 1H), 7.63 (t, *J* = 7.6 Hz, 1H), 7.57 (d, *J* = 7.3 Hz, 1H), 7.03–6.89 (m, 2H), 4.61 (s, 1H), 3.86 (s, 3H), 1.17 (s, 9H). ^{13}C NMR (100 MHz, Methanol-d4) δ = 171.5 (*C*O), 170.4 (*C*O), 168.6 (*C*O), 164.4 (*C*), 137.0 (*C*), 133.3 (*C*H), 131.0 (*C*H), 130.6 (*C*H, 2C), 129.9 (*C*H), 128.2 (q, *J* = 31.4 Hz, *C*), 127.4 (q, *J* = 4.6 Hz, *C*H), 125.6 (*C*), 125.2 (q, *J* = 271.2 Hz, *C*), 114.8 (*C*H, 2C), 61.4 (*C*H), 55.9 (*C*H$_3$), 35.7 (*C*), 27.2 (*C*H$_3$, 3C). ^{19}F NMR (376 MHz, Methanol-d4) δ = –60.2. HRMS-FAB (*m/z*): $[M+H]^+$ calcd for $C_{22}H_{24}F_3N_3O_4$: 451.1718; found 451.1794. HPLC analysis: CHIRALCEL AD-3 column [conditions, hexane:*i*PrOH = 87:13, flow rate = 1 mL/min, rt, Rt (major) = 50.97 min, Rt (minor) = 58.92 min], or [conditions, hexane:*i*PrOH = 9:1, flow rate = 1 mL/min, rt, Rt (major) = 52.30 min, Rt (minor) = 61.03 min]. For 80 %ee, $[\alpha]_D^{24.6}$ = –27.2 (c = 1.0, MeOH).

(*S*)-*N*-(3,3-Dimethyl-1-oxo-1-(2-(4-(trifluoromethyl)benzoyl)hydrazineyl)butan-2-yl)-2-(trifluoro methyl)benzamide ((*S*)-**3u**)

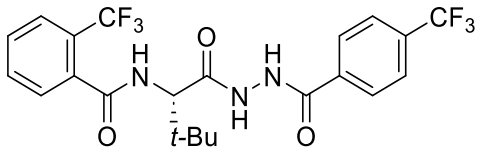

The title compound was synthesized from azlactone **2a** (28.5 mg, 0.1 mmol) and 4-(trifluoromethyl)benzoyl hydrazine (30.6 mg, 0.15mmol) following the general procedure and obtained in 69% yield with 69 %ee (33.8 mg, 0.069 mmol, white solid). mp = 271.4–272.6 °C. ^{1}H NMR (400 MHz, Methanol-d4) δ = δ 8.06 (d, *J* = 8.3 Hz, 2H), 7.81 (d, *J* = 8.1 Hz, 2H), 7.76 (d, *J* = 7.6 Hz, 1H), 7.69 (t, *J* = 7.3 Hz, 1H), 7.63 (t, *J* = 7.6 Hz, 1H), 7.57 (d, J = 7.3 Hz, 1H), 4.63 (s, 1H), 1.18 (s, 9H). ^{13}C NMR (100 MHz, Methanol-d4) δ = 171.5 (*C*O), 170.5 (*C*O), 167.5 (*C*O), 137.5 (*C*), 137.0 (*C*), 134.5 (q, *J* = 32.1 Hz, *C*), 133.3 (*C*H), 131.0 (*C*H), 129.9 (*C*H), 129.5 (*C*H, 2C), 128.2 (q, *J* = 31.3 Hz, *C*), 127.4 (q, *J* = 4.9 Hz, *C*H), 126.6 (q, *J* = 3.6 Hz, *C*H, 2C), 125.22 (q, *J* = 269.7 Hz, *C*), 125.16 (q, *J* = 271.2 Hz, *C*), 61.4 (*C*H), 35.7 (*C*), 27.2 (*C*H$_3$, 3C). ^{19}F NMR

(376 MHz, Methanol-d4) δ = –60.2, –64.5. Elemental Analysis calcd for $C_{22}H_{21}F_6N_3O_4$: C, 53.99; H, 4.33; N, 8.59. Found: C, 54.15; H, 4.44; N, 8.49. HPLC analysis: CHIRALCEL AD-3 column [conditions, hexane:*i*PrOH = 8:2, flow rate = 1 mL/min, rt, Rt (minor) = 8.85 min, Rt (major) = 10.86 min]. $[\alpha]_D^{19.6}$ = –22.0 (c = 1.0, $CHCl_3$).

Methyl (*S*)-2-(3,3-dimethyl-2-(2-(trifluoromethyl)benzamido)butanoyl)hydrazine-1-carboxylate ((*S*)-**3v**)

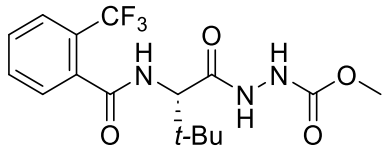

The title compound was synthesized from azlactone **2a** (28.5 mg, 0.1 mmol) and methoxycarbonyl hydrazine (13.5 mg, 0.15mmol) following the general procedure and obtained in 81% yield with 74 %ee (30.4 mg, 0.081 mmol, white solid). mp = 214.0–215.9 °C. ^{1}H NMR (400 MHz, Methanol-d4) δ = 7.76 (d, *J* = 7.8 Hz, 1H), 7.69 (t, *J* = 7.1 Hz, 1H), 7.63 (t, *J* = 7.3 Hz, 1H), 7.53 (d, *J* = 7.3 Hz, 1H), 4.50 (s, 1H), 3.71 (s, 3H), 1.11 (s, 9H). ^{13}C NMR (100 MHz, Methanol-d4) δ = 172.1 (*C*O), 170.5 (*C*O), 158.8 (*C*O), 137.0 (*C*), 133.3 (*C*H), 131.0 (*C*H), 129.8 (*C*H), 128.2 (q, *J* = 31.4 Hz, *C*), 127.3 (q, *J* = 4.7 Hz, *C*H), 125.1 (q, *J* = 271.8 Hz, *C*), 61.1 (*C*H), 53.1 (*C*H_3), 35.7 (*C*), 27.1 (*C*H_3, 3C). ^{19}F NMR (376 MHz, Methanol-d4) δ = –60.3. HRMS-FAB (*m/z*): $[M+H]^+$ calcd for $C_{16}H_{20}F_3N_3O_4$: 375.3482; found 375.1481. HPLC analysis: CHIRALCEL OD-3 column [conditions, hexane:*i*PrOH = 9:1, flow rate = 1 mL/min, rt, Rt (minor) = 8.79 min, Rt (major) = 14.82 min]. $[\alpha]_D^{19.8}$ = –22.3 (c = 1.0, $CHCl_3$).

Ethyl (*S*)-2-(3,3-dimethyl-2-(2-(trifluoromethyl)benzamido)butanoyl)hydrazine-1-carboxylate ((*S*)-**3w**)

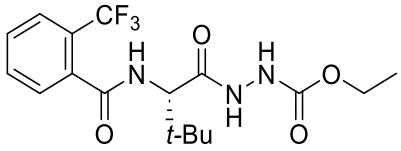

The title compound was synthesized from azlactone **2a** (28.5 mg, 0.1 mmol) and ethoxycarbonylhydrazine (15.6 mg, 0.15mmol) following the general procedure and obtained in 54% yield with 68 %ee (21.0 mg, 0.054 mmol, white solid). mp = 215.6–217.2 °C. ^{1}H NMR (400 MHz, Methanol-d4) δ = 7.75 (d, *J* = 7.8 Hz, 1H), 7.69 (t, *J* = 7.6 Hz, 1H), 7.63 (t, *J* = 7.3 Hz, 1H), 7.53 (d, *J* = 7.3 Hz, 1H), 4.50 (s, 1H), 4.19–4.07 (m, 2H), 1.30–1.21 (m, 3H), 1.11 (s, 9H). ^{13}C NMR (100 MHz, Methanol-d4) δ = 172.9 (*C*O), 170.4 (*C*O), 158.4 (*C*O), 137.0 (*C*), 133.2 (*C*H), 131.0 (*C*H), 129.8 (*C*H), 128.2 (q, *J* = 32.1 Hz, *C*), 127.3 (d or q, *J* = 2.9 Hz, *C*H), 125.1 (q, *J* = 271.1 Hz, *C*), 61.5 (*C*H), 35.7 (*C*), 27.1 (*C*H_3, 3C), 20.9 (*C*H_2), 14.5 (*C*H_3). ^{19}F NMR (376 MHz, Methanol-d4) δ = –60.2. HRMS-FAB (*m/z*): $[M+H]^+$ calcd for $C_{17}H_{22}F_3N_3O_4$: 389.1562; found 389.1643. HPLC analysis: CHIRALCEL OJ-H column [conditions, hexane:*i*PrOH = 95:5, flow rate = 1 mL/min, rt, Rt (minor) = 9.89 min, Rt (major) = 16.91 min]. $[\alpha]_D^{23.7}$ = –26.7 (c = 1.2, $CHCl_3$).

Benzyl (*S*)-2-(3,3-dimethyl-2-(2-(trifluoromethyl)benzamido)butanoyl)hydrazine-1-carboxylate ((*S*)-**3x**)

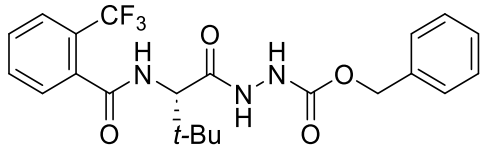

The title compound was synthesized from azlactone **2a** (28.5 mg, 0.1 mmol) and benzyl hydrazine carboxylate (24.9 mg, 0.15mmol) following the general procedure and obtained in 75% yield with 56 %ee (33.8 mg, 0.075 mmol, white solid). The product **3x** (33.8 mg, 0.075 mmol) was subjected to preferential enrichment (method B, see Section 2-3-1), affording **3x** in 44% (14.8 mg, 0.033 mmol) recovery with 96 %ee from the supernatant and 56% (18.9 mg, 0.042 mmol) recovery with 50 %ee from the crystals. mp = 149.8–152.1 °C. ^{1}H NMR (400 MHz, Methanol-d4) δ = 7.75 (d, *J* = 8.2 Hz, 1H), 7.70–7.59 (m, 2H), 7.54 (d, *J* = 4.1 Hz, 1H), 7.41–7.27 (m, 5H), 5.15 (dd, *J* = 15.1, 12.4 Hz, 2H), 4.50 (s, 1H), 1.12 (s, 9H). ^{13}C NMR (100 MHz, Methanol-d4) δ = 172.0 (*C*O), 170.5 (*C*O), 158.2 (*C*O), 137.7 (*C*), 136.9 (*C*), 133.2 (*C*H), 131.0 (*C*H), 129.8 (*C*H), 129.5 (*C*H, 2C), 129.2 (*C*H, 2C), 129.0 (*C*H), 128.2 (q, *J* = 32.4 Hz, *C*), 127.4 (d or q, *J* = 3.8 Hz, *C*H), 125.1 (q, *J* = 268.9 Hz, *C*), 68.2 (*C*H$_2$), 61.2 (*C*H), 35.7 (*C*), 27.1 (*C*H$_3$, 3C). ^{19}F NMR (376 MHz, Methanol-d4) δ = –60.2. Elemental Analysis calcd for $C_{22}H_{24}F_3N_3O_4$: C, 58.53; H, 5.36; N, 9.31. Found: C, 59.08; H, 5.59; N, 9.03. HPLC analysis: CHIRALCEL OD-3 column [conditions, hexane:*i*PrOH = 8:2, flow rate = 1 mL/min, rt, Rt (minor) = 6.29 min, Rt (major) = 9.63 min], or [conditions, hexane:*i*PrOH = 85:15, flow rate = 1 mL/min, rt, Rt (minor) = 6.94 min, Rt (major) = 11.71 min]. For 56 %ee, $[\alpha]_D^{19.3}$ = –8.2 (c = 1.0, $CHCl_3$).

***t*-Butyl (*S*)-2-(3,3-dimethyl-2-(2-(trifluoromethyl)benzamido)butanoyl)-1-methylhydrazine -1-carboxylate** ((*S*)-**3y**)

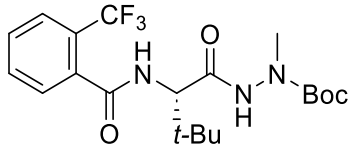

The title compound was synthesized from azlactone **2a** (28.5 mg, 0.1 mmol) and 1-Boc-1-methylhydrazine (21.9 mg, 0.15mmol) following the general procedure and obtained in 53% yield with 18 %ee (22.9 mg, 0.053 mmol, white solid). mp = 193.3–197.4 °C. ^{1}H NMR (400 MHz, Methanol-d4) δ = 7.76 (d, *J* = 7.8 Hz, 1H), 7.69 (t, *J* = 7.8 Hz, 1H), 7.63 (t, *J* = 7.6 Hz, 1H), 7.53 (d, *J* = 8.2 Hz, 1H), 4.42 (s, 1H), 3.09 (s, 3H), 1.46 (s, 9H), 1.11 (s, 9H). ^{13}C NMR (100 MHz, Methanol-d4) δ = 170.7 (*C*O), 170.6 (*C*O), 157.0 (*C*O), 136.9 (*C*), 133.3 (*C*H), 131.0 (*C*H), 129.8 (*C*H), 128.2 (q, *J* = 21.1 Hz, *C*), 127.4 (d, *J* = 2.9 Hz, *C*H), 125.2 (q, *J* = 181.3 Hz, *C*), 82.6 (*C*), 61.3 (*C*H), 40.0 (*C*H$_3$), 35.5 (*C*), 28.6 (*C*H$_3$, 3C), 27.2 (*C*H$_3$, 3C). ^{19}F NMR (376 MHz, Methanol-d4) δ = –60.2. HRMS-FAB (*m/z*): $[M+H]^+$ calcd for $C_{20}H_{28}F_3N_3O_4$: 431.2031; found 431.2109. HPLC analysis: CHIRALCEL OD-3 column [conditions, hexane:*i*PrOH = 97:3, flow rate = 1 mL/min, rt, Rt (minor) = 6.71 min, Rt (major) = 8.13 min]. $[\alpha]_D^{19.9}$ = –4.5 (c = 1.0, MeOH).

***t*-Butyl (*S*)-2-(2-benzamido-2-phenylacetyl)hydrazine-1-carboxylate** ((*S*)-**3z**)

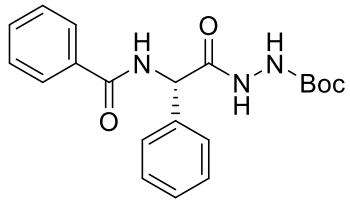

The title compound was synthesized from 2,4-diphenyloxazol-5(4*H*)-one **2z**[6] (23.7 mg, 0.1 mmol) following the general procedure. Unlike the other azlactone substrates examined in this study, **2z** underwent exceptionally rapid hydrolysis, occurring even immediately after column chromatography and evaporation. Although the subsequent asymmetric ring-opening reaction was carried out without delay, consistent selectivity could not be obtained. Results from two independent experiments are summarized.: 1st run, 58%, 40 %ee (21.5 mg, 0.058 mmol, colorless oil). 2nd run, 52%, 32 %ee (19.2 mg, 0.052 mmol, colorless oil). ^{1}H NMR (400 MHz, Methanol-d4) δ = 7.92–7.81 (m, 2H), 7.60–7.52 (m, 3H), 7.48–7.42 (m, 2H), 7.41–7.29 (m, 3H), 5.81 (s, 1H), 1.45 (s, 9H). ^{13}C NMR (100 MHz, Methanol-d4) δ = 172.2 (CO), 169.6 (CO), 157.5 (CO), 138.6 (C), 135.0 (C), 132.9 (CH), 129.7 (CH, 2C), 129.5 (CH, 2C), 129.3 (CH), 128.9 (CH, 2C), 128.6 (CH, 2C), 81.9 (C), 57.4 (CH), 28.5 (CH3, 3C). HRMS-FAB (m/z): $[M+H]^+$ calcd for $C_{20}H_{23}N_3O_4$: 369.1688; found 369.1763. HPLC analysis: CHIRALPAK IB column [conditions, hexane:*i*PrOH = 9:1, flow rate = 1 mL/min, rt, Rt (minor) = 12.37 min, Rt (major) = 14.96 min]. For 32 %ee, $[\alpha]_D^{27.8}$ = –6.9 (c = 1.6, MeOH).

3-4. Mechanistic Investigation via DFT Calculation

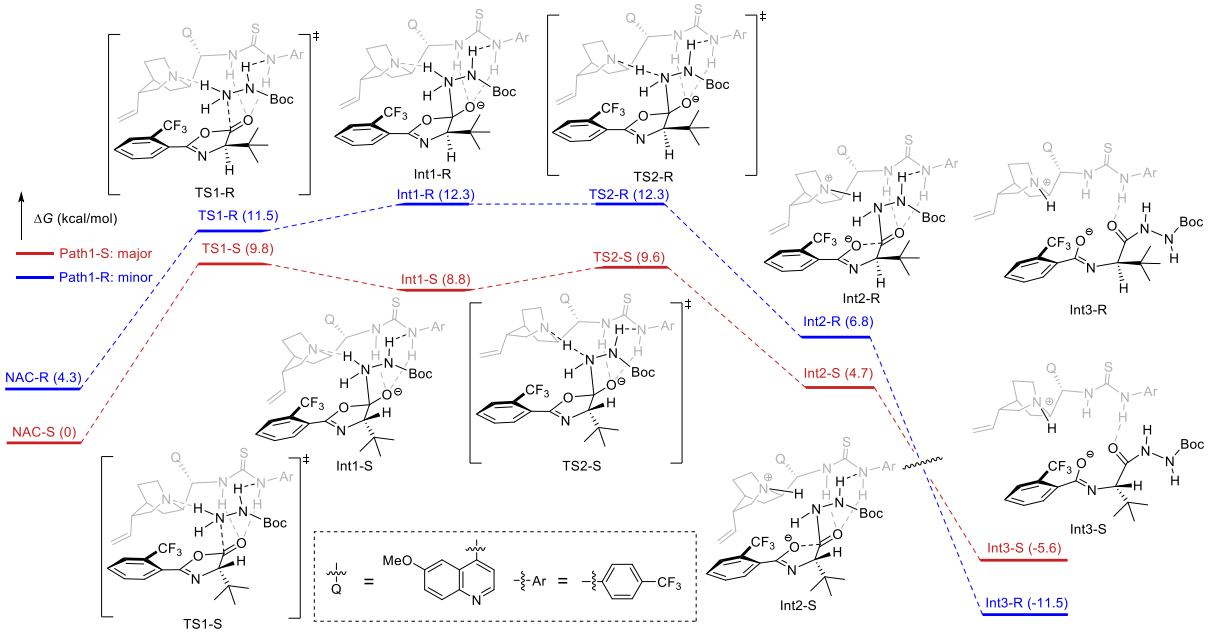

Figure 1. Density functional theory-calculated reaction energy diagram of the nucleophilic ring-opening of azlactone **2a** by Boc-hydrazine with catalyst **1a**. The relative free energy values were calculated at the M06-2X/TZVP level of theory.[a]

State	*S* (FreeE, Hartree)	*S* (FreeE, kcal/mol)[a]	*R* (FreeE, Hartree)	*R* (FreeE, kcal/mol)[a]
NAC	-3579.774141	0	-3579.767321	4.2796182
TS1	-3579.758496	9.81739395	-3579.755797	11.51104344
Int1	-3579.760182	8.75941209	-3579.754466	12.34625925
TS2	-3579.758860	9.58898031	-3579.754604	12.25966287
Int2	-3579.766715	4.65988926	-3579.763298	6.80409093
Int3	-3579.783027	-5.57605386	-3579.792421	-11.4708828

[a]Relative free energies (kcal/mol) are calculated with respect to the NAC structure of the Path1-S, set as the energy reference (0 kcal/mol).

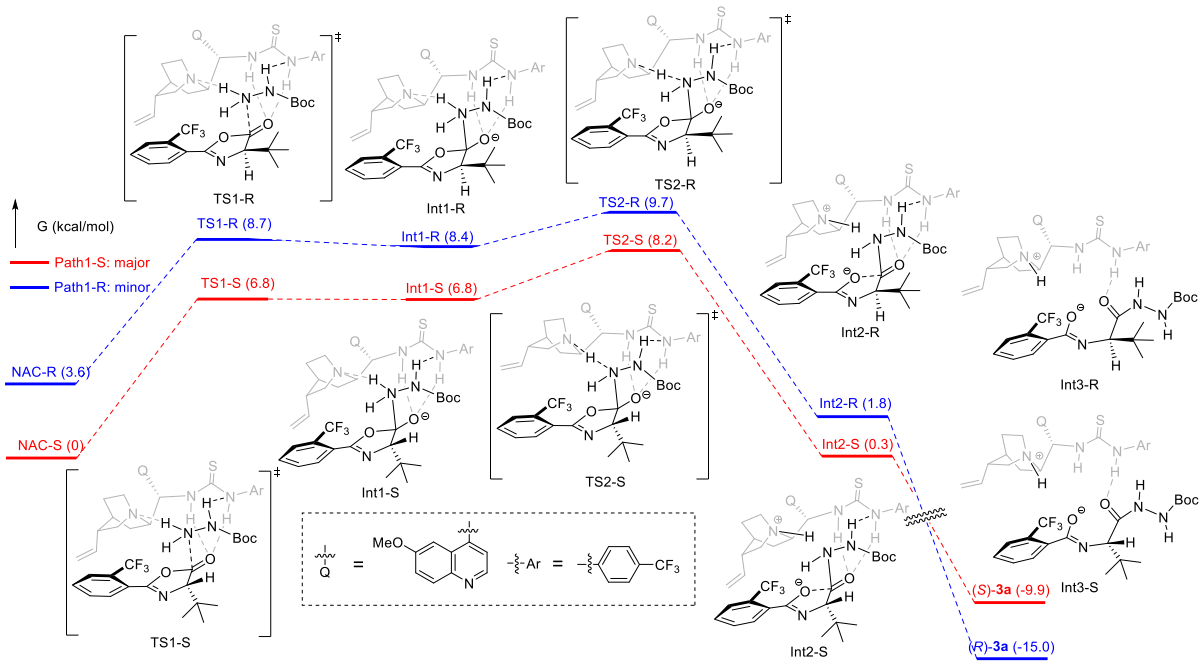

Figure 2. Density functional theory-calculated reaction energy diagram of the nucleophilic ring-opening of azlactone **2a** by Boc-hydrazine with catalyst **1a**. Self-consistent field (SCF)-based energy diagram.[a]

State	*S* (SCF, Hartree)	*S* (SCF, kcal/mol)[a]	R (SCF, Hartree)	E (SCF, kcal/mol)[a]
NAC	-3580.6552862	0	-3580.649534	3.609675974
TS1	-3580.6444797	6.781211915	-3580.641442	8.686978611
Int1	-3580.6444900	6.774742287	-3580.641875	8.415888016
TS2	-3580.6422571	8.175884266	-3580.639876	9.669759672
Int2	-3580.6548672	0.26290159	-3580.652356	1.838497623
Int3	-3580.6711110	-9.930395951	-3580.679143	-14.97012956

[a]Relative SCF energies (kcal/mol) are calculated with respect to the NAC structure of the Path1-S, set as the energy reference (0 kcal/mol).

3-5. Cartesian Coordinates and Energies

Structure: NAC-S

E(M06-2X/TZVP) = -3580.65528620 a.u.

Zero-point correction = 0.987683

Thermal correction to Energy = 1.051399

Thermal correction to Enthalpy = 1.052343

Thermal correction to Gibbs Free Energy (300K) = 0.882204

C	-0.964341	2.573307	-1.615229
C	-1.452201	1.793577	-2.633496
C	-1.906798	2.390623	-3.823895
N	-1.908341	3.682924	-4.030155
H	-1.487224	0.714496	-2.530025
H	-2.292775	1.770357	-4.627424
C	-1.404191	4.475937	-3.053343
C	-0.890544	3.976443	-1.825953
C	-0.340531	4.885603	-0.881806
C	-0.321036	6.227727	-1.153460
C	-0.867039	6.731044	-2.364543
C	-1.385029	5.878475	-3.285843
H	0.118712	4.505396	0.017476
H	-0.834177	7.800205	-2.528626
H	-1.789291	6.232134	-4.225143
C	-0.557671	1.915720	-0.303872
N	0.440315	0.886411	-0.523908
C	1.773642	1.093175	-0.446661
S	2.441702	2.464215	0.272694
N	2.492759	0.072195	-0.995195
C	6.535690	-0.956983	-0.682413
C	6.193714	0.376346	-0.854358
C	4.863727	0.749921	-0.973946
C	3.867682	-0.217783	-0.880108
C	4.218681	-1.560560	-0.731005
C	5.546472	-1.931567	-0.635727
H	6.968583	1.128910	-0.915968
H	4.596565	1.783613	-1.123407
H	3.441386	-2.313717	-0.672904
H	5.813262	-2.973486	-0.513857
C	-1.799747	1.348622	0.400015
N	-1.438118	0.563243	1.591180
C	-2.679343	0.130320	2.247232
C	-3.432533	1.317781	2.910277
H	-3.313817	-0.335211	1.486604
H	-2.435471	-0.634394	2.988312
C	-2.782712	2.492573	0.779143
C	-2.827428	2.602989	2.308895
H	-3.232573	1.317974	3.985843
C	-0.665419	1.379310	2.545369
C	-1.385077	2.722831	2.820372
C	-4.909602	1.200175	2.707295
C	-5.798430	1.005456	3.672009
C	7.968431	-1.357231	-0.490052
F	8.246543	-2.527253	-1.083995
F	8.820357	-0.449269	-0.981184
F	8.272100	-1.510135	0.810830
O	0.207434	7.168667	-0.337440
C	0.814491	6.723370	0.860001
H	-0.090959	2.645964	0.347384
H	0.110319	0.005738	-0.901783
H	1.947871	-0.659768	-1.437989
H	-2.287788	0.652722	-0.288538
H	-3.775511	2.292774	0.369804
H	-2.456628	3.445687	0.357378
H	-3.419268	3.469124	2.607609
H	-0.562695	0.785552	3.453422
H	0.342758	1.529215	2.154968
H	-1.375697	2.951442	3.887524
H	-0.882093	3.549796	2.309070
H	-5.253407	1.258606	1.676045
H	-5.495697	0.930259	4.710719
H	-6.856797	0.915387	3.460647
H	0.083669	6.234275	1.510773
H	1.633058	6.029239	0.651343
H	1.201092	7.611680	1.351284
N	-0.446864	-2.271605	1.104960

N	0.922423	-2.008385	1.250113
C	1.376699	-1.366537	2.374839
O	0.746947	-1.308662	3.405481
O	2.599661	-0.879117	2.147943
C	3.421057	-0.371363	3.249782
C	3.661264	-1.489235	4.255448
C	4.713721	0.028571	2.556326
C	2.765540	0.847861	3.884856
H	-0.707107	-2.978342	1.785047
H	-0.947770	-1.404739	1.330442
H	1.417999	-1.829202	0.389821
H	2.738448	-1.775496	4.756719
H	4.375344	-1.145992	5.005573
H	4.085516	-2.360166	3.752656
H	5.150767	-0.824051	2.033335
H	5.428908	0.390548	3.296198
H	4.517208	0.821733	1.834090
H	2.548163	1.589228	3.113700
H	3.464170	1.288319	4.598774
H	1.849084	0.579861	4.405926
C	-6.016980	-1.409824	0.333514
C	-4.846644	-2.133945	0.157489
C	-3.946431	-1.758880	-0.849419
C	-4.231287	-0.644801	-1.635357
C	-5.402455	0.075699	-1.452576
C	-6.299619	-0.313239	-0.471352
H	-6.698143	-1.687516	1.125196
H	-3.526905	-0.344712	-2.399616
H	-5.604706	0.937929	-2.074641
H	-7.215011	0.242635	-0.315271
C	-4.563564	-3.270553	1.120032
C	-2.689942	-2.477806	-1.118468
N	-2.454349	-3.710858	-1.062858
C	-1.061075	-3.900845	-1.443807
C	-0.547215	-2.485828	-1.601438
O	-1.632054	-1.659140	-1.517424
C	-0.907968	-4.753171	-2.731540
H	-0.519913	-4.381314	-0.626654
C	0.579703	-4.997079	-2.990353
C	-1.536587	-4.027620	-3.922657
C	-1.617556	-6.087633	-2.497367
O	0.549186	-2.049761	-1.816300
F	-5.393505	-3.220838	2.171003
F	-4.720187	-4.470098	0.563677
F	-3.320221	-3.201056	1.617318
H	1.121213	-4.066564	-3.161707
H	1.042191	-5.514457	-2.146673
H	0.694359	-5.626178	-3.874923
H	-2.591803	-3.812306	-3.741682
H	-1.016417	-3.091202	-4.142788
H	-1.471833	-4.655352	-4.812779
H	-1.487526	-6.727321	-3.372385
H	-2.682972	-5.942493	-2.322324
H	-1.196951	-6.605628	-1.632663

Structure: TS1-S

E(M06-2X/TZVP) = -3580.64447966 a.u.

Zero-point correction = 0.988881

Thermal correction to Energy = 1.050542

Thermal correction to Enthalpy = 1.051487

Thermal correction to Gibbs Free Energy (300K) = 0.887007

C	-0.972805	2.932149	-1.304024
C	-1.606695	2.319654	-2.355978
C	-2.113720	3.092974	-3.417455
N	-2.035134	4.398269	-3.463529
H	-1.720586	1.240336	-2.381189
H	-2.612756	2.606493	-4.249934
C	-1.390847	5.026836	-2.450005
C	-0.809934	4.342787	-1.348109
C	-0.106843	5.085341	-0.360693
C	-0.008032	6.447254	-0.469864
C	-0.622524	7.135644	-1.549698
C	-1.285914	6.443144	-2.511391
H	0.403975	4.564806	0.434886
H	-0.522852	8.212615	-1.585711

H	-1.745326	6.939354	-3.356088	H	-2.215283	0.815971	-0.230768
C	-0.492050	2.090114	-0.131767	H	-3.634886	2.416321	0.629284
N	0.504288	1.127670	-0.561225	H	-2.278363	3.467650	0.979366
C	1.833249	1.243544	-0.354697	H	-3.451747	2.932453	3.090816
S	2.513166	2.396179	0.676297	H	-0.355311	0.319229	3.407187
N	2.542544	0.307303	-1.052996	H	0.424566	1.433009	2.302801
C	6.533714	-0.930540	-0.843431	H	-1.446197	2.178383	4.331149
C	6.241154	0.415906	-0.683972	H	-0.938642	3.216703	3.004452
C	4.931993	0.866784	-0.760433	H	-4.978176	0.752744	1.361230
C	3.900433	-0.047532	-0.966351	H	-5.678931	0.171988	4.286044
C	4.207127	-1.396620	-1.165161	H	-6.820885	0.210504	2.831926
C	5.514088	-1.838261	-1.101717	H	0.651943	6.083272	2.119292
H	7.040461	1.125192	-0.513826	H	2.087970	5.890870	1.080711
H	4.709271	1.914955	-0.649035	H	1.851392	7.395137	2.010023
H	3.409211	-2.104140	-1.363406	N	-0.396514	-1.998611	0.457680
H	5.740920	-2.886668	-1.246115	N	0.961174	-2.272401	0.680507
C	-1.696788	1.402968	0.528972	C	1.453207	-1.907458	1.927645
N	-1.268088	0.432689	1.554643	O	0.745549	-1.807642	2.900072
C	-2.463164	-0.220419	2.108219	O	2.763145	-1.752167	1.843909
C	-3.375652	0.777554	2.873746	C	3.576485	-1.458313	3.033922
H	-3.013679	-0.665216	1.275363	C	3.495456	-2.634086	3.995879
H	-2.133390	-1.032009	2.760574	C	4.971446	-1.315294	2.448328
C	-2.666143	2.456580	1.129787	C	3.119847	-0.151983	3.667382
C	-2.799283	2.188864	2.631623	H	-0.969986	-2.702966	0.923618
H	-3.325049	0.572186	3.946600	H	-0.650299	-1.029685	0.828931
C	-0.546582	1.090471	2.661708	H	1.512185	-1.978366	-0.120743
C	-1.392816	2.250815	3.243500	H	2.491724	-2.743262	4.402939
C	-4.798037	0.628076	2.428815	H	4.189305	-2.464509	4.820570
C	-5.816162	0.322485	3.220775	H	3.783723	-3.556799	3.489913
C	7.938279	-1.427242	-0.675649	H	5.272725	-2.233868	1.943651
F	8.208605	-2.457755	-1.489335	H	5.685440	-1.102467	3.244518
F	8.847100	-0.475750	-0.920667	H	4.992999	-0.496760	1.726724
F	8.163753	-1.863055	0.577560	H	3.069368	0.632620	2.909542
O	0.665780	7.239149	0.395911	H	3.850753	0.143093	4.422136
C	1.350829	6.604453	1.458458	H	2.147531	-0.258398	4.143830
H	-0.007006	2.718175	0.608122	C	-6.390626	-1.585890	0.124934
H	0.198724	0.390117	-1.194772	C	-5.136886	-2.169007	-0.002459
H	1.972041	-0.348985	-1.580906	C	-4.199939	-1.611786	-0.881476

C	-4.528535	-0.447831	-1.574139	0.885347
C	-5.782061	0.130682	-1.440366	
C	-6.718781	-0.446682	-0.597271	
H	-7.105241	-2.012685	0.814390	
H	-3.792003	-0.007385	-2.233562	
H	-6.021496	1.029124	-1.994264	
H	-7.700009	-0.004524	-0.484846	
C	-4.821087	-3.364185	0.874584	
C	-2.857748	-2.185263	-1.118865	
N	-2.549466	-3.408335	-1.186996	
C	-1.126772	-3.472988	-1.537750	
C	-0.635052	-2.028393	-1.297621	
O	-1.867014	-1.263664	-1.313564	
C	-0.922134	-3.985314	-2.983846	
H	-0.614492	-4.164986	-0.864039	
C	0.574051	-4.198766	-3.230097	
C	-1.486609	-2.993646	-4.004112	
C	-1.647665	-5.327795	-3.114957	
O	0.356772	-1.486873	-1.817488	
F	-5.714080	-3.472206	1.868999	
F	-4.843440	-4.518185	0.213717	
F	-3.618681	-3.246783	1.465211	
H	1.124365	-3.261650	-3.165246	
H	0.989131	-4.902930	-2.503876	
H	0.722057	-4.621188	-4.226084	
H	-2.549428	-2.809901	-3.827826	
H	-0.950747	-2.043990	-3.971619	
H	-1.386174	-3.408430	-5.008958	
H	-1.462923	-5.746499	-4.106322	
H	-2.722088	-5.213252	-2.976066	
H	-1.284129	-6.042286	-2.372334	

Structure: Int1-S

E(M06-2X/TZVP) = -3580.64448997 a.u.

Zero-point correction = 0.989022

Thermal correction to Energy = 1.051452

Thermal correction to Enthalpy = 1.052396

Thermal correction to Gibbs Free Energy (300K) =

O	-1.891107	-1.247901	-1.299158
C	-2.873798	-2.179428	-1.124830
N	-2.556829	-3.399680	-1.205115
C	-1.130352	-3.450715	-1.546215
C	-0.645553	-2.004641	-1.282379
C	-4.221862	-1.618503	-0.888152
C	-5.150132	-2.179270	-0.002794
C	-6.407547	-1.605042	0.129296
C	-6.747646	-0.471279	-0.595779
C	-5.819614	0.109329	-1.446447
C	-4.562219	-0.459784	-1.583820
C	-4.819591	-3.368769	0.876069
F	-3.614408	-3.239132	1.459453
C	-0.912049	-3.949084	-2.994300
C	-1.625785	-5.296341	-3.141834
O	0.335862	-1.450450	-1.821091
N	-0.403933	-1.975293	0.427447
N	0.951822	-2.263423	0.654352
C	1.433322	-1.914277	1.911072
O	2.742612	-1.756979	1.839545
C	3.547598	-1.473608	3.038201
C	3.081294	-0.176558	3.683523
O	0.716100	-1.828179	2.877777
C	3.464446	-2.660810	3.985609
C	4.945001	-1.318243	2.461803
F	-5.705608	-3.481194	1.876155
F	-4.835107	-4.524991	0.219274
C	0.587290	-4.149590	-3.233174
C	-1.478213	-2.953653	-4.010027
N	-1.267599	0.434722	1.536956
C	-1.692349	1.417696	0.520529
C	-2.658209	2.468156	1.131898
C	-2.791881	2.186937	2.631023
C	-3.373334	0.775560	2.860345
C	-2.466254	-0.218592	2.084331
C	-1.384973	2.237862	3.242663
C	-0.543702	1.079103	2.651215

C	-0.484627	2.107166	-0.132405	H	-3.018684	-0.651759	1.246760
N	0.507345	1.144954	-0.571814	H	-2.139949	-1.038193	2.728385
C	1.835897	1.246085	-0.357971	H	-3.321591	0.560022	3.931147
N	2.539095	0.310256	-1.063358	H	0.002023	2.726163	0.614184
C	3.892392	-0.060362	-0.972128	H	0.198000	0.410759	-1.208831
C	4.932968	0.841071	-0.754737	H	1.963141	-0.336843	-1.597301
C	6.236510	0.375112	-0.674285	H	-2.212454	0.839521	-0.244528
C	6.514949	-0.973575	-0.840764	H	-3.627206	2.435602	0.631465
C	5.486810	-1.868160	-1.110546	H	-2.267096	3.479270	0.990610
C	4.185168	-1.411371	-1.178644	H	-3.441332	2.928539	3.097588
C	7.913404	-1.485946	-0.668957	H	-0.357488	0.300342	3.390017
F	8.132120	-1.919392	0.586340	H	0.429220	1.420379	2.296056
C	-4.797334	0.634537	2.417087	H	-1.437928	2.156306	4.329666
C	-5.814793	0.330599	3.210522	H	-0.926734	3.203710	3.011508
C	-0.961881	2.962777	-1.296382	H	-4.979501	0.764071	1.350321
C	-1.610858	2.365934	-2.348075	H	-5.675334	0.175197	4.274807
C	-2.113209	3.153239	-3.401567	H	-6.821037	0.224987	2.823926
N	-2.016604	4.457528	-3.439812	H	0.737433	6.067017	2.133464
C	-1.357173	5.070512	-2.426446	H	2.160966	5.861826	1.080420
C	-0.778786	4.371225	-1.332833	H	1.954105	7.362810	2.022198
C	-0.057862	5.097268	-0.346012	H	-0.984636	-2.675608	0.892018
C	0.059888	6.458308	-0.447517	H	-0.653439	-1.000760	0.804275
C	-0.552662	7.162357	-1.518248	H	1.506336	-1.951831	-0.137954
C	-1.232665	6.485520	-2.479532	H	2.457969	-2.779122	4.383401
O	0.751846	7.234750	0.417967	H	4.150751	-2.497552	4.817833
C	1.437480	6.583071	1.469836	H	3.760975	-3.576314	3.471467
S	2.523348	2.380549	0.688759	H	5.252057	-2.229230	1.946969
F	8.173114	-2.522492	-1.478293	H	5.654077	-1.113148	3.264391
F	8.833493	-0.545833	-0.916064	H	4.967086	-0.490398	1.750863
H	-1.740781	1.288582	-2.379614	H	3.030335	0.615723	2.933732
H	-2.624143	2.679171	-4.233943	H	3.807441	0.114097	4.444520
H	0.452052	4.564398	0.441967	H	2.107612	-0.293071	4.154847
H	-0.437898	8.238019	-1.548189	H	-7.115395	-2.034555	0.824069
H	-1.690894	6.993617	-3.317776	H	-3.831311	-0.016503	-2.247741
H	7.042869	1.074312	-0.495666	H	-6.069088	1.003417	-2.002953
H	4.721153	1.890927	-0.637696	H	-7.731590	-0.035985	-0.480342
H	3.380867	-2.108475	-1.388202	H	-0.620359	-4.147477	-0.875015
H	5.702761	-2.917929	-1.261389	H	1.128742	-3.207974	-3.161241

H	1.003853	-4.853513	-2.507416
H	0.744270	-4.566958	-4.229951
H	-2.544346	-2.782992	-3.840557
H	-0.952401	-1.999198	-3.963198
H	-1.365550	-3.358103	-5.017847
H	-1.432396	-5.704319	-4.136040
H	-2.701842	-5.191955	-3.007672
H	-1.260297	-6.014815	-2.403958

Structure: TS2-S

E(M06-2X/TZVP) = -3580.64225729 a.u.

Zero-point correction = 0.986135

Thermal correction to Energy = 1.047695

Thermal correction to Enthalpy = 1.048639

Thermal correction to Gibbs Free Energy (300K) = 0.884419

O	-2.054560	-1.196339	-1.277576
C	-2.996032	-2.160222	-1.116508
N	-2.639724	-3.370977	-1.177584
C	-1.203152	-3.376708	-1.494734
C	-0.751141	-1.911417	-1.217144
C	-4.366047	-1.639724	-0.899290
C	-5.259883	-2.171672	0.036533
C	-6.525053	-1.614866	0.175717
C	-6.907362	-0.527979	-0.597889
C	-6.015526	0.021432	-1.506623
C	-4.749505	-0.527400	-1.646557
C	-4.879180	-3.310164	0.960436
F	-3.668898	-3.117349	1.516493
C	-0.951827	-3.892720	-2.929336
C	-1.613596	-5.268670	-3.059744
O	0.184692	-1.333350	-1.854325
N	-0.502668	-1.798690	0.354867
N	0.860481	-2.090729	0.594739
C	1.309399	-1.795441	1.867856
O	2.613004	-1.573393	1.831603
C	3.392531	-1.361826	3.058783
C	2.853598	-0.164793	3.830449
O	0.576416	-1.793235	2.830627
C	3.374783	-2.641245	3.880654
C	4.779585	-1.062250	2.515257
F	-5.744357	-3.403741	1.981773
F	-4.868652	-4.493808	0.356739
C	0.555672	-4.046017	-3.153540
C	-1.544518	-2.939650	-3.970422
N	-1.329144	0.447425	1.386964
C	-1.660288	1.473705	0.360121
C	-2.610616	2.538411	0.962482
C	-2.722940	2.303134	2.470947
C	-3.376605	0.932714	2.746105
C	-2.590404	-0.114436	1.923580
C	-1.301178	2.282775	3.049263
C	-0.562848	1.034814	2.516675
C	-0.388125	2.119182	-0.209211
N	0.564123	1.111372	-0.624510
C	1.892396	1.156192	-0.394330
N	2.564810	0.213326	-1.119979
C	3.895709	-0.230128	-0.993445
C	4.973182	0.626470	-0.781972
C	6.250595	0.101676	-0.659249
C	6.464346	-1.263584	-0.781763
C	5.399544	-2.115554	-1.047546
C	4.122344	-1.598924	-1.153617
C	7.832201	-1.838976	-0.565156
F	7.998879	-2.255812	0.703634
C	-4.833493	0.869202	2.396691
C	-5.806183	0.616217	3.260451
C	-0.769723	3.024448	-1.371165
C	-1.394517	2.486178	-2.467718
C	-1.806951	3.325872	-3.520303
N	-1.647559	4.624559	-3.515269
C	-1.011610	5.178355	-2.454051
C	-0.520036	4.422965	-1.355798
C	0.182688	5.087038	-0.313525
C	0.364613	6.443776	-0.366972
C	-0.162008	7.205048	-1.444089

C	-0.821752	6.587121	-2.457919	H	2.370883	-2.864101	4.239242
O	1.045922	7.162564	0.554943	H	4.033229	-2.519979	4.742029
C	1.648195	6.450752	1.618574	H	3.740741	-3.477803	3.283603
S	2.613076	2.227671	0.697403	H	5.133684	-1.883647	1.891008
F	8.060652	-2.903451	-1.346850	H	5.477630	-0.922564	3.341369
F	8.802583	-0.949628	-0.807654	H	4.752014	-0.151835	1.914414
H	-1.574177	1.417546	-2.538252	H	2.755762	0.690701	3.159341
H	-2.298401	2.899549	-4.389048	H	3.568627	0.092756	4.613624
H	0.633419	4.509786	0.479237	H	1.892253	-0.383334	4.289974
H	0.001321	8.274762	-1.435648	H	-7.205487	-2.021706	0.910407
H	-1.214178	7.139093	-3.301776	H	-4.041817	-0.105298	-2.348847
H	7.086934	0.765110	-0.482270	H	-6.300880	0.876959	-2.105033
H	4.808409	1.688573	-0.699771	H	-7.896718	-0.106125	-0.478687
H	3.287420	-2.262483	-1.352370	H	-0.688940	-4.054351	-0.805982
H	5.567188	-3.178634	-1.162652	H	1.058100	-3.081659	-3.110806
H	-3.180699	-0.451847	1.070220	H	0.992643	-4.707870	-2.400213
H	-2.334061	-0.987581	2.525633	H	0.735067	-4.493169	-4.133753
H	-3.268939	0.715992	3.812457	H	-2.619834	-2.815356	-3.818868
H	0.091852	2.697250	0.573792	H	-1.061594	-1.963259	-3.926648
H	0.234133	0.371551	-1.259015	H	-1.398843	-3.355035	-4.969896
H	1.970241	-0.384192	-1.692438	H	-1.400329	-5.684787	-4.046672
H	-2.159805	0.926314	-0.438270	H	-2.693444	-5.203003	-2.931591
H	-3.588237	2.492742	0.480974	H	-1.224888	-5.961481	-2.309057
H	-2.216870	3.541004	0.780194				
H	-3.316259	3.092013	2.933725	Structure: Int2-S			
H	-0.483906	0.256094	3.272640	E(M06-2X/TZVP) = -3580.65486724 a.u.			
H	0.448108	1.263988	2.178157	Zero-point correction = 0.990603			
H	-1.329706	2.263029	4.139486	Thermal correction to Energy = 1.052780			
H	-0.776111	3.195790	2.754508	Thermal correction to Enthalpy = 1.053725			
H	-5.081942	1.010363	1.345098	Thermal correction to Gibbs Free Energy (300K) =			
H	-5.599665	0.448241	4.311814	0.889176			
H	-6.841284	0.565754	2.946679	O	-1.754196	-1.272236	-1.056955
H	0.893285	5.947421	2.230053	C	-2.673355	-2.241433	-1.121682
H	2.359044	5.709552	1.243623	N	-2.318505	-3.430397	-1.382453
H	2.168742	7.190175	2.220419	C	-0.871196	-3.392150	-1.642857
H	-1.061676	-2.509560	0.832480	C	-0.372468	-2.053362	-1.007827
H	-0.810488	-0.661707	0.814547	C	-4.072286	-1.792975	-0.896920
H	1.425644	-1.741022	-0.171356	C	-4.990654	-2.477830	-0.095254

C	-6.295839	-2.012643	0.017292	C	5.646381	-1.457616	-1.187457
C	-6.692150	-0.857769	-0.641792	C	4.316728	-1.120728	-1.055490
C	-5.774045	-0.147839	-1.402860	C	8.071054	-0.948646	-0.872298
C	-4.472200	-0.611724	-1.521309	F	8.443081	-1.648530	0.216569
C	-4.593076	-3.687151	0.724022	C	-4.829471	0.140670	2.433301
F	-3.416063	-3.492161	1.350444	C	-5.837434	-0.246192	3.200380
C	-0.575082	-3.578849	-3.148508	C	-1.110177	2.727365	-1.257512
C	-1.273845	-4.859709	-3.617779	C	-1.570025	1.956792	-2.296078
O	0.578032	-1.376357	-1.514242	C	-2.131724	2.578380	-3.428144
N	-0.264302	-2.196619	0.489403	N	-2.266088	3.874565	-3.551686
N	1.030946	-2.527604	0.887441	C	-1.789887	4.656720	-2.552671
C	1.648952	-1.719707	1.793713	C	-1.168998	4.140573	-1.383533
O	2.949115	-1.982093	1.837187	C	-0.643288	5.042631	-0.418110
C	3.779889	-1.515492	2.955692	C	-0.755915	6.394114	-0.612428
C	3.701041	-0.005048	3.134071	C	-1.419037	6.910564	-1.757610
O	1.054239	-0.911531	2.483489	C	-1.911388	6.065554	-2.699944
C	3.345092	-2.261644	4.208352	O	-0.256038	7.333692	0.223101
C	5.178675	-1.921480	2.520719	C	0.486323	6.883302	1.339155
F	-5.492294	-3.919655	1.694836	S	2.320757	2.731240	0.821135
F	-4.499305	-4.805416	0.015018	F	8.331434	-1.730815	-1.929892
C	0.934514	-3.741871	-3.351563	F	8.891086	0.107486	-0.945777
C	-1.088783	-2.391402	-3.967796	H	-1.506685	0.872973	-2.256210
N	-1.274321	0.448169	1.789761	H	-2.493938	1.970649	-4.251613
C	-1.767311	1.285059	0.640289	H	-0.086351	4.658962	0.423232
C	-2.903693	2.198900	1.138417	H	-1.489697	7.985549	-1.859718
C	-3.094413	1.988300	2.642575	H	-2.397718	6.431476	-3.594582
C	-3.469455	0.519101	2.941486	H	7.027150	1.408461	-0.035177
C	-2.397213	-0.389259	2.297846	H	4.655916	2.017587	0.191220
C	-1.760786	2.309760	3.329820	H	3.544331	-1.822430	-1.350683
C	-0.706741	1.273101	2.902556	H	5.924019	-2.425903	-1.583609
C	-0.598983	2.044671	0.001752	H	-2.787919	-0.937431	1.440597
N	0.477426	1.123145	-0.267224	H	-1.971132	-1.107451	2.996680
C	1.787812	1.357958	-0.006041	H	-3.454602	0.384628	4.026157
N	2.556891	0.334476	-0.465013	H	-0.218630	2.782254	0.702426
C	3.937020	0.129434	-0.543826	H	0.277322	0.298680	-0.850734
C	4.926754	1.045739	-0.186477	H	2.005833	-0.431048	-0.874315
C	6.263870	0.694788	-0.316819	H	-2.136668	0.557635	-0.077892
C	6.629269	-0.547777	-0.809112	H	-3.819911	1.986851	0.586487

H	-2.651448	3.244664	0.947487
H	-3.882235	2.641771	3.016590
H	-0.456497	0.570297	3.693133
H	0.227277	1.709407	2.549532
H	-1.874172	2.296138	4.414120
H	-1.441473	3.315146	3.046664
H	-4.961978	0.170029	1.352615
H	-5.739072	-0.308377	4.278733
H	-6.794698	-0.518989	2.774382
H	-0.140873	6.294282	2.015155
H	1.342038	6.279706	1.025161
H	0.832911	7.775951	1.851940
H	-0.896218	-2.929451	0.807872
H	-0.541225	-0.208131	1.460917
H	1.616940	-3.059543	0.255602
H	2.317145	-2.009713	4.469615
H	3.990632	-1.976911	5.040509
H	3.426406	-3.339225	4.058691
H	5.215074	-2.987255	2.293051
H	5.888832	-1.707502	3.320000
H	5.474419	-1.361644	1.632270
H	3.788066	0.501096	2.173454
H	4.538287	0.310018	3.759940
H	2.769962	0.305461	3.600089
H	-6.997069	-2.546526	0.643544
H	-3.749474	-0.068950	-2.118492
H	-6.068921	0.762899	-1.908308
H	-7.711834	-0.507926	-0.547423
H	-0.404503	-4.230595	-1.112684
H	1.467984	-2.839905	-3.058297
H	1.311831	-4.587551	-2.768118
H	1.143789	-3.948826	-4.403543
H	-2.162762	-2.250744	-3.818061
H	-0.565289	-1.475394	-3.694651
H	-0.927111	-2.584046	-5.030837
H	-1.020210	-5.054293	-4.662263
H	-2.356200	-4.776146	-3.527377
H	-0.951494	-5.719710	-3.024900

Structure: Int3-S

E(M06-2X/TZVP) = -3580.67111128 a.u.

Zero-point correction = 0.990941 (Hartree/Particle)

Thermal correction to Energy = 1.053669

Thermal correction to Enthalpy = 1.054613

Thermal correction to Gibbs Free Energy (300K) = 0.889113

C	-2.400734	6.100490	-2.398509
C	-2.301432	4.684746	-2.315401
C	-1.628760	4.108767	-1.203776
C	-1.039899	4.960423	-0.229520
C	-1.137351	6.320486	-0.360723
C	-1.844741	6.896783	-1.448777
C	-1.592114	2.690114	-1.141977
C	-2.143559	1.974197	-2.172930
C	-2.748694	2.651491	-3.248629
N	-2.849435	3.954908	-3.317659
C	-1.000676	1.935821	0.039241
N	0.122702	1.093605	-0.341069
C	1.411299	1.419074	-0.071943
S	1.816418	2.768046	0.876659
O	-0.580082	7.214132	0.490198
C	0.209632	6.700091	1.544299
C	-2.134751	1.140832	0.705888
N	-1.577387	0.106276	1.644890
C	-2.716674	-0.617398	2.290184
C	-3.393635	0.313707	3.317900
C	-2.950976	1.759457	2.996309
C	-3.105390	2.040841	1.497577
C	-1.465837	1.878026	3.355837
C	-0.706766	0.713667	2.701237
C	-4.880441	0.122812	3.295308
C	-5.603453	-0.224422	4.349308
N	2.305466	0.551270	-0.607777
C	3.707019	0.459361	-0.525140
C	4.571876	1.401237	0.033470
C	5.936686	1.145894	0.070968

C	6.457128	-0.024467	-0.454327	H	-0.451665	4.531673	0.567420
C	5.604936	-0.951640	-1.045774	H	-1.899728	7.976206	-1.502752
C	4.248583	-0.709424	-1.084074	H	-2.925730	6.512048	-3.250484
C	7.918336	-0.331250	-0.333993	H	6.598318	1.881132	0.510392
F	8.662944	0.774178	-0.208015	H	4.188422	2.321345	0.437270
F	8.179058	-1.095023	0.744898	H	3.579246	-1.420891	-1.552517
F	8.381721	-1.006978	-1.394945	H	6.005780	-1.858728	-1.479691
O	0.740528	-1.535916	1.549654	H	-3.404803	-0.895762	1.493079
C	1.701109	-2.131668	1.108885	H	-2.318746	-1.526761	2.738489
O	2.951815	-2.089433	1.557716	H	-3.033446	0.072198	4.321791
C	3.323620	-1.561141	2.870189	H	-0.605002	2.637872	0.765481
C	4.840206	-1.664785	2.841013	H	-0.098593	0.249608	-0.876686
N	1.673705	-3.009044	0.060799	H	1.916022	-0.210070	-1.174686
N	0.602625	-3.190236	-0.763382	H	-2.654864	0.558927	-0.045947
C	0.454460	-2.445473	-1.900176	H	-4.130720	1.862285	1.170565
O	-1.530052	-1.111945	-0.933434	H	-2.884260	3.090977	1.291531
C	-2.220910	-2.132596	-1.273881	H	-3.547875	2.461636	3.577393
N	-1.931294	-3.093066	-2.085535	H	-0.479618	-0.091047	3.398619
C	-0.662918	-2.988971	-2.794658	H	0.221443	1.029821	2.234487
C	-3.604977	-2.205437	-0.665546	H	-1.327140	1.844227	4.436662
C	-4.016132	-3.170117	0.254469	H	-1.065408	2.832186	3.004169
C	-5.291370	-3.122730	0.811407	H	-5.368750	0.273291	2.334672
C	-6.173642	-2.115920	0.451203	H	-5.144719	-0.400327	5.316308
C	-5.776959	-1.149548	-0.465096	H	-6.676860	-0.346658	4.283996
C	-4.501121	-1.193911	-1.007232	H	-0.392282	6.088635	2.223678
C	-0.791495	-2.315873	-4.185187	H	1.036900	6.098138	1.158339
C	-1.227771	-0.855382	-4.079140	H	0.597893	7.562008	2.079556
O	1.233952	-1.543475	-2.167565	H	-0.131016	-3.820279	-0.467466
C	-3.072759	-4.249697	0.721548	H	-1.033298	-0.568996	1.078091
F	-2.929587	-5.254722	-0.138115	H	2.552751	-3.416435	-0.222013
F	-1.837597	-3.756947	0.967851	H	1.623897	-2.425193	3.890424
F	-3.486772	-4.790283	1.881323	H	3.029727	-2.121695	4.921950
C	-1.855520	-3.094777	-4.967636	H	3.043189	-3.491825	3.799552
C	0.533931	-2.416475	-4.948471	H	5.150427	-2.693822	2.658016
C	2.895448	-0.113177	3.034426	H	5.252574	-1.336350	3.795524
C	2.713411	-2.460908	3.934587	H	5.240698	-1.031726	2.046731
H	-2.106372	0.889950	-2.162084	H	3.168842	0.474058	2.158572
H	-3.174050	2.083943	-4.070501	H	3.411247	0.308523	3.898865

H	1.824783	-0.030178	3.191092
H	-5.586646	-3.867618	1.537674
H	-4.183150	-0.436868	-1.716030
H	-6.461028	-0.362332	-0.757362
H	-7.164228	-2.086857	0.885977
H	-0.350097	-4.020427	-3.004265
H	1.308076	-1.797314	-4.500186
H	0.885726	-3.451962	-4.977953
H	0.385026	-2.090582	-5.980249
H	-2.206970	-0.789476	-3.598998
H	-0.512254	-0.264932	-3.506694
H	-1.313965	-0.424315	-5.079848
H	-1.963200	-2.666277	-5.966652
H	-2.818493	-3.061793	-4.459823
H	-1.567894	-4.143646	-5.077833

Structure: NAC-R

E(M06-2X/TZVP) = -3580.64953382 a.u.

Zero-point correction = 0.987763

Thermal correction to Energy = 1.051314

Thermal correction to Enthalpy = 1.052258

Thermal correction to Gibbs Free Energy (300K) = 0.883264

C	-1.151599	2.706289	-1.570320
C	-1.549446	1.961659	-2.652132
C	-1.999513	2.601006	-3.822006
N	-2.078180	3.901035	-3.950630
H	-1.512659	0.878076	-2.615083
H	-2.314727	2.008822	-4.675784
C	-1.663867	4.662337	-2.908753
C	-1.164230	4.121477	-1.693209
C	-0.712312	5.003647	-0.674202
C	-0.772842	6.358504	-0.863951
C	-1.304415	6.900049	-2.065039
C	-1.728979	6.075054	-3.056406
H	-0.264603	4.598490	0.220000
H	-1.336747	7.977243	-2.163615
H	-2.120080	6.459714	-3.989065
C	-0.749514	1.995032	-0.286060
N	0.297175	1.021495	-0.533408
C	1.618400	1.297329	-0.443073
S	2.205759	2.672947	0.334230
N	2.393614	0.343346	-1.032169
C	6.471993	-0.526557	-0.691935
C	6.075506	0.798467	-0.797238
C	4.732818	1.121561	-0.924178
C	3.778510	0.108657	-0.905701
C	4.185092	-1.224489	-0.824229
C	5.525499	-1.543520	-0.720059
H	6.817876	1.585559	-0.800451
H	4.423924	2.149754	-1.021950
H	3.440354	-2.012239	-0.825496
H	5.835084	-2.578339	-0.650127
C	-1.981565	1.334921	0.348852
N	-1.614664	0.489881	1.495530
C	-2.853462	-0.033773	2.087912
C	-3.654667	1.077022	2.824024
H	-2.599126	-0.845079	2.774259
H	-3.457766	-0.458601	1.278900
C	-3.025007	2.405080	0.776954
C	-3.097899	2.421306	2.310292
H	-3.454595	1.013757	3.897737
C	-0.894668	1.273118	2.516420
C	-1.670834	2.569421	2.855069
C	-5.126655	0.921781	2.612252
C	-6.003979	0.611886	3.557183
C	7.916853	-0.874990	-0.489823
F	8.255118	-2.003620	-1.130715
F	8.737942	0.089583	-0.922207
F	8.203608	-1.074879	0.808552
O	-0.341140	7.279194	0.028573
C	0.242951	6.800870	1.224470
H	-0.331700	2.707800	0.415916
H	0.007966	0.118071	-0.892143
H	1.892246	-0.383440	-1.532097
H	-2.421038	0.664156	-0.394607

H	-2.742750	3.396285	0.416250	C	-5.340033	-0.170268	-1.357086
H	-4.001126	2.179683	0.341115	C	-6.164761	-0.769615	-0.419017
H	-3.731421	3.241872	2.649407	H	-6.412572	-2.412269	0.935407
H	-0.787383	0.628684	3.388633	H	-3.493063	-0.310993	-2.434180
H	0.115045	1.484658	2.158766	H	-5.621684	0.765960	-1.821661
H	-1.192845	3.443889	2.402414	H	-7.100718	-0.305560	-0.136238
H	-1.688715	2.734967	3.933667	C	-4.200575	-3.845602	0.565023
H	-5.476371	1.060953	1.591252	C	-2.484032	-2.573389	-1.572527
H	-7.059675	0.504470	3.340659	N	-2.216939	-3.776862	-1.820073
H	-5.693959	0.457061	4.584893	C	-0.841077	-3.812306	-2.306217
H	0.548482	7.680103	1.784414	C	-0.341786	-2.405469	-2.029527
H	1.114195	6.174788	1.013737	O	-1.462034	-1.651991	-1.792443
H	-0.480837	6.227095	1.810864	C	-0.012391	-5.030827	-1.859971
N	-0.432749	-2.211496	0.828501	H	-0.895331	-3.862458	-3.405339
N	0.915233	-1.889330	1.035671	C	-0.782505	-6.278308	-2.303616
C	1.314491	-1.316573	2.216269	C	0.181104	-5.064227	-0.346439
O	0.663914	-1.365557	3.234284	C	1.346222	-4.989194	-2.564166
O	2.515866	-0.754420	2.052419	O	0.745631	-1.908352	-2.074517
C	3.283364	-0.271330	3.201725	F	-4.984896	-4.041042	1.633156
C	3.566100	-1.433144	4.144489	F	-2.941609	-3.783467	1.025054
C	4.564701	0.241669	2.563705	F	-4.305446	-4.935059	-0.193612
C	2.545641	0.868577	3.891823	H	-1.752703	-6.333531	-1.809846
H	-0.669441	-2.983136	1.442606	H	-0.207185	-7.169791	-2.048208
H	-0.986454	-1.390874	1.099648	H	-0.945269	-6.278870	-3.384417
H	1.429916	-1.631593	0.207627	H	0.802010	-4.235642	-0.003447
H	2.650396	-1.801568	4.603336	H	0.674547	-5.997881	-0.069344
H	4.051275	-2.246023	3.601247	H	-0.781615	-5.018925	0.165630
H	4.242114	-1.096695	4.932050	H	1.229252	-4.979035	-3.650906
H	5.245556	0.593510	3.339949	H	1.917217	-5.880188	-2.297421
H	5.056935	-0.551179	1.997294	H	1.924373	-4.112256	-2.273209
H	4.337660	1.067341	1.888278				
H	2.300352	1.640814	3.160179	Structure: TS1-R			
H	3.202831	1.305310	4.646188	E(M06-2X/TZVP) = -3580.64144263 a.u.			
H	1.636116	0.518115	4.374841	Zero-point correction = 0.989064			
C	-5.784899	-1.964653	0.178138	Thermal correction to Energy = 1.050699			
C	-4.587979	-2.576662	-0.165599	Thermal correction to Enthalpy = 1.051643			
C	-3.756563	-1.982968	-1.124203	Thermal correction to Gibbs Free Energy (300K) =			
C	-4.140273	-0.775375	-1.701708	0.886672			

C	-0.972481	3.035932	-1.332849	H	-3.382672	0.530824	3.797873
C	-1.579176	2.498245	-2.440089	C	-0.690650	0.979027	2.512265
C	-2.025274	3.340676	-3.476256	C	-1.471022	2.185637	3.088529
N	-1.913652	4.643934	-3.447812	C	-4.941966	0.673917	2.377018
H	-1.718135	1.425418	-2.529395	C	-5.911609	0.319631	3.208847
H	-2.502569	2.912833	-4.352476	C	7.880286	-1.370180	-0.671113
C	-1.296396	5.200175	-2.376661	F	8.160817	-2.393737	-1.489956
C	-0.776320	4.442748	-1.292575	F	8.798778	-0.421133	-0.889106
C	-0.099647	5.113138	-0.237530	F	8.079115	-1.818960	0.581607
C	0.033128	6.476249	-0.266162	O	0.686327	7.202577	0.670015
C	-0.519664	7.237354	-1.330226	C	1.312095	6.493251	1.722022
C	-1.157292	6.614623	-2.355179	H	-0.090023	2.698119	0.600496
H	0.366383	4.538160	0.547854	H	0.161274	0.484867	-1.330685
H	-0.394965	8.311973	-1.302364	H	1.962481	-0.193344	-1.768454
H	-1.569966	7.167393	-3.188805	H	-2.284547	0.875431	-0.430528
C	-0.553096	2.120262	-0.192152	H	-2.405521	3.467798	0.847062
N	0.451488	1.171637	-0.637907	H	-3.746552	2.393408	0.506822
C	1.777546	1.282398	-0.403629	H	-3.513183	2.927664	2.976738
S	2.432309	2.354869	0.725039	H	-0.575427	0.186932	3.251613
N	2.508661	0.412240	-1.161061	H	0.311511	1.261239	2.188233
C	6.481824	-0.863223	-0.861803	H	-0.978177	3.126939	2.826438
C	6.192722	0.480457	-0.671993	H	-1.507692	2.132336	4.177917
C	4.889527	0.941145	-0.777779	H	-5.188850	0.884191	1.337246
C	3.861541	0.039101	-1.040327	H	-6.941704	0.250570	2.881269
C	4.163319	-1.305668	-1.265720	H	-5.707538	0.085829	4.248042
C	5.466230	-1.757624	-1.175953	H	1.804499	7.239804	2.338576
H	6.990964	1.178840	-0.457398	H	2.049940	5.785571	1.334638
H	4.666941	1.987234	-0.644128	H	0.574966	5.951416	2.321962
H	3.365573	-1.999406	-1.508709	N	-0.471262	-2.028121	0.178296
H	5.692392	-2.802473	-1.344606	N	0.896568	-2.103492	0.464657
C	-1.792151	1.414262	0.380714	C	1.285412	-1.790254	1.758260
N	-1.421361	0.388405	1.373622	O	0.556371	-1.925208	2.710612
C	-2.654100	-0.225233	1.889074	O	2.548549	-1.392354	1.739199
C	-3.492254	0.771365	2.736507	C	3.307748	-1.186751	2.979646
H	-2.379864	-1.104523	2.476036	C	3.425793	-2.515493	3.711050
H	-3.238218	-0.566612	1.030617	C	4.655089	-0.709185	2.464022
C	-2.773003	2.449479	0.997214	C	2.651306	-0.109126	3.831184
C	-2.888355	2.171715	2.499681	H	-0.958819	-2.823120	0.588876

H	-0.850504	-1.123468	0.565495
H	1.443508	-1.681513	-0.278986
H	2.453129	-2.863262	4.056076
H	3.869069	-3.267645	3.056554
H	4.076550	-2.388259	4.577333
H	5.341383	-0.571269	3.300362
H	5.083135	-1.438039	1.773560
H	4.533761	0.240448	1.941125
H	2.483029	0.783769	3.226276
H	3.329561	0.149522	4.646225
H	1.708242	-0.450391	4.252286
C	-6.324862	-1.595731	-0.113245
C	-5.077711	-2.163483	-0.335807
C	-4.177304	-1.540204	-1.208750
C	-4.532881	-0.329922	-1.799194
C	-5.781201	0.232167	-1.573496
C	-6.682760	-0.408643	-0.738428
H	-7.009370	-2.071783	0.574460
H	-3.823448	0.161769	-2.452257
H	-6.043462	1.168029	-2.049712
H	-7.658706	0.020995	-0.554070
C	-4.716535	-3.411543	0.443547
C	-2.845998	-2.092869	-1.534362
N	-2.553931	-3.304528	-1.739222
C	-1.139853	-3.328147	-2.115129
C	-0.618302	-1.950868	-1.676181
O	-1.843941	-1.169221	-1.656410
C	-0.422121	-4.644183	-1.768048
H	-1.099221	-3.240315	-3.210812
C	-1.086600	-5.727496	-2.628465
C	-0.564886	-5.049898	-0.296995
C	1.057196	-4.532104	-2.141428
O	0.400744	-1.392788	-2.082903
F	-5.570113	-3.603261	1.458381
F	-3.493496	-3.312955	0.998535
F	-4.740993	-4.519867	-0.292296
H	-2.146424	-5.815306	-2.385874
H	-0.605393	-6.690323	-2.448207
H	-0.992850	-5.495999	-3.692129
H	0.105033	-4.484730	0.353546
H	-0.288112	-6.099974	-0.187563
H	-1.599609	-4.946743	0.039479
H	1.181795	-4.219986	-3.180766
H	1.540035	-5.503218	-2.014383
H	1.570711	-3.811635	-1.504363

Structure: Int1-R

E(M06-2X/TZVP) = -3580.64187464 a.u.

Zero-point correction = 0.989834

Thermal correction to Energy = 1.051749

Thermal correction to Enthalpy = 1.052694

Thermal correction to Gibbs Free Energy (300K) = 0.888430

O	-1.882703	-1.114347	-1.551492
C	-2.864757	-2.054941	-1.496894
N	-2.551291	-3.257210	-1.727594
C	-1.124750	-3.253187	-2.065656
C	-0.608556	-1.884944	-1.562279
C	-4.218775	-1.534369	-1.202892
C	-5.129061	-2.182441	-0.359820
C	-6.393255	-1.641938	-0.164853
C	-6.758295	-0.456343	-0.788005
C	-5.847830	0.209548	-1.593862
C	-4.582843	-0.325065	-1.790813
C	-4.762271	-3.430817	0.415533
F	-4.743234	-4.531862	-0.331077
C	-0.417270	-4.576732	-1.722992
C	1.063155	-4.482037	-2.097801
N	-0.417484	-1.931384	0.109126
N	0.952684	-2.060955	0.391009
C	1.327917	-1.802936	1.702310
O	2.594461	-1.429755	1.712495
C	3.340358	-1.248110	2.965785
C	2.675963	-0.181735	3.824740
O	0.372374	-1.297932	-2.069382
O	0.577918	-1.962311	2.634910

C	3.442491	-2.589313	3.675508	O	0.751227	7.216681	0.745203
C	4.693512	-0.767478	2.469014	C	1.402727	6.484357	1.765263
F	-5.637498	-3.651726	1.406198	S	2.453110	2.345212	0.744872
F	-3.556078	-3.312069	1.003485	F	8.099834	-2.474019	-1.541948
C	-1.089125	-5.654418	-2.584727	F	8.782806	-0.512016	-0.956102
C	-0.568117	-4.982063	-0.251913	H	-1.758566	1.513117	-2.505654
N	-1.371862	0.375386	1.347257	H	-2.579888	3.039523	-4.279429
C	-1.766237	1.427250	0.386865	H	0.412912	4.556511	0.581324
C	-2.751024	2.432749	1.041947	H	-0.376664	8.369199	-1.175414
C	-2.875590	2.091063	2.529410	H	-1.605225	7.266982	-3.052966
C	-3.461304	0.673825	2.704546	H	7.001281	1.111578	-0.428058
C	-2.590789	-0.282488	1.845241	H	4.695184	1.971533	-0.601817
C	-1.463303	2.104858	3.129699	H	3.327494	-1.950830	-1.642933
C	-0.651613	0.943626	2.506160	H	5.636022	-2.806350	-1.481515
C	-0.539625	2.158589	-0.181351	H	-2.291887	-1.162828	2.418512
N	0.464051	1.228609	-0.665168	H	-3.158655	-0.625431	0.977489
C	1.788864	1.315700	-0.419567	H	-3.372827	0.400728	3.759891
N	2.511201	0.456441	-1.198661	H	-0.071785	2.720632	0.620299
C	3.856201	0.056190	-1.081708	H	0.171549	0.551085	-1.369519
C	4.898806	0.927266	-0.773971	H	1.952769	-0.132649	-1.813662
C	6.191703	0.437449	-0.675860	H	-2.262769	0.903903	-0.430164
C	6.457296	-0.903546	-0.914720	H	-2.382344	3.456540	0.938196
C	5.428171	-1.765041	-1.272785	H	-3.720864	2.397635	0.542825
C	4.135126	-1.284205	-1.358534	H	-3.516029	2.816880	3.031760
C	7.845138	-1.440097	-0.728349	H	-0.512921	0.128190	3.215108
F	8.040982	-1.884579	0.526725	H	0.340220	1.265686	2.188133
C	-4.900724	0.562674	2.306333	H	-0.988322	3.066789	2.915125
C	-5.886423	0.192351	3.111649	H	-1.506423	1.999861	4.215037
C	-0.982241	3.097793	-1.293575	H	-5.123578	0.773918	1.260968
C	-1.615088	2.583664	-2.397293	H	-6.906613	0.112188	2.756897
C	-2.081487	3.448276	-3.405943	H	-5.705879	-0.044734	4.154479
N	-1.964977	4.750357	-3.353642	H	1.916334	7.216664	2.381627
C	-1.320657	5.283125	-2.286518	H	2.125462	5.780567	1.343787
C	-0.778322	4.502558	-1.230144	H	0.680100	5.934650	2.375563
C	-0.070774	5.148886	-0.180251	H	-0.929266	-2.715272	0.519876
C	0.068948	6.511690	-0.186585	H	-0.774079	-1.003646	0.525437
C	-0.507604	7.295929	-1.220798	H	1.496591	-1.602341	-0.333885
C	-1.174442	6.696231	-2.240901	H	2.463134	-2.939042	3.999340

H	3.893407	-3.331981	3.015614
H	4.079589	-2.479066	4.554149
H	5.373378	-0.644045	3.312763
H	5.124690	-1.487425	1.771086
H	4.578827	0.189725	1.958237
H	2.512385	0.718655	3.229622
H	3.346540	0.066682	4.649119
H	1.729573	-0.528865	4.233790
H	-7.085957	-2.139139	0.499383
H	-3.865562	0.185904	-2.420143
H	-6.116828	1.143997	-2.069154
H	-7.747447	-0.048212	-0.626804
H	-1.049873	-3.136286	-3.154953
H	-2.147158	-5.742700	-2.336074
H	-0.606125	-6.618397	-2.414423
H	-1.002678	-5.414904	-3.647188
H	0.099666	-4.420583	0.405252
H	-0.295746	-6.032812	-0.137944
H	-1.604716	-4.875672	0.078634
H	1.186916	-4.169745	-3.137061
H	1.534679	-5.459292	-1.974038
H	1.589090	-3.769865	-1.462058

Structure: TS2-R

E(M06-2X/TZVP) = -3580.63987647 a.u.

Zero-point correction = 0.986655

Thermal correction to Energy = 1.047967

Thermal correction to Enthalpy = 1.048911

Thermal correction to Gibbs Free Energy (300K) = 0.886284

O	-1.958263	-1.062946	-1.526241
C	-2.909300	-2.026346	-1.488891
N	-2.567267	-3.220781	-1.721436
C	-1.136528	-3.179785	-2.047953
C	-0.636542	-1.809793	-1.513103
C	-4.278334	-1.538604	-1.196995
C	-5.176995	-2.203792	-0.354642
C	-6.444339	-1.675811	-0.142202
C	-6.824553	-0.485662	-0.746916
C	-5.927300	0.195483	-1.555189
C	-4.659729	-0.326263	-1.768785
C	-4.793375	-3.458023	0.403358
F	-4.746413	-4.545972	-0.359271
C	-0.413822	-4.497533	-1.714658
C	1.063042	-4.389335	-2.099876
N	-0.430230	-1.808735	0.062749
N	0.946193	-1.974271	0.330999
C	1.340561	-1.796108	1.638358
O	2.618449	-1.450583	1.658144
C	3.367356	-1.316423	2.912328
C	2.723944	-0.258198	3.797983
O	0.309756	-1.197453	-2.090502
O	0.598582	-1.983878	2.576518
C	3.448435	-2.675118	3.590961
C	4.729002	-0.847532	2.426703
F	-5.674359	-3.711649	1.382778
F	-3.596725	-3.323903	1.006385
C	-1.078189	-5.581675	-2.574124
C	-0.551425	-4.906195	-0.243337
N	-1.372254	0.315810	1.258139
C	-1.757947	1.412090	0.326952
C	-2.732458	2.388994	1.030506
C	-2.797697	2.034822	2.518288
C	-3.397581	0.624889	2.700061
C	-2.604117	-0.326120	1.773177
C	-1.361674	2.018572	3.059217
C	-0.601676	0.837463	2.417548
C	-0.522452	2.152890	-0.208127
N	0.480846	1.229091	-0.695802
C	1.804736	1.319874	-0.444875
N	2.530312	0.471789	-1.231904
C	3.873201	0.065085	-1.104737
C	4.914886	0.932600	-0.785277
C	6.205272	0.438592	-0.674389
C	6.468308	-0.903027	-0.912159
C	5.440151	-1.760755	-1.282076

C	4.149542	-1.275790	-1.380246	H	-3.404570	2.764218	3.055180
C	7.851347	-1.446012	-0.708830	H	-0.488436	0.006750	3.111032
F	8.025749	-1.901224	0.545671	H	0.395335	1.122840	2.080803
C	-4.861122	0.541826	2.386069	H	-0.871087	2.966852	2.821803
C	-5.798484	0.170882	3.246257	H	-1.360995	1.916423	4.145223
C	-0.959692	3.113421	-1.304132	H	-5.144973	0.775225	1.360438
C	-1.568753	2.618022	-2.429523	H	-6.840141	0.112634	2.956329
C	-2.030755	3.503243	-3.422445	H	-5.555387	-0.089532	4.270613
N	-1.932838	4.805047	-3.333814	H	1.817774	7.172320	2.528986
C	-1.312867	5.318683	-2.243380	H	2.067184	5.768589	1.456517
C	-0.775907	4.518180	-1.199505	H	0.601778	5.872671	2.466375
C	-0.094120	5.145953	-0.121510	H	-0.932738	-2.598891	0.474460
C	0.024598	6.510372	-0.088667	H	-0.824461	-0.735753	0.589386
C	-0.547140	7.313746	-1.110917	H	1.499311	-1.516029	-0.384438
C	-1.188204	6.732124	-2.157645	H	2.464534	-3.014041	3.911877
O	0.681027	7.199502	0.872908	H	3.880580	-3.410078	2.910191
C	1.326353	6.449611	1.883918	H	4.093890	-2.597993	4.467120
S	2.460409	2.335773	0.737692	H	5.410066	-0.749228	3.272785
F	8.115087	-2.474362	-1.526389	H	5.149837	-1.561553	1.716845
F	8.795817	-0.519596	-0.914222	H	4.630120	0.119940	1.931948
H	-1.695180	1.548415	-2.568198	H	2.578659	0.659467	3.224429
H	-2.509541	3.111199	-4.314159	H	3.397778	-0.042216	4.628783
H	0.389608	4.540563	0.629825	H	1.770858	-0.597674	4.198184
H	-0.432852	8.387151	-1.034762	H	-7.128160	-2.187967	0.519838
H	-1.613914	7.318258	-2.961380	H	-3.950824	0.197653	-2.397324
H	7.014460	1.109295	-0.416365	H	-6.209269	1.131778	-2.019358
H	4.712617	1.977335	-0.613734	H	-7.815722	-0.087940	-0.572543
H	3.342030	-1.940134	-1.669975	H	-1.055025	-3.046013	-3.134232
H	5.646380	-2.802852	-1.488596	H	-2.132527	-5.685524	-2.316577
H	-2.309842	-1.239721	2.292669	H	-0.579769	-6.539456	-2.412168
H	-3.206635	-0.606782	0.908476	H	-1.005070	-5.336379	-3.636350
H	-3.250947	0.326974	3.741923	H	0.101925	-4.326860	0.412602
H	-0.063669	2.700337	0.608837	H	-0.255412	-5.950728	-0.128838
H	0.195917	0.535254	-1.395709	H	-1.589396	-4.821158	0.088792
H	1.971796	-0.109053	-1.856802	H	1.175440	-4.070881	-3.138582
H	-2.254865	0.917368	-0.504604	H	1.544196	-5.363065	-1.984070
H	-2.382784	3.417823	0.917134	H	1.586695	-3.675427	-1.464621
H	-3.719215	2.339703	0.567771				

Structure: Int2-R

E(M06-2X/TZVP) = -3580.65235645 a.u.

Zero-point correction = 0.990893

Thermal correction to Energy = 1.053069

Thermal correction to Enthalpy = 1.054013

Thermal correction to Gibbs Free Energy (300K) = 0.890078

O	-1.678302	-1.173394	-1.234210
C	-2.588657	-2.136704	-1.383826
N	-2.228604	-3.278683	-1.803956
C	-0.796581	-3.159852	-2.099238
C	-0.266939	-1.964382	-1.252008
C	-3.994202	-1.763947	-1.071907
C	-4.853855	-2.560190	-0.308691
C	-6.179611	-2.181403	-0.131443
C	-6.656182	-1.003934	-0.689824
C	-5.796782	-0.183761	-1.407319
C	-4.473550	-0.560259	-1.587082
C	-4.367911	-3.806458	0.399326
F	-4.242362	-4.863478	-0.395954
C	-0.078112	-4.519744	-2.052625
C	1.392740	-4.341885	-2.435801
N	-0.166821	-2.215777	0.217407
N	1.130912	-2.437685	0.658096
C	1.660343	-1.622365	1.608058
O	2.969127	-1.820725	1.701586
C	3.736756	-1.329891	2.852961
C	3.580032	0.172605	3.043277
O	0.674334	-1.252961	-1.716305
O	0.999256	-0.857965	2.288647
C	3.295922	-2.110621	4.082211
C	5.166718	-1.664158	2.460020
F	-5.217719	-4.159199	1.377700
F	-3.178539	-3.599864	0.999900
C	-0.749859	-5.412573	-3.104699
C	-0.206566	-5.219443	-0.694610
N	-1.318784	0.453519	1.670359
C	-1.856937	1.297789	0.547736
C	-3.029751	2.143683	1.079290
C	-3.196237	1.886526	2.579518
C	-3.497628	0.394079	2.847729
C	-2.397371	-0.448656	2.162688
C	-1.872405	2.254125	3.261406
C	-0.781110	1.271224	2.804772
C	-0.724372	2.120633	-0.077345
N	0.382688	1.247760	-0.387812
C	1.685223	1.514083	-0.105831
N	2.490369	0.533409	-0.587647
C	3.877443	0.370260	-0.640251
C	4.832684	1.307966	-0.246190
C	6.181790	0.996846	-0.351951
C	6.592580	-0.226785	-0.855697
C	5.644316	-1.156535	-1.272636
C	4.302965	-0.858944	-1.166587
C	8.045950	-0.586686	-0.891452
F	8.412186	-1.294923	0.194155
C	-4.847742	-0.032801	2.353693
C	-5.823996	-0.484396	3.126437
C	-1.272907	2.833998	-1.302641
C	-1.713960	2.091265	-2.368864
C	-2.313971	2.737914	-3.466929
N	-2.501231	4.031645	-3.532615
C	-2.043761	4.788723	-2.505844
C	-1.388981	4.248084	-1.366743
C	-0.887821	5.128338	-0.368711
C	-1.055633	6.481391	-0.503476
C	-1.752409	7.019503	-1.618218
C	-2.222494	6.196525	-2.590916
O	-0.582697	7.403512	0.366446
C	0.189663	6.935601	1.454566
S	2.162971	2.878110	0.771270
F	8.352926	-1.342865	-1.955440
F	8.837900	0.492736	-0.927619
H	-1.605025	1.010674	-2.375178
H	-2.662529	2.152553	-4.312028
H	-0.305945	4.731881	0.449516

H	-1.866652	8.094199	-1.673003	H	-6.834198	-2.801822	0.464953
H	-2.733864	6.580640	-3.463701	H	-3.799580	0.069187	-2.155592
H	6.918422	1.726606	-0.041960	H	-6.154176	0.745427	-1.832646
H	4.526279	2.265416	0.140917	H	-7.691716	-0.722656	-0.549821
H	3.555532	-1.571980	-1.497085	H	-0.701346	-2.786838	-3.126998
H	5.958311	-2.109026	-1.679860	H	-1.796122	-5.582073	-2.850470
H	-1.931458	-1.169086	2.833104	H	-0.237808	-6.375899	-3.158784
H	-2.774480	-0.985915	1.292405	H	-0.707549	-4.948425	-4.092790
H	-3.456298	0.234607	3.928402	H	0.422735	-4.774755	0.078645
H	-0.360223	2.844477	0.645548	H	0.103109	-6.262113	-0.791889
H	0.210261	0.447754	-1.007148	H	-1.246740	-5.210209	-0.359110
H	1.968024	-0.241648	-1.024618	H	1.483199	-3.904186	-3.432108
H	-2.197719	0.574324	-0.187659	H	1.898558	-5.309848	-2.436064
H	-2.829980	3.205010	0.913900	H	1.926468	-3.677004	-1.754912
H	-3.940210	1.901361	0.529974				
H	-4.010348	2.492667	2.976243	Structure: Int3-R			
H	-0.503185	0.557160	3.575885	E(M06-2X/TZVP) = -3580.67914260 a.u.			
H	0.134630	1.752549	2.462815	Zero-point correction = 0.990977 (Hartree/Particle)			
H	-1.599246	3.277302	2.993825	Thermal correction to Energy = 1.053818			
H	-1.973837	2.215521	4.346266	Thermal correction to Enthalpy = 1.054762			
H	-4.999712	0.019631	1.276995	Thermal correction to Gibbs Free Energy (300K) =			
H	-6.775561	-0.788341	2.708696	0.887760			
H	-5.704511	-0.569974	4.201072	O	-1.575961	-0.924767	-0.976171
H	0.506810	7.818538	2.002061	C	-2.268723	-1.968659	-1.230924
H	1.064759	6.380469	1.106444	N	-1.923893	-3.001955	-1.924527
H	-0.406107	6.293652	2.110530	C	-0.615309	-2.860815	-2.538296
H	-0.755558	-2.999069	0.489498	C	0.491781	-2.706197	-1.508518
H	-0.551346	-0.152734	1.328140	C	-3.691898	-1.948318	-0.712708
H	1.775497	-2.962476	0.082299	C	-4.230625	-2.856657	0.200579
H	2.249840	-1.907857	4.312537	C	-5.542243	-2.722056	0.649098
H	3.429735	-3.181539	3.922800	C	-6.336183	-1.683383	0.188901
H	3.901262	-1.808784	4.938220	C	-5.811347	-0.767954	-0.714466
H	5.841943	-1.415337	3.279226	C	-4.500747	-0.898603	-1.148117
H	5.263505	-2.726389	2.233579	C	-3.388967	-3.960921	0.786469
H	5.458371	-1.089358	1.579587	F	-3.171604	-4.981309	-0.041173
H	3.686834	0.693554	2.092750	C	-0.343139	-4.036963	-3.516277
H	4.372155	0.518491	3.710208	C	1.045270	-3.898382	-4.142813
H	2.615272	0.434511	3.469245	N	0.334223	-3.442203	-0.378000

N	1.276838	-3.415271	0.615356	N	-2.769162	4.049400	-3.589249
C	1.444147	-2.293250	1.391045	C	-2.206664	4.805581	-2.615573
O	2.632440	-2.367822	1.982619	C	-1.523766	4.258162	-1.496147
C	2.999153	-1.513983	3.117846	C	-0.913359	5.134483	-0.557195
C	3.079052	-0.057793	2.690432	C	-1.004298	6.490646	-0.727532
O	1.490493	-2.020060	-1.680059	C	-1.726608	7.039087	-1.820591
O	0.612385	-1.422136	1.533145	C	-2.300810	6.218908	-2.738317
C	2.003899	-1.739709	4.247899	O	-0.426946	7.405546	0.085997
C	4.376010	-2.034920	3.496769	C	0.374694	6.919046	1.144313
F	-3.951880	-4.476282	1.891278	S	1.974182	2.876025	0.556047
F	-2.176247	-3.500124	1.172288	F	8.394747	-1.111417	-1.075053
C	-1.404292	-3.952544	-4.616562	F	8.650410	0.936646	-0.445934
C	-0.466327	-5.387077	-2.807935	H	-2.014562	1.012452	-2.363432
N	-1.503890	0.424267	1.536419	H	-3.104761	2.162250	-4.288879
C	-2.059707	1.408596	0.543450	H	-0.311914	4.726183	0.240813
C	-3.009864	2.370714	1.282804	H	-1.776791	8.116756	-1.905103
C	-2.893386	2.134093	2.792273	H	-2.835937	6.608412	-3.594317
C	-3.362485	0.705714	3.152038	H	6.610839	2.206200	-0.551153
C	-2.636507	-0.278712	2.209872	H	4.186805	2.559511	-0.799159
C	-1.415420	2.258098	3.180279	H	3.559098	-1.670660	-0.682695
C	-0.637447	1.084718	2.562431	H	5.998020	-2.028509	-0.451027
C	-0.912475	2.129930	-0.180322	H	-2.221709	-1.140236	2.731174
N	0.165007	1.218998	-0.524843	H	-3.294811	-0.637852	1.419694
C	1.473978	1.506654	-0.315378	H	-3.062349	0.509777	4.185185
N	2.312794	0.571385	-0.819805	H	-0.476541	2.854128	0.500677
C	3.713778	0.467506	-0.706080	H	-0.106203	0.352865	-0.999222
C	4.576871	1.559721	-0.704994	H	1.880133	-0.276515	-1.193490
C	5.942718	1.355585	-0.563912	H	-2.590651	0.786760	-0.168218
C	6.453260	0.071993	-0.456004	H	-2.745542	3.404821	1.049682
C	5.598084	-1.023790	-0.510928	H	-4.034329	2.219552	0.941027
C	4.237512	-0.828440	-0.639263	H	-3.496267	2.860336	3.336618
C	7.918767	-0.166144	-0.250002	H	-0.387621	0.312481	3.287147
F	8.182587	-0.591957	0.999596	H	0.280531	1.406538	2.077239
C	-4.847863	0.521848	3.051859	H	-1.012088	3.206505	2.816696
C	-5.639823	0.269556	4.083244	H	-1.299289	2.247425	4.264199
C	-1.494316	2.841828	-1.391519	H	-5.273260	0.589254	2.052365
C	-2.049907	2.097392	-2.401490	H	-6.708030	0.147091	3.959118
C	-2.667131	2.748339	-3.487015	H	-5.245588	0.174040	5.089209

H	0.777716	7.794445	1.645575	H	-5.935359	-3.425454	1.370122
H	1.191342	6.298080	0.766336	H	-4.085450	-0.181767	-1.847010
H	-0.221935	6.335256	1.851956	H	-6.422394	0.047155	-1.082218
H	-0.553792	-3.883234	-0.181260	H	-7.355991	-1.588614	0.538211
H	-0.957098	-0.279442	1.010891	H	-0.553949	-1.930674	-3.117973
H	2.115239	-3.952867	0.441649	H	-2.402874	-4.034858	-4.188115
H	1.015395	-1.367885	3.984164	H	-1.259265	-4.759388	-5.338380
H	1.931053	-2.803176	4.480960	H	-1.332583	-3.001757	-5.151223
H	2.349089	-1.214219	5.139103	H	0.335044	-5.535857	-2.080883
H	4.767043	-1.458345	4.335642	H	-0.400163	-6.194636	-3.540436
H	4.324907	-3.085702	3.783483	H	-1.426067	-5.459899	-2.294169
H	5.059773	-1.928600	2.653730	H	1.171049	-2.919714	-4.611563
H	3.843468	0.077998	1.925392	H	1.181032	-4.665009	-4.908759
H	3.350801	0.553562	3.552713	H	1.840603	-4.015244	-3.404252
H	2.130448	0.297842	2.298396				

3-6. References

[1] (a) Liu, J.; Wei, Z.; Cao, J.; Liang, D.; Lin, Y.; Duan, H. *Tetrahedron* **2023**, *140*, 133471. (b) Qi, J.; Fan, G.-T.; Chen, J.; Sun, M.-H.; Dong, Y.-T.; Zhou, L. *Chem. Commun.* **2014**, *50*, 13841–13844. (c) Xu, J.; Hu, Y.; Huang, D.; Wang, K.-H.; Xu, C.; Niu, T. *Adv. Synth. Catal.* **2012**, *354*, 515–526. (d) Bera, K.; Namboothiri, I. N. N. *Org. Lett.* **2012**, *14*, 4, 980–983. (e) Yang, W.; Du, D.-M. *Org. Lett.* **2010**, *12*, 23, 5450–5453. (f) Li, X.; Deng, H.; Zhang, B.; Li, J.; Zhang, L.; Luo, S.; Cheng, J.-P. *Chem. Eur. J.* **2010**, *16*, 450–455. (g) Song, J.; Wang, Y.; Deng, L. *J. Am. Chem. Soc.* **2006**, *128*, 6048–6049. (h) Vakulya, B.; Varga, S.; Csámpai, A.; Soós, T. *Org. Lett.* **2005**, *7*, 10, 1967–1969.

[2] Carter, H. E.; Handler, P.; Melville, D. B. *J. Biol. Chem.* **1939**, *129*, 359–369.

[3] (a) Wang, L.; Liu, M.; Lu, M.; Wang, B.; Han, Q.; Jin, J.; Yu, S.; Wu, Y.; Guo, H. *Org. Chem. Front.* **2023**, *10*, 813–818. (b) Zhu, D.-Y.; Zhang, X.-J.; Yan, M. *Org. Lett.* **2021**, *23*, 4228–4232. (c) Arp, F. O.; Fu, G. C. *J. Am. Chem. Soc.* **2006**, *128*, 14264–14265.

[4] Tallon, S.; Manoni, F.; Connon, S. J. *Angew. Chem. Int. Ed.* **2015**, *54*, 813–817.

[5] Boudreault, N., Ball, R. G., Bayly, C., Bernstein, M. A., Leblanc, Y. *Tetrahedron* **1994**, *50*, 7947–7956.

[6] Liang, J.; Ruble, J. C.; Fu, G. C. *J. Org. Chem.* **1998**, *63*, 3154–3155.

4. Acknowledgment

I would like to express my deepest gratitude to Professor Makoto Tokunaga for his continuous support and guidance. I once thought that such an opportunity would never come again, and I am truly thankful for being given a second chance. I am also grateful to Professor Eiji Yamamoto for his constant and stimulating discussions, which not only contributed to this research but also deepened my overall insight into chemistry and beyond. I sincerely thank Professor Takashi Kamachi of Fukuoka Institute of Technology for his guidance. Despite being conducted online, his instruction greatly broadened my understanding of computational chemistry, a field I never expected to explore within my research curriculum, making it an invaluable experience. My appreciation also goes to Assistant Professor Akina Yoshizawa, whose sharp questions from different perspectives prevented the research from becoming one-sided and ensured a balanced approach.

I am indebted to Dr. Kawai, Mr. Ichikawa, and Mr. Kono, who departed before the completion of this study; without their prior work, this research could not have been completed so smoothly. I also wish to thank Mr. Yamaguchi, whose exceptional ability to identify aspects I had overlooked or not fully considered was of great help throughout the course of this research. His insights not only enriched the present work but also played a significant role in shaping the prospective direction of this study.

Finally, I would like to acknowledge the unusual origins of this work. It traces back to four international students (three PhD students and one master's student) whose academic paths were thrown into considerable difficulty when their former supervisor abruptly and without due responsibility departed. It is fortunate that each of us was given a second chance, and I am grateful that this could ultimately lead to the present study.

5. List of Publication

5-1. List of Principal Publication

1) Dynamic Kinetic Resolution of Azlactones with Hydrazines via Negative Catalysis: Synthesis of *α*-Chiral Amino Acid Hydrazides and Their Preferential Enrichment Phenomenon
Sungyong Won, Yuta Yamaguchi, Yasutaka Kawai, Yuki Kono, Masato Ichikawa, Eiji Yamamoto, Takashi Kamachi, Akina Yoshizawa, and Makoto Tokunaga
ACS Catal. **2025**, *accepted*.

5-2. List of Other Publications

1) Economical and Readily Accessible Preparation of *o*,*o*-Disubstituted Arylboronates through Palladium-Catalyzed Borylation of Haloarenes
Ryoichi Kuwano, Eunhyung Lee, and Sungyong Won
Org. Lett. **2021**, *23*, 9649–9653.

2) Room-Temperature Benzylic Alkylation of Benzylic Carbonates: Improvement of Palladium Catalyst and Mechanistic Study
Ryoichi Kuwano, Masashi Yokogi, Ken Sakai, Shigeyuki Masaoka, Takashi Miura, and Sungyong Won
Org. *Process Res*. *Dev*. **2019**, *23*, 1568–1579.

3) Highly Stereoselective Reactions of 2-(*t*-Butyl)dimethylsilyl-3,3-difluoro-1-phenylprop-2-en-1-one with Nucleophiles
Ye Rim Jeong, Hyun Gyu Ryu, Sung Yong Won, and In Howa Jeong
Bull. *Korean Chem*. *Soc*. **2018**, *39*, 111–114.